KUOPION YLIOPISTON JULKAISUJA G. – A.I. VIRTANEN – INSTITUUTTI 36
KUOPIO UNIVERSITY PUBLICATIONS G.
A.I. VIRTANEN INSTITUTE FOR MOLECULAR SCIENCES 36

PIIA VALONEN

A Multimodal NMR study of Apoptosis Induced by HSV-tk Gene Therapy in a Rat Experimental Glioma Model

Doctoral dissertation

To be presented by permission of the Faculty of Natural and Environmental Sciences of the University of Kuopio for public examination in Medistudia ML3, University of Kuopio, on Friday 17th June, 2005, at 12 noon

Department of Biomedical NMR and National Bio-NMR Facility
A.I. Virtanen Institute for Molecular Sciences
University of Kuopio

Distribution: Kuopio University Library
P.O.Box 1627
FIN-70211 KUOPIO
FINLAND
Tel. +358 17 163 430
Fax +358 17 163 410

Series editors: Professor Karl Åkerman
Department of Neurobiology
A.I. Virtanen Institute for Molecular Sciences
University of Kuopio, Finland

Research Director Jarmo Wahlfors
Department of Biotechnology and Molecular medicine
A.I. Virtanen Institute for Molecular Sciences
University of Kuopio, Finland

Author's address: Department of Anatomy
University of Kuopio
P.O.Box 1627
FIN-70211 KUOPIO
FINLAND
Tel. +358 17 163 178
Fax +358 17 163 032
Piia.Valonen@uku.fi

Supervisors: Professor Risto Kauppinen, M.D., Ph.D.
School of Sport & Exercise Sciences
The University of Birmingham, UK

Professor Seppo Ylä-Herttuala, M.D., Ph.D.
Department of Biotechnology and Molecular medicine
A.I. Virtanen Institute for Molecular Sciences
University of Kuopio, Finland

Reviewers: Professor Peter Barker, Ph.D.
Russel H Morgan Department of Radiology and Radiological Science
Johns Hopkins University School of Medicine
Baltimore, MD, USA

Professor Veli-Matti Kähäri, M.D., Ph.D.
Department of Medical Biochemistry and Molecular Biology
University of Turku, Finland

Opponent: Professor Arend Heerschap, Ph.D.
Department of Radiology
UMC Nijmegen, The Netherlands

ISBN 951-781-395-3
ISBN 951-27-0099-9 (PDF)
ISSN 1458-7335

Kopijyvä
Kuopio 2005

Valonen, Piia. A Multimodal NMR study of Apoptosis Induced by HSV-tk Gene Therapy in a Rat Experimental Glioma Model. Kuopio University Publications G. –A.I. Virtanen Institute for Molecular Sciences 36. 2005. 87 p.
ISBN 951-781-395-3
ISBN 951-27-0099-9 (PDF)
ISSN 1458-7335

Abstract

In vivo nuclear magnetic resonance (NMR) techniques are widely used nowadays, both in experimental and clinical cancer research. Advantages of NMR include the ability to reveal abnormal tissue types non-invasively, and to provide a wealth of information from cancer tissue *in situ*, which can be used to assess the degree of malignancy and treatment responses. This study was devised to search for endogenous NMR detectable biomarkers for apoptotic cell death in a rat BT4C glioma model treated with Herpes Simplex virus thymidine kinase gene (HSV-tk) ganciclovir (GCV) gene therapy. To this end, multimodal NMR methods *in vivo*, *ex vivo*, and *in vitro* were used.

Altered microenvironments of water were observed in the apoptosing BT4C glioma *in vivo*, as revealed with diffusion MR imaging (MRI). Increases both in extracellular volume and net water content, as well as decrease in intracellular space was also detected in the gene therapy treated apoptosing gliomas. These changes preceded or coincided with the collapse of tumour cell count determined by histology and were expressed before a decline in the tumour volume observed in T_2 weighted MR images. Therefore, diffusion MRI proved to be a sensitive imaging method for the detection of a tumour's response to gene therapy –induced apoptosis prior to tumour shrinkage.

A Carr-Purcell (CP) T_2 MRI method was introduced for imaging of rat brain tumours. CP T_2 MRI contrast at a 4.7 T magnetic field strength, acquired with a short (6.1 ms) interpulse interval, highlighted tissue changes associated with gene therapy -induced cytotoxicity. This was also evident well before any cell loss or decrease in tumour growth rate could be observed. This MRI contrast is expected to provide valuable information about early cytotoxic tumour responses and might be useful in clinics.

Ex vivo high resolution magic angle spinning (HRMAS) NMR spectroscopy revealed that none of the chemical species containing a choline moiety contributing to the *in vivo* choline ^{1}H NMR signal at 3.2 ppm, were found to decrease with cell density early in the apoptosing glioma. In contrast, the concentration of taurine resonating close to 3.2 ppm followed the cell density and this may explain the decrease in the intensity of the choline peak *in vivo* in early phase of tumour apoptosis. Accumulation of polyunsaturated fatty acids (PUFA) was found to be the most significant contributor to the increase in ^{1}H NMR lipid resonances during the apoptotic cell death. Multidimensional NMR analyses of tissue samples *ex vivo* and extracts *in vitro* showed that ^{1}H NMR detectable PUFAs were mainly 18:1 and 18:2 fatty acids. This argues that membrane breakdown products may be the source for the ^{1}H NMR detected PUFAs.

The present results show that several potential endogenous biomarkers for apoptosis can be revealed with NMR methods *in vivo*. These results expand our understanding of the biomolecular and biophysical changes behind the NMR data in the apoptotic BT4C glioma. They also show the ability of *in vivo* NMR techniques to reveal apoptosis in the experimental glioma prior to tumour growth arrest or shrinkage. It is believed that NMR methods used here may provide a way of visualising treatment response in early phase of therapy. Some or all of these may also have uses in the clinical environment, thus allowing for the more efficient management of cancer.

National Library of Medicine Classification: WN 185, QZ 380, QU 375,QZ 52
Medical Subject Headings: diagnostic imaging; neoplasms; glioma; magnetic resonance imaging; magnetic resonance spectroscopy; simplexvirus; thymidine kinase; gene therapy; ganciclovir; apoptosis; biological markers; diffusion; fatty acids, unsaturated; choline; taurine; rats

Acknowledgements

This study was carried out in the A. I. Virtanen Institute for Molecular Sciences, University of Kuopio, during the years 2000-2005.

I own my deepest gratitude to my principal supervisor, Professor Risto Kauppinen, M.D. Ph.D., who gave me the possibility to work in his laboratory with state-of-art methods in the field of *in vivo* NMR. His enthusiasm and devotion towards science is breathtaking. His endless capability to produce new ideas, as well as his patience has made the completion of this thesis possible.

My second supervisor, Professor Seppo Ylä-Herttuala, M.D. Ph.D, has provided me the opportunity to work as a part of a highly recognized group. His knowledge and inspiring attitude has shown me a way to practice science with 'relaxed dedication'. I thank him for the encouragement and support I received from him during the years.

Docent Juhana Hakumäki, M.D. Ph.D, has served as my third supervisor after Risto's departure to Manchester. It has been educative to work with him. I thank him for the talks, support and criticism he has provided me during the years.

I thank the official reviewers, Professor Peter Barker, Ph.D, and Professor Veli-Matti Kähäri, M.D. Ph.D, for their comments and constructive criticism of this work. I would also like to thank Tom Dunlop, Ph.D, for revising the language of the manuscript and Professor Asla Pitkänen, M.D. Ph.D, for her invaluable help concerning histology.

The basics of my cell culturing techniques were kindly provided to me by technician Anne Martikainen. The animal handling and the glioma model were introduced to me by Pauliina Lehtolainen, Ph.D, whose *in vitro* study expertise was also invaluable. I will also thank her for the time she always had for me, and for the nice discussions. It was always a pleasure to work with her.

I think there is nobody in the NMR group who has survived without helping me in the issues concerning the use or the handling of the results of NMR, thank you for all of you, but the contribution of Kimmo Lehtimäki, B.Sc., overrides everybody else's. He has made most of the *in vivo* and *in vitro* measurements, and he has always had time for my silly questions. Thank you. Olli Gröhn, Ph.D, and Mikko Kettunen, Ph.D, have been crucial factors in programming, and they have had a big part in introducing me to the secrets of Varian. I will also thank Tuula Väisänen, M.Sc., who has also had a big contribution into the studies included in this book in official, as well as in unofficial way. I also thank Julian Griffin, Ph.D, whose expertise in HRMAS has been conclusive.

I would also like to thank our technicians Niina Kuhmonen, Tuula Salonen and Maarit Pulkkinen for their significant contribution and help with histology, but also for their friendship that developed between the slices.

I am deeply grateful to my family, who have managed to say the right words at the right places, even though I am not that sure they have really known what this all has been about… My friends have also had a significant contribution to my life during this time by understanding and supporting me, especially Kaija, who has been there for me when ever needed and who has always believed in me.

This study was financially supported by the Academy of Finland, the Finnish Cancer Foundation, the Finnish Cultural Foundation of Northern Savo, Ella and Georg Ehrnrooth Foundation, Ida Montin Foundation, Maud Kuistila Foundation and the Sigrid Juselius Foundation.

Kuopio, June 2005

Piia Valonen

Abbreviations

AA	anaplastic astrocytoma
AAV	adeno-associated viruses
ADC	apparent diffusion coefficient
Ala	alanine
ANOVA	analysis of variance
ANN	artificial neural networks
B_0	external magnetic field
B_1^{max}	peak RF amplitude
BBB	blood brain barrier
BCNU	carmustine
B_{eff}	effective magnetic field
Bid	BH3 interacting domain death agonist
CBV	cerebral blood volume
CCD	computerized consensus diagnosis
CCM	choline containing metabolites
CCT	CTP:phosphocholine cytidylyltransferase
CDP-Cho	cytidine diphosphocholine
CH_2	methylene-group
CH_3	methyl-group
Cho	free choline
tCho	total choline
CD	*Escherichia coli* cytosine deaminase
CDP	cytidine diphosphate
CK	choline kinase
CNS	central nervous system
COSY	chemical shift correlated spectroscopy
CP	Carr-Purcell
CPMG	Carr-Purcell-Meiboom-Gill
CP-T_2	Carr-Purcell T_2
Cr	creatine + phosphocreatine
CT	computed tomography
1D	one dimensional
2D	two dimensional
D	diffusion coefficient
D_{av}	1/3 of the trace of the diffusion tensor
D_i	diffusion constant of the i^{th} component
DMEM	Dulbecco's modified eagle's medium
DWI	diffusion weighted imaging
ΔE	energy difference
f_i	population fraction of the i^{th} component
FADD	Fas-associated death domain protein
FBS	fetal bovine serum
5-FC	5-fluorocytosine
5-FU	5-fluorouracil
FFA	free fatty acids
FGF	fibroblast growth factor
FID	free induction decay
FOV	field of view

FT	Fourier transformation
δ	duration of the diffusion-sensitizing gradient pulse
G	amplitude of the diffusion-sensitizing gradient pulse
GBM	glioblastoma multiforme
GCV	ganciclovir
Glx	glutamate + glutamine
Gly	glycine
GMT	Glioma Meta-analysis Trialists
GN	Gauss-Newton
GPC	glycerophosphocholine
γ	gyromagnetic ratio
HMBC	heteronuclear multiple bond correlation
HPF	high-power microscopy field
HRMAS	high resolution magic angle spinning
HSV-tk	Herpes Simplex viruses thymidine kinase gene
HSQC	heteronuclear single quantum coherence
I	nuclear spin quantum number
IL-4	interleukin 4
i.p.	intraperitoneal
J_{XX}	spin-spin coupling constant
JRES	J-resolved 2D spectrum
Lac	lactate
LASER	localization by adiabatic selective refocusing method
LDA	linear discriminant analysis
LGA	low-grade astrocytoma
M_0	net magnetization at equilibrium
MAS	magic angle spinning
MeP	6-methylpurine
MEN	meningiomas
MET	metastasis
MM	broad unassigned macromolecular resonances
MRI	magnetic resonance imaging
MRS	magnetic resonance spectroscopy
M_z, M_{xy}	magnetization components along the z axis and in the xy plane, respectively
myo-Ins	myo-Inositol
n^- and n^+	the relative numbers of nuclei of the higher and lower energy levels
NAA	N-acetyl-aspartate
NMR	nuclear magnetic resonance
OCT	optimal cutting temperature
ω_0	the Larmor frequency
PBS	phosphate buffered saline
PC	phosphocholine
PCA	perchloric acid
PCD	programmed cell death
PCV	combination of procarbazine, lomustine and vincristine
PE	phosphoethanolamine
PET	positron emission tomography
PL	phospholipid
PLA_1	phospholipase A_1
PLA_2	phospholipase A_2

PLC	phospholipase C
PLD	phospholipase D
ppm	parts per million
PS	phosphatidylserine
PtdCho	phosphatidylcholine
PUFA	polyunsaturated fatty acids
r	mean displacement of water
RF	radio frequency pulse
RT	radiation therapy
σ	shielding constant
s.c.	subcutaneously
SI	signal intensity
STEAM	stimulated echo acquisition mode
SW	sweep width
τ	mean apparent residence time
τ_{CP}	interpulse interval time in CP-T_2 sequence
T_1	longitudinal relaxation time
T_2	transverse relaxation time
$T_{1\rho}$	longitudinal relaxation in the rotating frame
$T_2^{\dagger}$	apparent transverse relaxation time
$T_{2,\ Intrinsic}$	intrinsic transverse relaxation time
$T_{2,\ Diffusion}$	diffusion contribution to transverse relaxation time
$T_{2,\ Exchange}$	exchange contribution to transverse relaxation time
Tau	taurine
t_D	diffusion time
T_p	pulse length
tBid	truncated Bid
TE	echo time
TI	inversion time
TM	middle period
TMZ	temozolomide
TOCSY	total correlation spectroscopy
TR	repetition time
TSL	duration of the spin lock pulse
TSP	trimethylsilyl propionic acid
TUNEL	transferase-mediated dUTP nick end labeling
UDP	uridine diphosphate
VAPOR	a variable pulse power and optimized relaxation delay
VEGF	vascular endothelial growth factor
WHO	World Health Organization

List of original publications

This thesis is based on the following publications which will be referred to by their corresponding Roman numerals in the thesis:

I **Valonen P.K**, Lehtimäki K.K, Väisänen T.H, Kettunen M.I, Gröhn O.H.J, Ylä-Herttuala S, Kauppinen R.A. Water diffusion in a rat glioma during ganciclovir-thymidine kinase gene therapy-induced programmed cell death *in vivo*: Correlation with cell density. *J Magn Reson Imag*, 9:389-396, 2004

II Gröhn O.H.J, **Valonen P.K**, Lehtimäki K.K, Väisänen T.H, Kettunen M.I, Ylä-Herttuala S, Kauppinen R.A, Garwood M. Novel Magnetic Resonance Imaging Contrasts for Monitoring Response to Gene Therapy in Rat Glioma. *Cancer Res*, 63:7571-7574, 2003

III Lehtimäki K.K, **Valonen P.K**, Griffin J.L, Väisänen T.H, Gröhn O.H, Kettunen M.I, Vepsäläinen J, Ylä-Herttuala S, Nicholson J, Kauppinen R.A. Metabolite changes in BT4C rat gliomas undergoing ganciclovir-thymidine kinase gene-therapy induced programmed cell death as studied by ^{1}H NMR spectroscopy *in vivo, ex vivo* and *in vitro*. *J Biol Chem*, 278:45915-45923, 2003.

IV Griffin J.L, Lehtimäki K.K, **Valonen P.K**, Gröhn O.H, Kettunen M.I, Ylä-Herttuala S, Pitkänen A, Nicholson J.K, Kauppinen R.A. Assignment of ^{1}H nuclear magnetic resonance visible polyunsaturated fatty acids in BT4C gliomas undergoing ganciclovir-thymidine kinase gene therapy-induced programmed cell death. *Cancer Res*, 63:3195-3201, 2003.

V **Valonen P.K**, Griffin J.L, Lehtimäki K.K, Liimatainen T, Nicholson, J.K, Gröhn O.H.J, Kauppinen R.A. High resolution magic-angle-spinning ^{1}H NMR spectroscopy reveals the different responses in choline-containing metabolites upon gene therapy –induced programmed cell death in rat brain glioma. *NMR in Biomed*, *In Press.*

1 Introduction

Cancer is a major public health problem in the developed countries and accounts for approximately one quarter of all deaths in the United States each year (Jemal et al., 2003). Although brain tumours account for only about two percent of all cases of cancer, they are responsible for the highest number of years lost to cancer (Vincent and George, 2004). This is because the prognosis of glioblastoma patients has remained poor despite improvements in the treatments. The expected lifetime of these patients, post-diagnosis, is approximately one year.

However, new methods of cancer treatment are under development with gene therapy being one of the most studied. In experimental cancer models as well as studies with patients, cancer cells have been made to produce toxic compounds, enzymes to activate pro drugs and tumour suppressor proteins. Attempts have also been made to inhibit angiogenesis and enhance immune response, by the introduction of therapeutic transgenes into the tumour (Lam and Breakefield, 2001). In addition, many methods have been generated for the induction of programmed cell death in the tumours because deficiencies in the mechanisms of apoptosis are often found in cancer cells (Lowe and Lin, 2000a).

Since apoptosis is associated with a clear set of physical and chemical events, we wondered if any of these processes could be detected *in vivo* by NMR. In this study we have used the well characterized experimental rat BT4C glioma model, where apoptotic cell death is induced by Herpes Simplex viruses thymidine kinase gene (HSV-tk) expression and ganciclovir (GCV) mediated gene therapy (Hakumäki et al., 1998; Hakumäki et al., 1999; Poptani et al., 1998a; Sandmair et al., 2000b). Nuclear magnetic resonance (NMR) techniques are currently exploited extensively in clinical and preclinical settings to monitor cancer, and here we have used various NMR methods to characterize the BT4C-tk glioma before and during apoptotic cell death.

Since the aim of our research was to find endogenous NMR visible biomolecular markers that could reveal apoptosis, before cell death and tumour shrinkage become apparent, we used a variety of NMR methods *in vivo*. These included magnetic resonance imaging (MRI), magnetic resonance spectroscopy (MRS), diffusion weighted imaging (DWI) and diffusion spectroscopy to provide anatomical, biochemical and biophysical information. Furthermore, tissue samples were studied with high-resolution magic angle NMR spectroscopy (HRMAS) *ex vivo* and extracts from tissue samples were studied by ^{1}H and ^{31}P NMR spectroscopy *in vitro*. These latter studies were performed in order to identify some of the essential molecular changes occurring in our model. Finally, histological studies were performed in order to match the changes observed in NMR with physiological changes occurring during the treatment of the glioma.

2 Review of the literature

2.1 Cancer biology

2.1.1 Cancer

Cancer is characterized by uncontrolled growth (proliferation) of cells. This can occur by epigenetic reprogramming but it is most often caused by changes in the cells genetic material. Due to the mutations in the DNA, caused by factors such as radiation, carcinogenic compound or some viruses, cells are transformed to a cancerous state, where they no longer respond appropriately to the signals controlling their environment. Cancer cells can grow and divide in an uncontrolled manner, and invade blood and lymphatic vessels, which allows them to spread to other sites in the body to form metastases (Lowe and Lin, 2000b). Malignant brain tumours differ from other types of cancers in this respect because they do not commonly metastasize.

It is believed that before a cell can become cancerous, many mitosis and multiple mutations must happen. For the cells to gain the abilities of aggressive cancers, they must acquire some or all of the following characteristics. These include, fast population growth, resistance to apoptotic signals, the ability to survive in a suspension like environment, and to be able to secrete the proteases that are necessary for invasion into tissues. Thus, cancer cells have gone through many inherent changes to fight their way to survive and this is perhaps the main reason why they are so difficult to treat. Cancers are also very difficult to treat because even cancers from the same cell type can have different sets of cancer-promoting mutations. Despite this situation, the development of better methods for the treatment and the analysis of treatment success continue (Lowe and Lin, 2000b).

2.1.2 Classification

Tumours can result from the abnormal proliferation of many kinds of cells in the body. A tumour is any abnormal proliferation of cells which can be either benign or malignant. A benign tumour remains at its original location and it neither infiltrates neighboring tissues nor spreads to distant body sites. Malignant tumours on the other hand, have the ability of invasion and can spread throughout the body via blood and lymphatic vessels. Only malignant tumours are referred to as cancers (Cooper, 2000).

Most of the primary brain tumours in adulthood arise from glial cells and the first objective in treatment is to characterize which cell type the tumour has originated from and how much the cells differ histologically from this tissue.

Table 1. Tumours of neuroepithelial tissue as classified by the World Health Organization (WHO) (Zülch, 1979)

Gliomas
Pituitary tumours
Meningioma
Pineal tumours
Intracranial lymphoma
Acoustic
Chondroma
Neuronal tumours

Each of these tumour types have been classified into four different grades (I to IV) which are determined by the assessment of four morphological features.

1. atypical appearance of cell nuclei
2. evidence of cell division (mitotic bodies)
3. endothelial hyperplasia (microvascular proliferation)
4. areas displaying necrotic histology

The grades are assigned according to the following descriptions. None of these features are found in grade I tumours. Grade II, usually have nuclear atypia and often infiltrative capacity. Tumours of grade III usually exhibit mitosis, nuclear atypia and are clearly infiltrative. Grade IV tumours have all four features and show a remarkable degree of cellular heterogeneity and necrotic foci (Maidment and Pilkington, 2000; Zülch, 1979). However, despite the grading, histologically benign brain tumours can be malignant if they grow in vital areas or increase intracranial pressure.

2.1.2.1 Gliomas

Gliomas comprise 46 % of all primary intracranial tumours, glioblastoma multiforme (GBM) being the most aggressive one (Levin et al., 2001). GBM accounts for about 47 % of all the gliomas. It has been reported to be the leading and fifth leading cause of cancer related deaths in men and women in the 20 – 39 age group, respectively (Jemal et al., 2003; Levin et al., 2001). This is despite the fact that primary brain tumours account for only two percent of all cases of cancer in the UK (Vincent and George, 2004). In Finland, 3.5 % of all cases of cancer originate from the central nervous system. Prognosis of high-grade glioma patients has remained poor despite the improvements in the treatment procedures. Their expected lifetime after diagnosis is approximately one year.

Table 2. The four grades of gliomas of astrocytic origin

Pilocytic astrocytoma, grade I
Astrocytoma, grade II
Anaplastic astrocytoma, grade III
Glioblastoma, grade IV

2.2 Therapies

2.2.1 Surgery

The first step in the conventional treatment of patients with malignant gliomas is surgery. With this procedure, the main objective is to remove the tumour, however most of the time it is also the only way to make a reliable diagnosis. For many malignant gliomas the operation is usually considered as a resection. This is because clear boundaries can not be seen between the tumour cells and the neighboring normal tissues. For this reason, the tumour is removed, if possible, with about two centimeter margins of neighboring tissues in order to minimize the probability of recurrence. Despite successful surgery the tumour invariably recurs locally with a median survival from initial diagnosis of about 3 – 4 months (Walker et al., 1978).

2.2.2 Radiotherapy

Due to the poor outcome of malignant glioma patients when treated alone with surgery, radiation therapy (RT) has been applied to kill the remaining tumour cells after surgery without inducing permanent damage in the healthy tissue (Holsti et al., 1992). With combining surgery and RT, the median survival time has been raised up to 9 to 12 months (Nieder et al., 2004; Walker et al., 1978). Earlier the volume of the tumour was considered as the most precise and most relevant predictor of the RT outcome (Dubben et al., 1998), but lately this has been observed not to be so straightforward. The efficacy of treatment has been found to depend on the oxygen concentration in the tissue, which in turn depends on the local blood supply (Griebel et al., 1997; Kallinowski et al., 1989a; Kallinowski et al., 1989b; Lyng et al., 2000; Vaupel et al., 1987). Therefore a poor vascular supply and hypoxia are critical factors contributing to radiation treatment characterized with a poor outcome (Gatenby et al., 1988). This also explains why hypoxic tumours have been found to require three times higher doses of radiation to be killed off (Gatenby et al., 1988).

Radiation has been delivered to tumours by a variety of methods. A routinely used type of RT is teletherapy, where the source of the radiation is outside the body. The radiation is directed either into the entire brain or locally into the tumour with 2 cm margins of normal tissue (Holsti et al., 1992). Variations of this technique have been developed for the more specific delivery of radiation into the target tissue. One of these is the so-called gamma knife radiosurgery. Here the radiation is applied stereotacticly into the tumour, making it possible to deliver high doses of radiation directly into the locally confined target, thereby spearing more of the healthy tissue (Chan et al., 2004; Mogard et al., 1994). It has also been proven possible to give different doses of radiation into different areas of the tumour with the highest amounts directed into the most aggressive parts. Another form of teletherapy used is fractionated RT, where the total amount of radiation is delivered to the patient in smaller quantities. Even though many variants of RT has been developed and the treatment time can be shortened, no prolongation effect have been found in survival time with any of these RT variants (Bese et al., 1998; Nieder et al., 2004).

In brachytherapy a source of radiation (usually ^{125}I) is placed temporarily, or in some cases permanently, into the tumour (Koot et al., 2000; Mayr et al., 2002). Radiation can be restricted inside the tumour without affecting the surrounding tissue by calculating the penetration range of the radioactive particles emitted by the source. Even though it could be presumed that brachytherapy may prolong survival time of patients with malignant glioma, it

has not redeemed the expectations placed upon it. For example, promising results have been achieved (Koot et al., 2000), but this has been proposed to be at least in part due to coincident factors such as patient selection. A study by Florell *et al.* (Florell et al., 1992) reported that patients eligible for brachytherapy were young, had large resections and were in good general health. Therefore, it is possible that the patients lived longer because of these factors and not because of any benefits derived from the therapy. Furthermore, in studies where the patients have been randomized, no survival improving effect have been obtained with interstitial boost of radiation in addition to conventional RT (Laperriere et al., 1998; Selker et al., 2002).

Computed tomography combined with positron emission tomography (CT/PET) are emerging as the method of choice in evaluating tumour heterogeneity prior to RT or monitoring effectiveness of this therapy (Beuthien-Baumann et al., 2003; Gatenby et al., 1988; Mogard et al., 1994; Tsuyuguchi et al., 2004). With the CT/PET method the macroscopic pattern of vascularity and the variation of metabolic activity in different parts of the tumour can be detected. This enables PET/CT scanning to be a valuable method in defining which tumour regions should receive higher radiation doses (Gross et al., 1998). These imaging techniques can also be employed post therapeutically to assess their effectiveness. For example, by using CT or MRI, the detection of radiation induced necrosis or tumour progression can be made. However, these techniques are limited by having to wait longer to assess a therapy's efficiency. Whereas with PET, in conjunction with a [^{18}F]Fluorodeoxyglucose tracer injection the distinction can be revealed sooner after therapy (Mogard et al., 1994), thereby aiding decision-making in the therapy planning process.

2.2.3 Chemotherapy

Despite developments in surgical and radiation therapies, the survival of glioma patients has remained poor. Chemotherapy is a method of treatment where specific chemical compounds are used to interfere with tumour cell growth and survival. These compounds achieve their effectiveness from their ability to alter the cell cycle or kill the cell. Both these rely on the fact that tumour derived cells are actively dividing, whereas normal brain cells mostly are not. Therefore, non-dividing cells are usually unaffected by chemotherapy. However, the success of the treatment depends on dividing rate of cancer cells and thus, fraction of cells in this phase of the cell cycle.

Adjuvant chemotherapy on top of normal surgery and RT regimes have been found to have a possible positive effect on the treatment of primary malignant glioma patients (Fine et al., 1993; Stenning et al., 1987). Different kinds of chemotherapy drugs and combinations have been developed and a diverse set of results has been obtained. The combination of procarbazine, lomustine and vincristine (PCV) has been found to be more efficient than treatment with carmustine (BCNU) alone, especially with anaplastic gliomas (Levin et al., 1990). However, in a meta-analysis performed from the published literature, adjuvant PCV treatment has shown not to have a survival benefit over plain RT regimes (Party, 2001). However, the combination of temozolomide (TMZ) with antiangiogenic agent thalidomide seems to be relatively well tolerated with favorable survival outcome (Chang et al., 2004). This is not true for all drug combinations. For instance, a study with combination of TMZ and tamoxifen was discontinued due to a low positive response rate and a high frequency of toxicity (Spence et al., 2004). On the other hand, the Glioma Meta-analysis Trialists (GMT) Group has recently made a wide meta-analysis from randomized trials that compared RT with RT plus chemotherapy. This group reported a significant prolongation of survival associated

with the receival of adjuvant chemotherapy (Stewart, 2002). The results of adjuvant chemotherapy therefore appear to be controversial, but there seems to be at least some advance in extending the patient's mean survival times compared to conventional treatment methods.

There have been efforts to enhance the outcome of the radiation and chemotherapeutic treatments. For example, by combining the chemotherapy drugs with radiosensitizing agents, drug delivery into the tumour is enhanced due to radiation induced changes in the microcirculation (Griebel et al., 1997).

2.2.4 Gene therapy

2.2.4.1 Cytotoxic gene therapy

Due to the continued poor prognosis of glioma patients treated with traditional methods illustrated above, there is an urgent need to develop alternative therapies. One of the experimental new methods is gene therapy, where genetic material is delivered to a tumour. This is done either to correct a defect or to prime the cell for destruction. For instance, the latter may be caused by predisposing glioma cells to a cytotoxic agent. Herpes Simplex viruses thymidine kinase gene (HSV-tk) – ganciclovir (GCV) combination is one of the first and most commonly used pro-drug activation protocols (Lam and Breakefield, 2001; Moolten, 1986). In this model therapy HSV-tk phosphorylates GCV into a nucleotide analogue, which in turn blocks the function of the DNA phosphorylase enzyme. This leads to the death of the cell through programmed cell death (PCD) (Poptani et al., 1998b). HSV-tk gene is transferred into the tumour cells by stable transduction with retroviruses. This permanently combines the gene into the cells genome (Ram et al., 1993; Vincent et al., 1996). Alternatively, transient transduction of the gene with adenoviruses or plasmid DNA can be used. In this case, the gene is placed in the nucleus as an episome (Chen et al., 1994; Nanda et al., 2001; Ram et al., 1993; Tyynelä et al., 2002; Vincent et al., 1996). With both of these *in vivo* transfection methods clear prolongation of life in animals has been observed, when compared to non-treated ones (Vincent et al., 1996). This technique has another advantage. It has been found that phosphorylated GCV spreads to cells not expressing HSV-tk through gap junctions and this explains why a substantial reduction in tumour size can be achieved with as little as 10 % of HSV-tk positive cells (Sandmair et al., 2000b). This phenomenon is known as a bystander effect (Dilber et al., 1997; Mesnil and Yamasaki, 2000; Namba et al., 1996; Rubsam et al., 1999). HSV-tk mediated gene therapy method has also been tested in clinical settings in combination with other methods. Although longer survival times have been achieved with this method, compared to conventional treatment methods (surgery, RT, chemotherapy), the total clearance of the tumour has not been reported and it recurs (Sandmair et al., 2000a; Trask et al., 2000). Recently, one of the first randomized and controlled clinical study was established, where clear prolongation of survival was achieved with adenovirus mediated HSV-tk gene therapy after primary or recurrent malignant glioma resection (Immonen et al., 2004). The adenovirus was administered directly into the healthy tissue of the wound bed after tumour resection, to reach the remaining malignant cells scattered in the normal brain tissue in the walls of resection cavity. The therapy was well tolerated, and the survival was significantly increased both in primary and recurrent groups of malignant glioma. Results were not influenced by prognostic factors as age, tumour type, histology nor Karnofsky score (Immonen et al., 2004). ONYX-015 is replicative, tumour selective, oncolytic, and mutated adenovirus, that was used by Chiocca *et al.* (Chiocca et al.,

2004) when studying the treatment of malignant glioma. Even though no definite anti tumour efficacy was observed in this trial, they showed the relative safety of injections of this virus into the normal brain tissue surrounding resected malignant gliomas (Chiocca et al., 2004).

Table 3. Viral delivery methods for gene therapy, modified from (Aguilar and Aguilar-Cordova, 2003)

Vehicle	Immunogenicity	Advantages	Disadvantages
Non-integrating			
Adenovirus	High	1. Large insert capacity 2. Efficient transduction of dividing & and non-dividing cells 3. Established production & characterization 4. Clinical experience 5. Relative stability	1. Potential for toxicity at high-doses, especially with intravascular delivery 2. Persistence limited by immune response
Herpes	High	1. Very large insert capacity 2. Efficient transduction of many cell types including nervous system 3. Potential for replication competent specificity	1. Production capacity limited 2. Recombination common & sequencing impractical 3. Limited clinical experience 4. Persistence limited by immune response
Integrating			
Onco-retroviral	Low	1. Moderate insert capacity 2. Established production & characterization 3. Clinical experience 4. Persistence	1. Transduction limited to dividing cells 2. Potential for insertional mutagenesis
Lentivirus	Low	1. Moderate insert capacity 2. Transduce dividing & non-dividing cells 3. Persistence	1. Safety concerns 2. No clinical experience 3. Un-proven production capacity
AAV	Low	1. Transduce dividing & non-dividing cells 2. Persistence 3. Limited clinical experience	1. Limited insert capacity 2. Production capacity limited

AAV = adeno-associated viruses

Other cytotoxic gene therapy methods have been developed and examined. One of them is the well characterized *Escherichia coli* cytosine deaminase/5-fluorocytosine (CD/5-FC) system

(Mullen et al., 1992b), where the prokaryotic specific CD enzyme converts non-toxic 5-FC to highly toxic compound 5-fluorouracil (5-FU). Since CD is not produced in mammalian cells, the toxicity of 5-FC is experienced only by the cells that have been transduced with the CD gene (Miller et al., 2002). This method has been observed to possess significant anti-tumour effects both *in vivo* and *in vitro*. This cytotoxic gene therapy model may have potential uses also in clinical settings as well (Ge et al., 1997; Miller et al., 2002). As with chemotherapeutic drugs, combinations of gene therapies have also been examined. For instance, Chang *et al.* have produced recombinant adenoviruses which have both, the HSV-tk and CD genes, in the same virus. The resulting cytotoxicity experienced by transduced C6 glioma cells in the presence of both GCV and 5-FC prodrugs was greater than with either drug alone (Chang et al., 2000). This indicates that it is possible to obtain even greater effects by combining different cytotoxic enhancement regimes.

Gadi *et al.* succeeded to inhibit the growth of a slowly growing (10 to 15 day doubling time) human glioma in mice by selectively releasing 6-methylpurine (MeP) in the tumour cells (Gadi et al., 2003). A single intraperitoneal (i.p.) injection of a prodrug was transformed to MeP in the glioma, stopped tumour growth and caused it to regress, indicating destruction of both dividing and non-dividing tumour cells. This was facilitated by the long intratumoral half-life of MeP and a bystander effect. In addition to the specific delivery techniques mentioned above, many other methods of prodrug mediated therapy of cancer have been developed. These are beyond the scope of this thesis but have been excellently reviewed by Aghi *et al.* (Aghi et al., 2000).

A further strategy for killing tumour cells has been developed, where the main focus is to trigger apoptotic cell death pathway in tumour cells. For example, the cell cycle can be modulated to obtain the correct conditions for the optimal efficacy of an apoptosis inducing drug (Darzynkiewicz, 1995). Alternatively, the cellular 'death' receptor 'Fas' can be up-regulated and thus increase apoptosis mediated by this receptor (Frankel et al., 2001). One big branch of this kind of therapy is focused on the reactivation of silenced tumour suppressor genes, such as p53. Inactivation or mutation of these genes have been found to be important factors in the development of human cancers (Hollstein et al., 1996; Hollstein et al., 1991; Lang et al., 1999; Levine et al., 1991). When a competent p53 gene was introduced into glioma cells containing mutant p53, apoptosis was induced. This however only works for cells containing mutant p53 gene. Glioma cells with a wild type p53 are resistant to p53-mediated apoptosis. However, these cells also die but it appears to occur by another route which involves an enhancement in their radiosensitivity (Lang et al., 1999; Shono et al., 2002). Conversely, the absence of p53 expression in cells leads to an increased resistance to irradiation and treatment with chemotherapeutic agents (Lowe and Lin, 2000a; Lowe et al., 1993). As Lowe *et al.* (Lowe and Lin, 2000a) summarized, there seems to be a strong correlation between the treatment outcome and the p53 status. This group states that in cancers, where the p53 gene is often mutated, tumours respond poorly to either radiation or chemotherapy. Consequently, in these tumour types, mutations in p53 have been found to correlate with poor prognosis. In contrast, in types of cancers where the mutated p53 is rare, this type of chemotherapy is effective.

2.2.4.2 Immunotherapy in gene therapy

Another direction in glioma treatment is immunotherapy. Glioma patients are often characterized by a depression in their immunity, a phenomenon utilized by gliomas for

increased survival and growth (Roszman et al., 1991; Tada and de Tribolet, 1993). The rationale behind immunotherapy is that boosts to the immune system (by inoculation or by introducing key components of the immune system) may induce the host body to 'reject' the tumour and destroy it. So far, the animal based models for this type of therapy have given positive results. For instance, Benedetti *et al.* have attempted to improve the immunity of the animals with inoculated gliomas by over-expressing interleukin 4 (IL-4) in the C6 glioblastoma of Sprague Dawley rats and the 9L glioblastoma of Fischer 344 rats. The study was successful in that it significantly prolonged the life of the animals and achieved the total disappearance of the tumour in a majority of the animals (Benedetti et al., 1999). A number of other cytokine-mediated therapies have been developed for the activation of immune system. These include interleukin-6 (Mullen et al., 1992a), interleukin-17 (Benchetrit et al., 2002), γ-interferon (Gansbacher et al., 1990), murine granulocyte-macrophage colony-stimulating factor (Dranoff et al., 1993) and tumour necrosis factor-α (Asher et al., 1991). Successful treatment outcomes have been achieved with these as well. Uhl *et al.* (Uhl et al., 2004) studied the use of transforming growth factor β receptor (TGF-βR) I kinase inhibitor SD-208 in treatment of glioma. The biological effects of TGF-β1 and TGF-β2 were blocked, resulting in an enhanced release of proinflammatory cytokines and a reduced release of the immunosuppressive cytokine IL-10. Migration and invasion of glioma cells were inhibited, and the median survival of glioma bearing mice was prolonged significantly. The therapeutic effect of SD-208 was proposed to be mediated by the promotion of an antiglioma immune response, as there was found to be an interrelation between the amount of tumour shrinkage observed and the degree of immune cell infiltration detected in histological specimens (Uhl et al., 2004). Based on these initial results, the prospect for the growth of the use of this branch of cancer therapy is good.

2.2.4.3 Antiangiogenic gene therapy for cancer

Neovascularization or angiogenesis is a general prerequisite for neoplasia and is especially intense and comprehensive in high grade malignancies, where it increases the potential of metastasis (Folkman and Shing, 1992; Jackson et al., 2002; Macchiarini et al., 1992). Actually, enhanced neovascularization is associated with increasing rate of metastasis (Weidner et al., 1993; Weidner et al., 1991). Therefore, gene therapy methods for cancer treatment have been developed, where the main aim is to block angiogenesis. This stems from the rationalisation that if new blood vessel formation into the tumour can be curtailed, the tumour will start to die, or at least be restrained because of a lack of nutrients and oxygen. Additionally as a consequence of this, the metastatic capacity of tumour will decline. That is because tumour cells will be unable to enter circulation and metastasize to distant sites of body because there are no blood vessels (Folkman and Shing, 1992). These reasons, therefore, make the inhibition of angiogenesis an attracting strategy for the treatment of cancers.

To date, over 40 endogenous inhibitors of angiogenesis have been characterized, thirteen of which have been employed in gene therapy models. All of these have shown antitumour activity in experimental animals, as recently reviewed by Feldman and Libutti (Feldman and Libutti, 2000). Fibroblast growth factors (FGF), vascular endothelial growth factor (VEGF) and transforming growth factor-β were some of the first cytokines found to have angiogenic properties. Compared to FGF, VEGF can be secreted from producer cells without harm, whereas FGF has to be passively released by cell lysis in conditions such as programmed cell death or damage associated with tissue injury (Conn et al., 1990). Furthermore, VEGF expression has been found to be induced by hypoxia in tumor cells *in vivo* and *in vitro* for the

induction of angiogenesis (Ikeda et al., 1995; Plate et al., 1992; Shweiki et al., 1992) therefore it is not surprising that, today, it is one of the most actively studied molecule in this regard, possessing restricted mitogenic activity towards vascular endothelial cells (Conn et al., 1990; Ferrara and Henzel, 1989). In high grade tumours expression of VEGF mRNA has been found to be higher than in the low grade ones, and it appears to be associated with increased necrotic area volumes (Plate et al., 1992).

There are several procedures for the inhibition of VEGF's angiogenic activity. These include: (1) the use of anti-VEGF monoclonal antibodies (Kim et al., 1993); (2) modified soluble VEGF receptor expression in glioma cells for binding to VEGF and preventing it from binding to it's naturally expressed receptor on the surface of the target cell (Goldman et al., 1998); (3) blocking VEGF receptor function by gene delivery of a dominant-negative receptor (Machein et al., 1999; Millauer et al., 1994) and (4) the inhibition of transcription of the VEGF gene (Im et al., 1999; Kang et al., 2000). These methods have given promising anti-angiogenic results and thus inhibit tumour growth. Today, some of these approaches have even advanced to the clinical trial stage of development (Feldman and Libutti, 2000). However, the treatment of brain tumours with gene therapy in clinical settings has not been as successful as could have been expected from the promising preclinical tumour models in rodents. This unfortunate discrepancy could be due to variety of differences that exist between human and rodent brain tumours. First of all, human brain tumours are much bigger than in rodents. Even though they are bigger, they grow slower. This means that there is higher percentage of dividing cells in rodent tumours, resulting greater transduction efficiency via retroviral vectors and higher sensitivity to drugs and vectors that are selective for DNA replication or cell cycling (Lam and Breakefield, 2001). Another issue is that human GBMs are associated with immune suppression and evasion, but rodent gliomas usually are antigenic even in syngeneic animals (Nitta et al., 1994). Finally, human gliomas tend to send out single invasive cells to considerable distance from the main tumour mass (Dalrymple et al., 1994), whereas rodent gliomas grow in a single mass with infiltrating fronds. In summary, it is clear that more research is required into optimizing gene therapy regimes for human gliomas.

2.3 Types of cell death

2.3.1 Apoptosis

Programmed cell death (PCD), often called apoptosis (Steller, 1995), is an active ATP - requiring process where the cell commits suicide in a strictly controlled manner, depending upon the presence or absence of a signal from the environment. It was originally characterized and named by Kerr *et al.* in the 1970's (Kerr et al., 1972). From their studies, they concluded that the structural changes take place in two discrete stages. In the first stage, apoptotic bodies are formed. These are of membrane bound, compact, but well preserved cell remnants, which are derived from the condensation of the fragmented nucleus and cytoplasm. In the subsequent phase, the apoptotic bodies are degraded and 'eaten' by neighboring cells or phagocytes. This whole process therefore results in the disappearance of the cell, without the induction of an inflammatory response. Apoptosis is a gene directed program, which has important roles in developmental biology, tissue homeostasis and immunology, affecting often scattered single cells rather than contiguous groups of cells (Wyllie et al., 1980). It also has to compete with other latent signals in the environment. For instance, cell numbers in organs are regulated not only by apoptosis but also factors influencing cell survival, proliferation and differentiation (Lowe and Lin, 2000a).

To date, there has been two major pathways described in mammalian cells that induce apoptotic cell death (Hengartner, 2000) (Fig. 1). In the death receptor pathway, the signal for the activation of apoptosis comes from outside the cell via stimulation of a member of the death receptor superfamily (such as CD95). In this pathway, binding of an appropriate ligand (i.e. CD95L) to the receptor on the membrane of the cell, activates a proteolytic cascade. Via Fas-associated death domain protein (FADD), caspase-8 (cystein protease 8) is activated, leading to the death of the cell by apoptosis. The other way of apoptotic cell death is mitochondrial pathway, which is used extensively to respond to both extracellular cues and internal insults such as DNA damage. These lead first to the activation of pro-apoptotic members of the Bcl-2 family, such as Bax, Bad, Bim and Bid. These in turn, cause the release of certain molecules from mitochondria, the principal of these being cytochrome c. This event causes the activation of a cascade of enzymes and the formation of an apoptosome. The mitochondrial and death receptor pathways converge at the level of caspase-3 activation, whose activation is essential for the death of the cell by apoptosis (Fig. 1) (Hengartner, 2000). Activation of caspases precede the morphological changes of the cells undergoing apoptosis (Blankenberg et al., 2000a). Additionally, during caspase activation, phosphatidylserine (PS) is presented to the surface of the cell. This event plays a role in informing the neighboring cells that the cell is apoptotic and is ready to be phagocytosed (Verhoven et al., 1995). After caspase activation and PS expression, the execution phase of apoptosis occurs. This includes condensation of the cytoplasm, DNA fragmentation and finally apoptotic body formation (Blankenberg et al., 2000b).

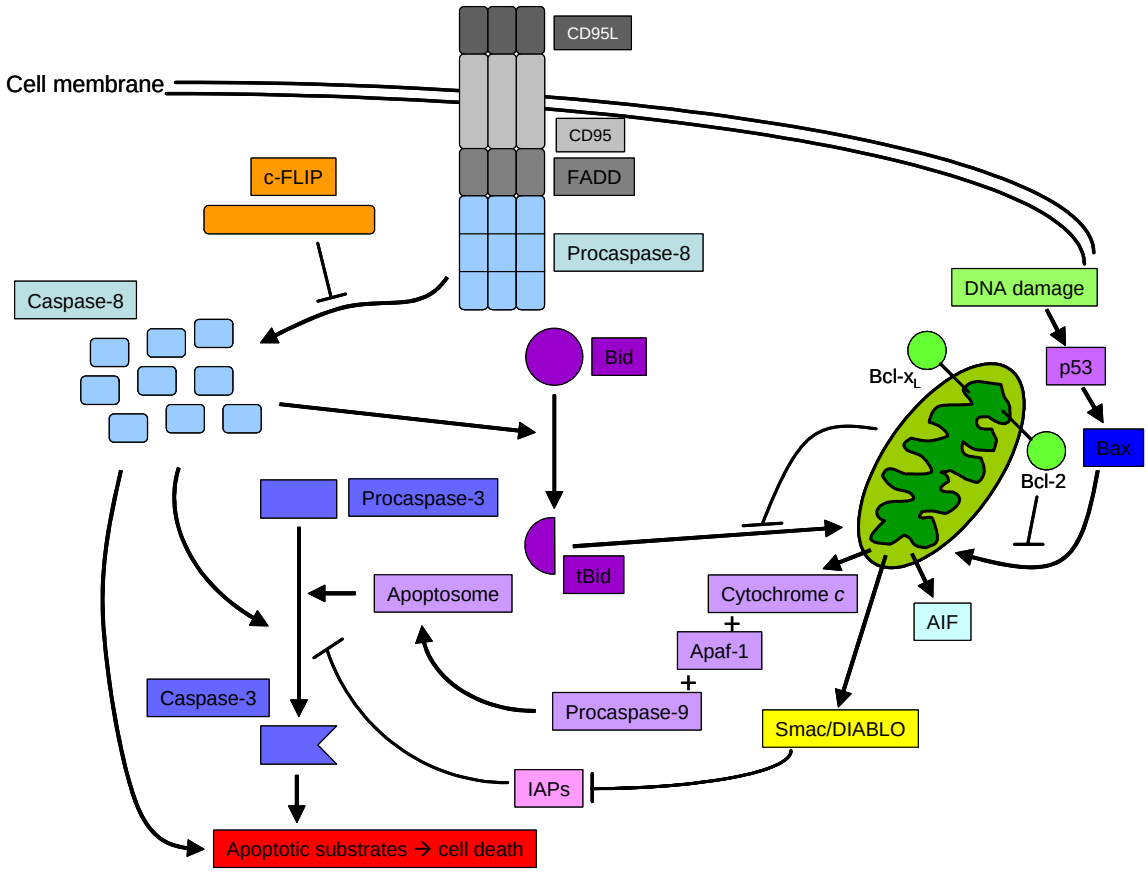

Figure 1. The two main apoptotic pathways of mammalian cells: the death receptor pathway and mitochondrial pathway. tBid = truncated Bid. Modified from (Hengartner, 2000).

2.3.2 Necrosis

Necrosis is a form of uncontrolled cell death, which usually is initiated when cells or tissues are exposed to acute insults such as toxins, hypoxia or ischemia, and physical injury. The first morphological marker indicating irreversible necrotic cell death, is the swelling of the matrix of mitochondria (Wyllie et al., 1980). Subsequent steps are the rupturing of the nuclear, organelle and plasma membranes, thus enabling extracellular fluid to enter the cell, causing it swell and finally burst (Escargueil-Blanc et al., 1994; Wyllie et al., 1980). All the harmful proteases and enzymes normally localized inside the lysosomes will now be floating free in the extracellular fluid, damaging the neighboring cells, often killing them too. This has the effect of spreading the inflammation process into the adjoining viable tissue. However, as in apoptosis, the cell remnants are eventually ingested and degradated by phagocytotic cells (Wyllie et al., 1980).

2.4 Principles of Nuclear Magnetic Resonance

Nuclear Magnetic Resonance (NMR) is a phenomenon that occurs when nuclei in a static magnetic field are exposed to a second oscillating magnetic field. For the generation of NMR, the nucleus has to possess a property known as spin, *I*. This spin is more precisely called (in quantum mechanical terms), a nuclear spin angular momentum. It comes about in the following way. If a nucleus has either an even atomic weight (number of protons and neutrons in nucleus) or even atomic number (number of protons), it possesses no spin ($I = 0$). Therefore, nuclei of this type will not interact with an external magnetic field and will be unobservable by NMR. However, if a nucleus has an even atomic weight and odd atomic number (e.g. $I = 1, 2, 3$), or an odd atomic number (e.g. $I = 1/2, 3/2, 5/2$), it will possesses a spin and can be detected. (Brown and Semelka, 1995; Gadian, 1995)

Nuclei with a spin ½ tend to have more favourable NMR characteristics for *in vivo* use than those with spin greater than ½. This together with the *in vivo* concentrations of any given biochemical compound and the natural abundance of isotopes, are the main reasons why most NMR studies of living systems use the nuclei of ^{1}H, ^{13}C and ^{31}P. In the future sections I have focused on ^{1}H, because it is the most abundant isotope of hydrogen (99,985 % natural abundance), and therefore water contains high concentration of it (Brown and Semelka, 1995; Gadian, 1995). Water, itself, is a focus of much attention in NMR studies since it is by far the most abundant molecule in the body.

A nucleus with a spin is viewed as a vector in the classical description of NMR. Here, nuclei have an axis of rotation with a specific orientation and magnitude. Each nucleus also has a magnetic property due to the spinning positive charge of the proton. In complex mixtures of organic molecules such as tissues, each proton has a spin vector of equal magnitude but have random orientations. This situation produces a zero net magnetization, because spin vectors in opposite directions cancel each others effects out. However, when the tissue is subjected to an external magnetic field (B_0), each proton will start to precess around the magnetic field. This occurs slightly tilted away from the axis of orientation, until the axis of rotation is parallel to the B_0 (the z direction). Rotation at the angular frequency occurs because of interaction of the magnetic field with the moving positive charge (the Zeeman interaction), and is proportional to the strength of the magnetic field as is expressed by the Larmor equation (Equation (1)).

$$\omega_0 = \gamma B_0 \qquad (1)$$

Where ω_0 is the Larmor frequency in MHz, B_0 is the magnetic field strength in Tesla (T), and γ (gyromagnetic ratio) is an inherent constant for each nucleus given in s^{-1} T^{-1}.

The protons have two different states of energy for spins: parallel and antiparallel to B_0, + ½ and – ½ respectively. The number of protons oriented parallel to B_0 exceeds the number of protons antiparallel, because the previous ones are in a lower energy state. The populations of these energy states are governed by the Boltzmann distribution in Equation (2).

$$n^- / n^+ = \exp(-\Delta E / kT) \qquad (2)$$

Where n^- and n^+ are the relative numbers of nuclei of the higher and lower energy levels (spins of - ½ and + ½ states, respectively), k is the Boltzmann constant, T is the temperature (in degrees of Kelvin) and ΔE is the energy difference between the two states, as given by Equation (3).

$$\Delta E = \gamma \hbar B_0 \qquad (3)$$

Where $\hbar$ is equal to $h/2\pi$, h being the Planck constant. From Eq. (3), it can be deduced that an increase in the magnitude of B_0, increases the energy difference between the adjacent states and hence the size of the difference in their populations (Eq. (2). As a result, higher magnetic field strengths are desirable because the higher magnetization yields a higher population difference and this improves the signal-to-noise ratio in the output data from *in vivo* NMR.

As described above, the number of protons of lower energy exceeds the number of higher energy and this means that the sum of the spin vectors will point parallel to the B_0 magnetic field. Thus, the net magnetization of the tissue (M_0) in an external magnetic field is oriented parallel to B_0, and will be constant over time. M_0 aligned along the magnetic field with no transverse components (in the xy plane), is the equilibrium state of protons with the lowest energy. Protons will always tend to return to this after any perturbation.

For the production of a NMR signal, the spins have to be moved away from the equilibrium configuration of lowest energy. When a proton is irradiated at the correct frequency (ω_0) by a radio frequency (RF) pulse, it will absorb energy. This absorption excites it from a lower energy state to a higher one. Additionally, if this energy is at the right frequency, it will cause M_0 to rotate away from its equilibrium orientation. Furthermore, if the RF pulse (also called the 90° pulse) is applied for long enough, at a high enough amplitude, the absorbed energy will cause M_0 to move entirely into the transverse plane (xy plane) with no magnetization along z axis. A net magnetization is now produced to the xy plane (M_{xy}), because the RF pulse has forced the individual magnetic moments of protons together which charactively possess phase coherence immediately after the 90° pulse. After the RF pulse is turned off, the individual nuclear spins will experience the B_0 field again and start to return to their equilibrium state and the phase coherence is lost. The net magnetization at the M_{xy} plane starts to rotate about B_0, again, and the protons will emit the extra energy at the Larmor frequency. This event can be captured as a current induced into a coil, tuned to the precession frequency, placed perpendicular to the transverse plane. This produces the NMR signal called free induction decay (FID). The FID is an induction signal as a function of time, from where the frequency distribution can be revealed by using a Fourier transformation algorithm (FT).

2.4.1 Spin-lattice relaxation, T_1

T_1 is defined as the time needed for the net M_0 to return to 63% of its original value after the excitation pulse. It is called a spin-lattice, or longitudinal relaxation time. This is because this process involves an exchange of energy between the nuclear spins and their molecular framework (the lattice). As mentioned above, after the 90° pulse there will be no longitudinal magnetization (along z axis). In T_1 relaxation, a return of the longitudinal magnetization will be observed, when the protons release their energy and return to equilibrium. The return of protons to equilibrium with the lattice is exponential and can be described by Equation (4).

$$\frac{dM_z}{dt} = \frac{M_0 - M_z}{T_1} \qquad (4)$$

This equation expresses the return of the magnetization M_z to its equilibrium value M_0 with a time constant T_1. After three T_1 periods, the net magnetization will be returned to 95% of the level prior to the excitation pulse, i.e. M_0.

An important factor governing the energy transfer from an excited proton to its surrounding, is the presence of molecular motion (e.g. vibration, rotation) in its vicinity. The frequency of the motion should be close to the Larmor frequency, to allow for the efficient transfer of energy. Consequently, the closer the frequencies are, the more rapidly the protons will return to their equilibrium configuration. In tissues, the frequency of the molecular vibrations of proteins is approximately 1 MHz. This means, that at lower B_0 the frequencies of the molecular motion and the ω_0 of spins will be closer. When this occurs, efficient energy transfer will occur and T_1 will be shorter, thus contributing to the observation that T_1 decreases with decreasing B_0. (Brown and Semelka, 1995; Gadian, 1995)

2.4.2 Spin-spin relaxation, T_2

T_2 relaxation is a process where the transverse magnetization is lost, a phenomenon also called spin-spin or transverse relaxation. This type of energy transfer from an excited proton to another nearby proton is called spin-spin relaxation, differing from T_1 in regard to the absence of an energy exchange with the lattice. After a 90° pulse is applied, all of the protons have absorbed energy and are subsequently oriented in the transverse plane. Additionally, they rotate at the same frequency (ω_0) and are synchronized at the same point or phase of the rotational cycle. Since nearby protons of the same type will experience the same type of environment and rotate at the same frequency, they will absorb the energy released by other protons in the vicinity. Energy transfer will also continue to happen as long as the protons are in close proximity to each other and rotate at the same frequency. If an irreversible loss of phase coherence occurs while the energy is being exchanged, the magnitude of the transverse relaxation is reduced. This event can be detected in the same way as with spin-lattice relaxation.

T_2 is defined as the time when the transverse magnetization (M_{xy}) value is 37% of its maximum, observed right after the 90° pulse and the irreversible spin-spin relaxation is the only cause for the loss of the phase coherence. Equation (5) expresses the exponential decay of the M_{xy} magnetization to zero with a time constant T_2:

$$\frac{dM_{xy}}{dt} = -\frac{M_{xy}}{T_2} \qquad (5)$$

It is important to note that T_2 will always be less or equal to T_1, because all processes that influence the spin-lattice relaxation affect the spin-spin relaxation as well.

The reasons for the decay of transverse coherence of protons can be several. However, the movement of the adjacent spins due to molecular motion is responsible for the true T_2 relaxation. Another factor of great significance for spin-spin relaxation is the field inhomogeneity. This phenomenon causes changes in Larmor frequency and subsequently a loss in the transverse phase coherence.

2.5 In vivo applications of NMR

2.5.1 Magnetic Resonance Imaging

The frequency of energy, at which a proton absorbs and reemits RF energies, is determined by the field strength it experiences. In magnetic resonance imaging (MRI) this field dependency is exploited to localize proton frequencies in different parts of space. To achieve this goal, small perturbations are induced into the main magnetic field B_0 by gradient pulses, which elicit distortions that are typically less much than 1% of the main field strength. In addition, three gradients are used in imaging, one each for the x, y and z directions. This gives coordinates for the position of the protons in the three dimensions. During a field gradient pulse, each proton resonates at an unique frequency that depends on its exact position. The MR image itself, is simply a frequency map of protons that is generated through the unique magnetic field strengths observed at each point throughout the image. The intensity of the visual picture element (pixel) is proportional to the number of protons contained within the volume element (voxel). Since the quantity of protons found is weighted by the T_1 and T_2 relaxation times of the tissues in the voxel, this enables the retrieval of information regarding the nature of the tissue. (Brown and Semelka, 1995)

Many recent technical modifications have improved the resolution of MRI. In 1986, MR microscopy was able to produce images from biological tissues at the cellular level (frog ovum cell, around 1 mm in diameter) in which the cell nucleus and cytoplasm were distinguishable (Aguayo et al., 1986). After this groundbreaking study, other studies have been carried out with plant and animal cells. For example, in 1995 a study was performed on the L7 neuron isolated from the sea hare *Aplysia californica*. This is still a relatively large cell (≈ 300 μm in diameter) but it indicates that neurons could be visualized with MR successfully. For a good review of the other studies please refer to ref. (Blackband et al., 1999).

2.5.1.1 T_1 contrast

Since water protons have different T_1 relaxation properties in different tissues, this forms the basis for the use of T_1 contrast MR imaging in oncology. The most often used method for the generation of T_1 contrasts is based on the inversion recovery sequence. This is implemented as follows. An inversion recovery pulse can be incorporated as a module virtually into any

imaging or spectroscopy sequence to produce the T_1 weighting of the scans. If a 180 ° pulse is now applied, it results in the inversion of magnetization relative to the -z axis. This is followed by a gradual recovery of the magnetization back to +z axis according to a time constant T_1. However, since magnetization in the z axis is undetectable, a 90° read-pulse is applied after a given inversion time (TI) to tilt the recovered magnetization into the MR readable xy plane. The NMR signal is then collected and the recovery of the longitudinal relaxation can be monitored, by varying the TI value. Therefore, T_1 can be determined by repeating the measurement with different TIs and fitting the signal intensity to Equation (6).

$$M_t = M_0\left(1 - 2\exp\left(-TI / T_1\right)\right) \quad (6)$$

Where M_0 is the net magnetization obtained at the equilibrium. The factor 2 in Eq. (6) derives from the fully inverted magnetization imposed by the 180^o inversion pulse.

2.5.1.2 T_2 contrast

Carr and Purcell were the first to introduce the so called spin echo sequence in 1954 (Carr and Purcell, 1954). It is widely used in imaging and spectroscopy, and it generates signals that are weighted according to the T_2 relaxation. In its simplest form, the 90° pulse is followed by a 180° pulse, after a time of TE/2. In this case, the echo signal is generated after another TE/2 has elapsed. Not all of the spins can be refocused by the 180° pulse, due to the diffusion of molecules. This causes the amplitude of the echo to diminish by a factor e^{-TE/T_2}. T_2 can be evaluated from the measurements of the echo intensities obtained from a range of different TE values. (Gadian, 1995)

The signal loss resulting from the translational diffusion of protons in T_2 measurements can be reduced by a sequence generated by Carr and Purcell in 1954 (Carr-Purcell T_2, CP-T_2 sequence). They found that, when they combined a 90° pulse with a train of 180° pulses during the time of TE, the effect of dynamic dephasing regime can be reduced. Dynamic dephasing is derived from the exchange and/or diffusion of spins between regions with different magnetic fields. By decreasing the interpulse interval time τ_{CP} between the 180° pulses, the effects of dynamic dephasing regime can be reduced. Each 180° pulse generates an echo and if each signal was detected midway between pulses, a train of echoes would be observed. (Bartha et al., 2002b; Gadian, 1995)

The apparent transverse relaxation time ($T_2^{\dagger}$) is related to the intrinsic transverse relaxation time ($T_{2,\,Intrinsic}$) through Equation (7).

$$\frac{1}{T_2^{\dagger}} = \frac{1}{T_{2,Intrinsic}} + \frac{1}{T_{2,Diffusion}} + \frac{1}{T_{2,Exchange}} \quad (7)$$

The term $T_{2,\,Intrinsic}$ is affected by various phenomenons. These include (i) (homonuclear) dipole-dipole interactions between protons; (ii) contact interactions, where the change in the transverse relaxation time is due to an interaction with a paramagnetic center and (iii) cross-relaxations, which can be significant in dipole-coupled systems. $T_{2,\,Diffusion}$ is a term, where the transverse relaxation time is determined by the diffusion of molecules and the $T_{2,\,Exchange}$ term is determined by the exchange of spins between regions with different magnetic properties.

The dynamic dephasing regime, where the net magnetization is reduced by the diffusion and exchange between regions with different magnetic field strengths, is described by the parameters mentioned above.

By decreasing the time interval between the 180° pulses (τ_{CP}), the effect of the translational diffusion of molecules can be reduced and the pulse sequence becomes more governed by the dipolar relaxation processes. *In vitro* and *in vivo* studies have successfully used the CP-T_2 sequence, or its modifications, to study the mechanisms of transverse relaxation and to improve MRI contrast (Bartha et al., 2002a; Bryant et al., 1990; Michaeli et al., 2002; Ye et al., 1996).

2.5.1.3 $T_{1\rho}$ contrast

In a $T_{1\rho}$ MRI experiment, a 90° pulse is used to tilt the magnetization into the x axis. Immediately after the 90° pulse, a continuous RF pulse, often referred to as the spin lock pulse, is applied with a 90° phase shift relative to the previous 90° pulse. This effectively 'locks' the spins of the nuclei into the xy plane. When this occurs, there is no net magnetization orthogonal to the spin lock pulse. Subsequently, the relaxation of the locked magnetization proceeds along the locking field with a time constant $T_{1\rho}$. After termination of the spin lock pulse, the magnetization that relaxes back to the z axis is read with any standard NMR sequence to generate the FID (Santyr et al., 1989).

The $T_{1\rho}$ relaxation time constant is determined by collecting the FID after the spin lock pulse is applied for varying lengths of time. The intensity of the measured magnetization can be derived from Equation (8), where TSL refers to the duration of the spin lock pulse.

$$M_t = M_0 \exp\left(-TSL / T_{1\rho}\right) \qquad (8)$$

2.5.1.4 Diffusion contrast for MRI

Molecular diffusion is a consequence derived from the random thermal, Brownian, motion of molecules, with small displacement distances. In an unrestricted situation, in 100 ms, water molecules will diffuse up to 20 μm in any possible direction. However, in a tissue, cell membrane and organelles restrict the movement of water molecules. This phenomenon can be used for probing cellular integrity and pathology, because these processes might alter the cellular environment and hence alter the observed diffusion distances. (Gadian, 1995) This makes these events detectable by NMR.

In diffusion weighted imaging (DWI), two strong gradient pulses are integrated into the standard spin echo sequence, thus making the images sensitive to the water displacements derived from the diffusion of molecules. The first gradient pulse is placed between the 90° and 180° pulses, and the second is inserted after the 180° pulse but before the echo signal. The first gradient pulse dephases the protons and causes a diminishment in the magnitude of M_{xy}. In the situation where the nuclei are stationary during the period of TE, the rephasing effect of the second gradient pulse will cancel out the effect of the first pulse. Consequently, the nuclei will end up in phase at the time of the echo with no loss of signal, other than that

derived from the intrinsic relaxation effects. However, where molecular diffusion occurs, each proton would experience different field strengths during the second pulsed gradient compared to that which they experienced during the first one. Here there would be no complete rephasing and loss of signal would be discovered due to the random phase shifts of the water protons. These phase shifts results from the translational motion of the ^{1}H nuclei along the direction of the field gradients (Gadian, 1995).

The signal attenuation due to diffusion is related to the gradient strength and its duration, as well as to the diffusion time. Equation (9) describes how the echo signal is attenuated.

$$A = \exp(-bD) \qquad (9)$$

Where D is the diffusion coefficient. The b-term (or b-value), is determined by the gradient strength and timing, and can be derived using Equation (10).

$$b = \gamma^2 \delta^2 G^2 (\Delta - \delta / 3) \qquad (10)$$

Here, γ is the gyromagnetic ratio, δ and G are the duration and amplitude of the diffusion-sensitizing gradient pulses, and Δ is the time interval between the leading edges of these pulses. The parameter (Δ-δ/3) is often referred as to the diffusion time, t_D. (Gadian, 1995; Nicolay et al., 1995)

The signal intensity (SI) of a voxel of tissue can be calculated using Equation (11) (see also reference (Schaefer et al., 2000a)).

$$SI = SI_0 \times \exp(-b \times D) \qquad (11)$$

In this equation, SI_0 refers to the signal intensity on the T_2 weighted (or $b \cong 0$ s/mm^2) image. The DW image has T_2 weighted contrast as well as contrast due to diffusion, which obstructs the detection of areas with increased diffusion. Reducing the effect of the T_2 relaxation from the DW image can be done, either by dividing DW images with an image, where the $b \cong 0$ sec/mm^2, or an apparent diffusion coefficient (ADC) map could be created (Schaefer et al., 2000b). The ADC method is used instead of D when studying the diffusivity of a molecule in a tissue, due to the heterogeneity therein. The movement of a molecule from one place to another is not straightforward in tissues, but in MR imaging the increased distance travelled is not taken into account. Therefore, only the ADC can be calculated, when measuring molecular motion with DWI (Schaefer et al., 2000b). The ADC map is calculated from absolute DW images, where the signal intensity is equal to the magnitude of the ADC. The signal intensity in a DW image is expressed by Equation (12).

$$SI = SI_0 \times \exp(-b \times ADC) \qquad (12)$$

As mentioned above, in tissues the movement of the water molecules is not isotropic. This can be due to the microscopic structure of tissues such as different kinds of cells and subcellular compositions. Biochemical parameters in different places of the tissue also contribute to the water anisotropy found in biological samples *in vivo*. Examples of these biophysical parameters include concentration, pressure and thermal gradients as well as ionic interactions. In the brain, for example, there are neurones, which along with their myelinated axons compose a neural network. The remaining space is taken up by other cell types (e.g.

glial cells), blood vessels and the fluid filled ventricles. This means that the brain tissue is highly anisotropic, as recently observed (Mori et al., 2002), and consequently the true movement of the molecules can not be found out when measured only from one direction. The orientation dependency of DWI complicates the comparison of data between different measurements. Therefore, an orientation unbiased method, the measurement of the trace of the diffusion tensor $D_{av} = 1/3 Trace\overline{\overline{D}} = 1/3\left(D_{xx} + D_{yy} + D_{zz}\right)$, has been developed to study the diffusion of water in anisotropic systems (Clark et al., 2002; Mori and van Zijl, 1995; Zhang et al., 2003). Mori and van Zijl presented a method, where the trace of the diffusion tensor can be measured within a single scan (Mori and van Zijl, 1995). They used series of bipolar gradients to measure D_{av} in a single scan, to produce diffusion images independent from the orientation of the patient relative to the gradient pulses. This is important, as individually measured diffusion constants can vary as much as a factor of two or three depending on the relative orientation of the diffusion gradients and the subject (van Zijl et al., 1994).

2.5.2 NMR spectroscopy

A molecule in the presence of a static magnetic field B_0, resonates at a given frequency, which is directly proportional to the local magnetic field it experiences. However, different molecules do not resonate at the same frequency because of their difference in chemical structures. These events can be observed by NMR spectroscopy (MRS). Different compounds produce different kinds of small magnetic fields inside B_0 due to the differences in their electronic environment. Subsequently, the total effective field (B_{eff}) at the nucleus can be written as Equation (13).

$$B_{eff} = B_0(1-\sigma) \qquad (13)$$

In this equation, σ represents the contribution of a small secondary field generated by electrons and is known as the shielding constant. Since the B_{eff} associated with each chemical group is different, this gives rise to signals at different frequencies. The separation of resonance frequencies from an arbitrarily chosen reference frequency is called the chemical shift, which is expressed in terms of dimensionless units of parts per million (ppm). The secondary fields are very small in comparison with the applied field, when the absolute spread in frequency is also small. As a consequence of this, it could be difficult to separate the various resonances. However, an improvement in the resolution of the data can be achieved by increasing the magnitude of B_0, since the frequency separation of the resonances is proportional to B_0. (Gadian, 1995)

This entire phenomenon is possible because the secondary magnetic fields induced by the motion of electrons, opposes the applied magnetic field B_0 and 'shields' the nucleus. This means that nuclei experience a smaller magnetic field than the one really applied. Consequently a resonance at specific frequency is formed. This phenomenon is also regulated by the size of the charge surrounding the nucleus. Therefore, the higher the electronic density around the nucleus, the lower the resonance frequency will be. Shielding can also be affected by the electronegativity of adjacent nuclei. This occurs where a more electronegative atom attracts the shield of electrons of another nucleus towards itself. This situation is exemplified by the case of a water molecule, where the oxygen atom pulls electrons towards itself. Finally, the motion of electrons from other molecules or groups of atoms in the vicinity of a nucleus, can also affect the amount of shielding that occurs. This is dependent on the condition that the

motion of the electrons of the other nuclei differs from the orientation of the molecule in the applied field.

The total number of peaks in a spectrum is affected by a phenomenon called spin-spin coupling. This happens between two nuclei, providing that they both have spins of ½, and the participating nuclei are covalently bonded together and separated by one or more bond. It is also not restricted interactions between nuclei of the same type (i.e. homonuclear) but can also develop between different species of nuclei (i.e. heteronuclear). Examples of these spin-spin interactions are the observed ^{13}C-^{1}H and ^{1}H-C-C-^{1}H specific coupling patterns. As a consequence of this coupling, any one nucleus will produce two peaks in spectra instead of one, when coupled with another nucleus. The separation of these two peaks is known as a spin-spin coupling constant (J_{XX}), which is a characteristic to particular molecule. It is independent of the applied magnetic field and is expressed in Hz. Spectra can become very complex quickly, because each pair of magnetic nuclei within a molecule produces a coupling. Nevertheless, these are very informative and it is even possible to determine the chemical structures of molecules by studying the patterns of coupling. (Gadian, 1995)

In summary, ^{1}H NMR spectroscopy is an excellent method for investigating not only molecules, but also their chemical structure and behavior in different micro-environments *in vivo*. From this, important information regarding the status of a tissue can be determined and matched with the existing biochemical knowledge of the tissue. It has been also applied widely to clinical studies, where it has shown its significance when evaluating the state of a tumour after treatment or assessing the level of damage after a stroke (Chenevert et al., 2000; Mardor et al., 2003).

2.5.2.1 Diffusion NMR spectroscopy

To utilise the occurrence of diffusion within *in vivo* NMR spectroscopy, the goal is to study the diffusivity of water and individual metabolites. This is made possible by the fact that diffusion spectroscopy measurements are sensitive to factors that are directly related to the architecture of cells and tissues. With this method, the evaluation of the physico-chemical properties of metabolites within cells and tissues can be made to reveal possible alterations therein. These changes can be caused by a variety of processes, including developmental, pathological or therapeutical changes amongst others. The ADCs of metabolites can be measured the same way as is done with water molecules. Furthermore, modifications can also be made to MRS sequences, so as to suppress unwanted resonances that interfere with the detection of the resonance of interest. For example Sotak *et al.* filtered out the signal derived from lipids at 1.3 ppm which overlaps the lactate (Lac) peak, when they were studying the diffusion of that biochemical in tumours (Sotak, 1988).

This method is not without its difficulties. For example, metabolite diffusion measurements are more demanding than water diffusion measurements, because the concentrations of the chemicals are only a fraction of that of water. In addition, the metabolite diffusivity is substantially slower than that of water. This means that higher gradient amplitudes and/or longer diffusion times are required to achieve sufficient diffusion-dependent signal attenuation in the time regime (Nicolay et al., 2001).

2.5.3 Magic angle spinning NMR spectroscopy in biological specimens

Tissue structure is highly organized and this restricts the motion and orientation of water protons. This causes three principle problems. There are a) intermolecular dipole-dipole interactions that shorten the T_2 relaxation time, b) chemical shift anisotropy and c) magnetic susceptibility, which causes a broadening of the spectral lines and a decrease in the signal intensity. These problems and their solutions are discussed next, in detail.

It has been observed that the orientation of the tissue, in relation to a constant B_0 magnetic field, affects the signal intensity by phenomenon arising from dipole-dipole interaction of different molecules. Therefore, in tissues, which resemble solids in consequence of molecular interaction and movement, it can be assumed that the dipolar interaction between two nuclei can be described by Equation (14).

$$3\cos^2\theta - 1 \qquad (14)$$

Here, θ is the angle between the static magnetic field and the internuclear vector. When $3\cos^2\theta - 1 = 0$, the dipolar interaction disappears. This so-called 'magic angle' condition is satisfied when the θ equals 54,74°. When the samples are rotated along an axis at this angle in relation to the B_0 magnetic field, the dipolar interactions disappear. Spectral resolution can also be improved significantly by reducing (i) the chemical shift anisotropy, (ii) the local susceptibility gradients near intracellular and extracellular structures (Weybright et al., 1998) and (iii) the residual dipolar interactions in heterogeneous solid-like biological samples (Cheng et al., 1996a; Cheng et al., 1997; Erickson et al., 1993). One of the first articles reviewing both the development of MAS and the improved spectral resolution of MAS compared to the conventional non-spinning system by Andrew in 1971 (Andrew, 1971). Nowadays, MAS has been successfully used *in vitro* (Chen et al., 2002; Weybright et al., 1998) and *ex vivo* (Bollard et al., 2003; Cheng et al., 1998; Cheng et al., 1996b; Griffin et al., 2000; Millis et al., 1997), revealing the metabolic profiles of studied samples as well as changes therein brought about by, for example, treatments.

2.6 Applications of NMR techniques in the field of oncology

2.6.1 MRI

MRI has been widely used in clinics to distinguish tissues and to visualize malformations and tumours in the body. MRI provides better soft-tissue contrast than plain radiography or CT, because the variations in T_1 and T_2 relaxation properties of tissues are much greater than variations in the density of the tissue. The success of MRI has also increased due to its non-invasive nature and its independence from the use of radioactive tracers. Additional freedom of measurement with this technique is also derived from the fact that images can be taken in any direction and from any part of the body (Edelman and Warach, 1993).

Therefore it is not surprising that the MRI has become an important part of clinical care in oncology. For example, the place and size of the tumours can be seen accurately, and the success of a treatment can be easily followed during and after the treatment. The reaction of the tumour to the treatment protocol can be usually observed by studying the T_1 and T_2 contrasts, often referred to as conventional MRI. With this technique, quantitative changes are

noticed even before other parameters, such as decreased tumour volumes become latent (Evelhoch et al., 2000; Hakumäki et al., 2002; Poptani et al., 1998b).

2.6.2 The use of DWI in oncology

Even though the volume of the tumour can, in most cases, be seen with conventional MRI, it does not always show the precise margins and the nature of it. New methods have been developed to overcome this problem. In particular, the possibilities of DWI have been exploited owing to its documented use in the detection of acute stroke (Kucharczyk et al., 1991). DWI can observe ischemic brain tissue within minutes of onset, when the characteristic decrease of ADC in the first stages of ischemia is observed. This is caused by several ischemia-induced tissue changes, including energy failure and the influx of extracellular water into the cells. Therefore, DWI has become a widely used and important method in clinical settings for imaging stroke, where it aids the making of appropriate diagnostic and treatment decisions (Huisman, 2003; Kucharczyk et al., 1991; Roberts and Rowley, 2003; Schaefer et al., 2000a).

The possibilities of DWI in cancer research has been studied widely with experimental tumour models (Chenevert et al., 1997; Chenevert et al., 2000; Hakumäki et al., 1998; Kauppinen, 2002) and in clinical settings (Castillo et al., 2001; Chenevert et al., 2000; Hein et al., 2003; Maier et al., 2001; Mardor et al., 2003). As far as the outcome of a treatment of tumours is concerned, ADC has been found to be inversely correlated to the cell density (Gauvain et al., 2001; Gupta et al., 2000; Kono et al., 2001; Sugahara et al., 1999), as well as to the concentration of choline containing compounds (tCho) (Gupta et al., 2000; Gupta et al., 1999). Increases in ADC during successful treatment is also associated with decreases in cell density (Chenevert et al., 2000; Mardor et al., 2001) or to increase in the extracellular volume due to the cell shrinkage (Galons et al., 1999). It additionally has been found to decrease due to recurrent tumour growth (Chenevert et al., 1997). However, to date, no correlation between the ADC value and grade of the tumour has been found (Lam et al., 2002).

DWI has proven its value in cancer research as well as in stroke, revealing the positive reaction of the tumour to the treatment substantially earlier than can be seen with the T_1 and T_2 weighted MRI, as discussed in the previous section (Chenevert et al., 1997; Chenevert et al., 2000). Therefore, when considering the treatment procedures, the decisions to alter the treatment protocol can be made substantially earlier (Mardor et al., 2001). Due to its wide availability around the world and the promising early results in clinical settings, DWI has become a valuable method in the field of cancer research.

2.6.3 Perfusion imaging

In order to meet the energy and oxygen metabolism of a tumour, new blood vessels and capillaries are formed inside of it. This angiogenic phenomenon is considered essential for cancer growth. In this light, several studies have been made by using the perfusion imaging NMR method to examine the cerebral blood volume (CBV) of brain tumours in order to reveal the extent and the state of the blood vessels (Cha et al., 2003). The basis of this method is related to the nature of the capillaries within the tumours. Within a tumour, the capillaries are newly formed and the epithelial cells have not yet formed tight connections between each other and this makes the capillary walls leaky. This leakiness can be utilised to allow the entry

of contrast agents into the tissue from the capillaries, a phenomenon that has been utilized in perfusion imaging. In the normal brain tissue, the blood brain barrier (BBB) highly regulates the molecules that can shift from the blood to the brain tissue and is therefore less detectable by perfusion imaging. Leaky BBB is characteristic to a tumour, establishing a way to characterize the nature and the state of the blood vessels therein. Tofts and Kermode (Tofts and Kermode, 1991) have presented a model for the quantification of BBB permeability and leakage space, that are very important and useful parameters in the study of conditions where BBB is disturbed. In this way physiological variables can be measured in an objective, reproducible and non-invasive way, and achieved results which are not dependent on intra- or inter-patient variations in the blood contrast agent concentrations. Reliable quantification procedures have an important role in studying patients in the clinics, understanding disease process, and evaluating the effectiveness of new treatments (Evelhoch et al., 2004; Tofts, 1997).

Contrast agent perfusion MRI of tumours has been widely used in clinical settings. By using this method, it has been found that increased malignancy is associated with increases in the CBV (Aronen et al., 1994; Jackson et al., 2002; Law et al., 2003; Preul et al., 2003). Aronen *et al.* (Aronen et al., 1994) have even managed to reveal areas of probable malignant dedifferentiation in a tumour by finding areas of high CBV from nonenhanced region of the tumour in the conventional MRI (after injection of a gadolinium based contrast agent). They also demonstrated the ability of perfusion measurements to reveal the high heterogeneity of the tumours and high CBV values therein. This phenomenon was also noticed by Preul *et al.* (Preul et al., 2003) in a high grade brain tumour.

Recently a study was made with glioblastomas, where an inverse relationship between the size of the tumour and CBV was found (Principi et al., 2003). This result was associated with necrosis, a well known phenomenon described in glioblastomas. Necrosis occurs in very malignant gliomas because the growth is so fast that the microvasculature can not meet the demands placed upon it by the tumour for nutrients and oxygen, creating conditions for ischemic necrosis. Therefore, they found out that lower CBV values were related to higher levels of necrosis in tumours. In support of this view, another study revealed that the density of microvessels was higher in the rim section of the tumour. Furthermore, the density of these vessels decreased towards the core of the tumour, where the necrosis was more abundant (Sun et al., 2004). Finally, they also found that the microvessel density was higher in the normal tissue compared to the tumour. This last finding is in contrast to the common assumption and many other studies. However, this phenomenon has also been reported by Silva *et al.* (Silva et al., 2000).

This MRI method has also been used to predict when to use RT as well as the effects of this treatment. A study has been made where perfusion imaging has been found to predict the outcome of a radiotherapy: Griebel *et al.* found that better responses to the treatment were related to higher initial tumour perfusion (Griebel et al., 1997). It has also been reported that better outcomes of the treatment were associated to higher reductions in blood volume (compared to the initial values) after RT, in the tumour (Hawighorst et al., 1997; Hawighorst et al., 1998).

Therefore according to the available evidence described above, contrast agent perfusion imaging appears to be a very promising tool in which to investigate the nature of the tumours at the level of the state of the BBB and capillaries. The data derived from the use of this

technique can be used in determining the correct kind of treatment for the individual patient as well as aiding the assessment and development of new anticancer drugs.

2.6.4 ^{1}H magnetic resonance spectroscopy

^{1}H MRS has been used to study brain tumours in more detail, where the goal is to monitor metabolic changes associated with malignancy as well as the 'metabolite phenotypes' of tumours (Ala-Korpela et al., 1996). It is a novel method of NMR that has had an important role in studying and characterizing normal and diseased brain *in vivo* (Ross and Bluml, 2001). In the use of MRS of the brain *in vivo*, the main parameters examined have been the spectral peaks derived from tCho, N-acetyl-aspartate (NAA) and creatine (Cr, comprising from creatine and phosphocreatine). These compounds were chosen on the basis of differing criteria. Choline containing compounds are almost exclusively located in the plasma membranes of a cell and therefore disturbances in these may indicate pathology associated membranes changes. On the other hand, NAA is used because it's exclusive association with neurons and therefore is considered as marker for this type of cell. Finally, Cr is used as a marker for metabolic activity because it was thought that it is a reliable marker for the energy status of a cell. Since this is an important method, the details of its use in various studies will be described next.

It has been found that the amount of tCho is higher in tumours than in normal brain tissue (Howe et al., 2003; Isobe et al., 2002; Negendank et al., 1996; Utriainen et al., 2003). In addition, this measurement has also a linear correlation with cell density (Gupta et al., 2000; Miller et al., 1996; Nafe et al., 2003) and the increase in the amount of tCho in tumours is due to the higher density of cells. NAA levels, on the other hand, are reduced because tumour cells replace normal brain tissue and thus decreases the numbers of neurons (Negendank et al., 1996). However, a discrepancy from the above results was obtained by Usenius *et al.* This group found no differences in the absolute choline concentration between astrocytomas and normal white matter *in vivo*, a result verified by their *in vitro* studies (Usenius et al., 1994b). It has been found in multiple studies that Cr concentrations are lower in gliomas compared to normal brain tissue (Gill et al., 1990; Howe et al., 2003; Isobe et al., 2002; Negendank et al., 1996; Rémy et al., 1994). The levels of Cr are kept relatively constant in the normal brain (Murphy et al., 2002), but a decline as a function of reduced cell density in a rat glioma model has been observed (**III)**. Consequently, the levels of Cr can be used as an internal reference for the calculation of specific metabolic concentrations within a sample.

Chemical specific spectra for these chemicals, obtained by ^{1}H MRS, have also been used to monitor responses to conventional glioma therapies. From these studies, it has been shown that after efficient RT, that has been shown to lead to extensive apoptosis (Thompson, 1995), the level of tCho decreases (Kizu et al., 1998; Nelson et al., 1999; Vigneron et al., 2001). However, in the case of poor RT, the concentration of tCho remains stable or increases even further. These individual parameters can also be combined to further increase the predictive purpose of the results. When the data derived from tCho, NAA and Cr were combined, in various studies from individual patients, the differentiation between active (possibly recurrent) tumours, necrotic tumours and normal brain tissue was possible (Dowling et al., 2001; Kizu et al., 1998; Nelson et al., 1997; Schlemmer et al., 2002; Schlemmer et al., 2001; Taylor et al., 1996; Vigneron et al., 2001). This makes MRS an useful extension to a conventional MRI in predicting the active area of the tumour (Croteau et al., 2001; Pirzkall et

al., 2001; Pirzkall et al., 2002; Wald et al., 1997) and quantifying the degree of tumour infiltration (Croteau et al., 2001).

Lipids and therefore tCho change over the life time of the tumour and therefore have the potential to predict the future behaviour of the tumour to therapy. This might speed up the therapeutic process. Therefore when it was found that concentration of lipids were found to increase proportionally with the aggressiveness of the tumour, and their presence is also observed in metastasis, it looked like that they may be useful (Ishimaru et al., 2001; Murphy et al., 2002). This notion has also been supported by other studies. For instance, it has been observed that the microscopic necrosis in high grade glioma correlates with poor prognosis of the patient (Burger et al., 1985; Daumas-Duport et al., 1988; Nelson et al., 1983) and additionally that the amount of mobile lipids increase with the amount of microscopic cellular necrosis (Kuesel et al., 1994). Due to these results there has been a belief that the more severe disease, the more there is necrosis and lipids due to the high speed of growth. This is the situation in most cases, however, lately it has been shown that abnormal lipid distributions are also present in viable tumours, further increasing during apoptotic cell death (Hakumäki et al., 1999; Negendank et al., 1996) (**IV**). This is probably due to the breakdown of membranes.

Many attempts have been made, in effort to grade the tumours non-invasively using MRS and the amount of tCho. However, this has not been easy due to the wide heterogeneity of tumours with large variations of the amounts of metabolites within each subtype, especially glioblastomas. Nevertheless, it has been possible to differentiate between low- and high grade gliomas (Castillo et al., 2000; Fulham et al., 1992; Howe et al., 2003; Law et al., 2003; Negendank et al., 1996; Tedeschi et al., 1997). Attempts have also been made to use Cr concentrations as a hall marker of possible malignancy, but contradictory results has been achieved. In some studies there is a decrease of Cr in malignancy (Isobe et al., 2002; Negendank et al., 1996), whereas in others no relationship could be found (Usenius et al., 1994a; Utriainen et al., 2003). Specific components of the choline pool have also been studied. For instance, Myo-Inositol (*myo*-Ins) concentrations have been examined, but only trends of decreased concentrations with increasing malignancy has been observed, with no substantial differences between grade to grade (Castillo et al., 2000; Howe et al., 2003; Murphy et al., 2002). Despite these inconclusive results, other variations of MRS have been tried to determine the grade of a tumour. For instance, by using single voxel ^{1}H MRS, Majós *et al.* have managed to differentiate tumours into four groups: GBM and metastases (MET), meningiomas (MEN), low-grade astrocytomas (LGA) or anaplastic astrocytomas (AA) with a 77 % success rate (Majos et al., 2003).

The concentrations of Lac and lipids have also been studied for the purposes of grading tumours. In this case, an increasing trend was found therein in concordance with malignancy (Howe et al., 2003). Meyerand *et al.* used single voxel MRS to study the viable area of the tumour, and found a relationship between the ratio of Lac and water signal to the different grades of the tumours (Meyerand et al., 1999). Unfortunately, when the signal from Lac was compared to the signal from Cr, as is often done, no such clear correlation could be found and only a division of low and high grade gliomas was possible. This was also the case when the ratios of tCho to water or Cr were examined in this study. Recently a study reported a correlation between an increasing tCho and a more irregular nuclear shape (Nafe et al., 2003). This study also investigated other parameters and found that even nuclear density correlated with the tCho. These results are in concordance to a previous study that explained them more thoroughly at the cellular level (Negendank et al., 1996).

Due to the wide heterogeneity of tumours and other abnormalities of the brain and to the complexity therein to grade them correctly, new methods have been developed for the analysis of the NMR spectra. In their study, Somorjai *et al.* managed to differentiate meningiomas, astrocytomas and epileptic brain tissue in an accuracy of 91.8 %, by using techniques which incorporated linear discriminant analysis (LDA), artificial neural network (ANN) and computerized consensus diagnosis (CCD) (Somorjai et al., 1996). An even better successful classification rate was achieved by Preul *et al.*, who managed to separate tissues from normal brain and from the five most common types of adult brain tumours (LGA, AA, GBM, MEN and MET) with an accuracy of 99 % (Preul et al., 1996). In the latter study a pattern recognition -based analysis was used to simultaneously take into account the six most measured ^{1}H MRS resonance peaks of brain tumours (Cho, Cr, NAA, alanine (Ala), Lac and lipids (at 0.9 ppm)). These pattern recognition and discriminant analyses are based on the comparison of unknown tumour samples to the databases of spectra from known tissue samples (Tate et al., 1998). To aid this process, automated classification methods has been lately developed and these improve the identification of the unknown lesions more reliable and less susceptible to the subjectivity of the person handling the data. An example of this type of improvement is the implementation of an ANN (Poptani et al., 1999; Tate et al., 1998; Tate et al., 2003).

2.6.5 *Ex vivo* ^{1}H MRS

The advantages of using excised tissue samples, *ex vivo* methods, compared to *in vivo* methods lies in the possibilities of using higher magnetic fields, longer measurement times, lower temperatures and spinning the samples. These parameters are all tightly fixed *in vivo* and therefore the freedom afforded *ex vivo* facilitates much better spectral resolution. In addition, by using *ex vivo* methods, some of the problems arising from *in vitro* studies (see section 2.6.6) can also be avoided. High resolution ^{1}H NMR spectroscopy, or more often, high resolution magic angle spinning (HRMAS) ^{1}H NMR spectroscopy, have been used successfully for the investigation and characterisation of different types of tumours and tissues. These techniques also allow for an improvement in the biochemical interpretation of lower resolution spectra *in vivo* (Barton et al., 1999; Kuesel et al., 1994; Millis et al., 1999; Rutter et al., 1995; Tzika et al., 2002).

Therefore, due to the higher resolution, the complexity underneath the so called choline peak around 3.2 ppm in tumour has been found to derive not only from free choline (Cho) but also glycerophosphocholine (GPC), phosphocholine (PC), taurine (Tau), *myo*-Ins and phosphoethanolamine (PE) (Rémy et al., 1994) (**V**). The concentration of tCho *in vivo* has been stated to be higher in tumours than in normal brain tissue due to higher cell numbers. However, Rémy *et al.* found no significant differences in their study, which was made by using *in vivo*, *ex vivo* and *in vitro* methods in a rat C6 glioma model (Rémy et al., 1994). This is in concordance with the results of other published studies (Peeling and Sutherland, 1992; Usenius et al., 1994b). Rémy and colleagues noticed instead a clear increase in Tau concentration within the glioma, which lead them to the conclusion that increases in the levels of Tau and PE could be responsible for the changes observed in the 3.2 ppm area of the spectra *in vivo*.

Even though the methods have been successfully used in cellular studies (Weybright et al., 1998), the main focus of research is tissues. In the case of, for instance, lymphatic cancer, the differentiation between the tumour from a healthy lymph node is very time consuming. With

convenient spectroscopic method it takes about 4 to 5 hours with two dimensional (2D) spectroscopy (Cheng et al., 1996b). This is due to the excessive amount of fat in this tissue. By using HRMAS the 1D spectral resolution was remarkably improved with the time needed for the detection of the malignancy was reduced to about half an hour. The results of improved spectral resolution and sensitivity achieved by HRMAS have also been noticed by many other researchers and from different kinds of tissues and diseases HRMAS therefore helps in facilitating better diagnosis (Cheng et al., 1998; Cheng et al., 1997; Griffin et al., 2000; Millis et al., 1997).

HRMAS has also been successfully used to monitor cell and tissue responses to differentiation therapy, using the drug thiazolidinedione, in liposarcoma (Chen et al., 2002). This agent makes the cells withdraw from the cell cycle. This event is associated both with an accumulation of triglycerides and an increase in the phosphatidylcholine : phosphocholine (PtdCho:PC) ratio. Since NMR can detect the latter variable, it was suggested that NMR could be used to quantify the effectiveness of the treatment. Indeed, in patients, the increase in the PtdCho:PC ratio was the observation that was most associated with differentiation. This indicates that this parameter may possibly serve as a NMR-detectable marker for efficient liposarcoma therapy (Chen et al., 2002). These results are in concordance with another study, where the classification of liposarcomas was made (Millis et al., 1999). This other group found that falls in triglyceride content were proportional to the amount of de-differentiation found in the tumour. This was also accompanied with a significant increase in the PtdCho level associated to increased cell numbers (Millis et al., 1999). It should be noted that a contradictory result concerning the PtdCho content was reported by Chen *et al.* This group explained this phenomenon by an increase in the activity of the CTP: phosphocholine cytidylyltransferase enzyme (CCT, the rate limiting enzyme in the conversion of PC to PtdCho) in this case of differentiation (Chen et al., 2002). HRMAS has been successfully used to monitor the metabolic patterns of a tumour after efficient gene therapy in another therapy model of tumour. Here, it has also revealed accurate changes occurring during the early stages of the treatment (**III, IV**).

2.6.6 *In vitro* ^{1}H MRS

In using ^{1}H MRS *in vitro* it is possible to study more accurately and more closely the phenomena seen *in vivo*. Additionally the extraction of the tissues, often used in the preparation of samples for *in vitro* studies, makes it possible to see the total concentrations of the metabolites therein. This is because some of sub-cellular compartments containing the compounds are non-NMR visible *in vivo* (Kauppinen and Williams, 1991). This means that *in vitro* the concentrations of the metabolites can be higher than measured *in vivo*.

Many *in vitro* studies from the extracts of tumours has been performed in order to find out special spectral characters exist for different types of tumours which might improve the identification of neoplasms *in vivo* (Gill et al., 1990; Gribbestad et al., 1994; Kinoshita et al., 1994). Despite the advantages of *in vitro* studies there are some drawbacks and these mainly concern the extraction procedures. For example, the widely used perchloric acid (PCA) extraction method removes lipids and proteins from the sample, even though they have important roles of a normal cellular metabolism and are known to contribute to the tCho peak seen *in vivo* (Peeling and Sutherland, 1992); they are a potential source of novel MRS visible markers. Extraction procedures also liberate metabolites from the different cellular compartments that are not possible to detect *in vivo*. This means that *in vitro* there could be

seen some metabolites in a certain area which are not apparent *in vivo*. This might ultimately lead researchers to the false assumptions that do not apply *in vivo*. The heterogeneity of different extraction techniques may also cause difficulties. With different methods, variable amounts of metabolites are extracted from the tissue (Le Belle et al., 2002) thus making the comparison of studies made by different ways very questionable. Not withstanding these problems, *in vitro* studies have been, and continue to be, successful in determining some useful parameters that can be used to detect cancers by NMR.

2.6.6.1 Choline containing compounds in malignancy

tCho is required for the integrity and maintenance of cell membranes. Furthermore, the amount of tCho have been found to be in a linear correlation to cell density in tumours (Gupta et al., 2000; Miller et al., 1996; Nafe et al., 2003), and after an efficient RT the amount of tCho has been found to decrease. Therefore, in this capacity, it has been used as the hallmark of a successful treatment procedure (Kizu et al., 1998; Nelson et al., 1997; Schlemmer et al., 2002). These are the results applied presently in clinics. However, when the so called choline area around 3.22 ppm in the spectra was examined more carefully, with *in vitro* and *ex vivo* methods, it was noticed to be composed of signals derived from different types of choline containing compounds (Ala-Korpela et al., 1996; Rémy et al., 1994).

PtdCho is the most abundant phospholipid in biological membranes consisting approximately 40 % of the lipid found in it (Miller et al., 1996). Despite this fact, the precursor and degradation products of PtdCho, but not the molecule itself, seems to be responsible for the Cho peak seen *in vivo* (Miller et al., 1996). The biosynthesis of PtdCho starts with the phosphorylation of Cho to PC. PC is then transformed to cytidine diphosphocholine (CDP-Cho) by a rate limiting enzyme CCT. Finally, CDP-Cho is finally transformed by phosphocholine transferase to PtdCho. When PtdCho is hydrolyzed by phospholipases, GPC, free fatty acids (FFA), Cho and 1,2-Diacylglycerol amongst other compounds are formed (Aboagye and Bhujwalla, 1999).

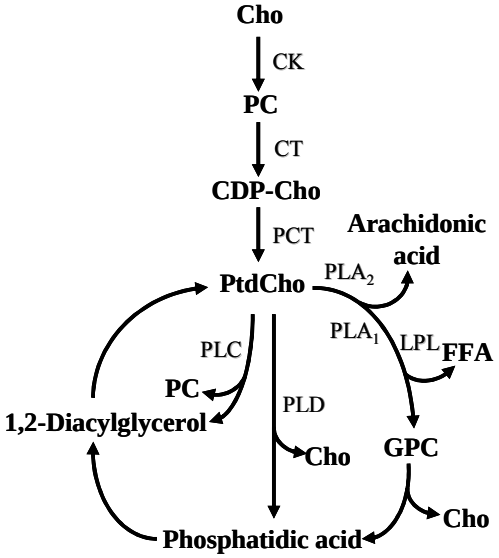

Figure 2. Biosynthesis and hydrolysis of PtdCho. Choline kinase (CK), phospholipase C (PLC), phospholipase D (PLD), phospholipase A_1 and A_2 (PLA_1 and PLA_2). Image modified from (Aboagye and Bhujwalla, 1999).

GPC has been found to be the main constituent of tCho observed *in vivo* by ^{1}H MRS in normal human mammary epithelium. However, during carcinogenesis a GPC to PC switch happens, with highly invasive metastatic cell lines showing the highest levels of PC (Aboagye and Bhujwalla, 1999). This is not true for all neoplasm types. In prostate cancer cells no such GPC to PC switch was observed. Instead there was a significantly higher PC and GPC concentrations than in normal prostate epithelial cells. This indicates that the elevation of tCho peak in clinical settings is connected to alterations in phospholipid metabolism and not only to increased cell numbers (Ackerstaff et al., 2001). In a study made by Bhakoo *et al.* (Bhakoo et al., 1996), the GPC levels were found to be approximately double that of PC in normal cells. Additionally it was observed that in tumour cells, the amount of PC was increased dramatically and a decrease in the levels of GPC was noticed. However, the PC:GPC levels did not correlate simply with the rate of cell division, because rapidly dividing primary cells examined had approximately twice as much GPC as PC (Bhakoo et al., 1996). This supports the assumption made later by Ackerstaff *et al.* (Ackerstaff et al., 2001). The accumulation of phospholipids (PL) (including PC) is also a periodic event associated with the cell cycle, with a net accumulation occurring in the S phase (Jackowski, 1994; Jackowski, 1996; Smith et al., 1991). Therefore this biochemical marker may be used as a marker of increased membrane synthesis and possibly increased cell numbers or increased cell division.

Although there seems to be no differences in the absolute concentration of tCho between healthy brain and astrocytic tumours of different grades, approximately 90 % greater values in the PC concentration have been observed in grade IV astrocytomas (Usenius et al., 1994b). Therefore PC concentration may be used as a biochemical marker for astrocytomas of highest malignancy in the future.

2.6.6.2 ^{1}H NMR detected lipids in malignancy

Even though cells contain a considerable amount of lipids in their membranes, ^{1}H NMR spectroscopy rarely detects lipid resonances in the brain tissue, because the membrane bound lipids are not detectable by ^{1}H NMR (Hakumäki and Kauppinen, 2000). Therefore, the ^{1}H NMR spectroscopy of lipids in brain tumours is an attractive tool by which malignancy may be monitored (Opstad et al., 2004).

Cancer cells usually die via apoptosis after efficient conventional RT, chemotherapy (Thompson, 1995), and gene therapy (Hakumäki et al., 1999). Blankenberg *et al.* have shown that the amount of apoptotic cell death can be quantified by ^{1}H NMR spectroscopy *in vitro* by studying the increase in the ratio of methylene (CH_2) and methyl (CH_3) resonances at 1.3 and 0.9 ppm, respectively (Blankenberg et al., 1997; Blankenberg et al., 1996). Over two fold - increase in the signal intensity of the CH_2 resonance were observed in the cell cultures undergoing apoptosis (Blankenberg et al., 1996). An increase in the methylene group signal was noticed also in *in vivo* experimental tumour model during apoptotic cell death, with additionally an increase in the methyl group concentration also detected (Hakumäki et al., 1999). They also detected an increase in the signal at 5.4 ppm during efficient gene therapy, and appearance of a peak at 2.8 ppm early on the treatment. These peaks were assigned to be the vinyl and *bis*-allylic protons of mobile polyunsaturated fatty acyl chains, respectively. Both of these also correlated quantitatively to the extent of apoptosis in the tumours. The increase in the lipid levels was not due to increased synthesis, because the total amounts of lipids did not change significantly during the treatment (Hakumäki et al., 1999). Proliferation arrest has been found to cause an accumulation of neutral lipids in the cellular cytosol in the

form of lipid droplets. These droplets have been found to be the source of the resonance at 1.3 ppm in the ^{1}H NMR spectra derived from mobile lipids (Barba et al., 1999; Hirakawa et al., 1991). Additionally, apoptotic cell death of Jurkat T-cells is associated with the accumulation of mobile triglycerides, mostly in the form of cytoplasmic lipid droplets (Al-Saffar et al., 2002). It should be noted that droplet formation is also observed *in vivo* (Hakumäki et al., 1999) and therefore may be considered as valid phenomenon occurring in tumours *in situ*.

2.6.6.3 Taurine in biology

Tau is a sulfur-containing amino acid, present in especially high levels in the central nervous system (CNS), heart and muscles (Saransaari and Oja, 2001). It has been shown to play an important role in several biological processes such as the development of the CNS, membrane stabilization, reproduction as well as being an essential nutrient (Huxtable, 1992; Schuller-Levis and Park, 2003; Timbrell et al., 1995). Tau also acts as an inhibitory neurotransmitter as well as neuroprotectant, a regulator of a cells water balance, a modulator of the rhythm and the power of contractions of the heart and participates in adjusting body temperature and hormone secretion (Huxtable, 1992; Rémy et al., 1994; Saransaari and Oja, 2001; Schuller-Levis and Park, 2003; Timbrell et al., 1995). The mechanisms of Tau actions in these processes are still unknown. With respect to brain cancer, the amount of Tau has been found to be higher in some tumours than in normal white matter (Peeling and Sutherland, 1992; Rémy et al., 1994). From this observation, it has been proposed that high Tau levels might represent increased cellular proliferation and tumour aggressiveness (Moreno et al., 1993).

2.6.6.4 *Myo*-Inositol in biology

The biochemical role of *myo*-Ins is not well understood, but it has been proposed to be an essential requirement for both cell growth and as an osmolite. It is mostly located in astrocytes and is therefore considered to be as a glial cell specific marker (Castillo et al., 2000; Ross and Bluml, 2001). In addition, *myo*-Ins is also involved in the activation of protein kinase C, which is associated with the activation of proteolytic enzymes, substances which are often secreted by malignant and aggressive tumours (Castillo et al., 2000). In relation to its behaviour in cancer, the amount of *myo*-Ins has been found to be higher in low-grade astrocytomas than high grade ones. It has been proposed to be a result of non-activation of pathway to activate protein kinase C, a phenomenon activated in high grade gliomas (Castillo et al., 2000).

3 Aims of the present study

In the present work we have used multimodal NMR methods for the characterization of BT4C-tk glioma before and during apoptotic cell death, for the better understanding of the biochemical and biophysical processes occurring therein. A well defined tumour model for glioma was used, where the apoptotic cell death in rat's BT4C glioma model is induced by HSV-tk GCV mediated gene therapy (Hakumäki et al., 1998; Hakumäki et al., 1999; Poptani et al., 1998a; Sandmair et al., 2000b).

The specific aims of the present study were:

1. to examine water diffusion by NMR methods in the apoptosing BT4C glioma model
2. to study CP-T_2 contrast during cytotoxic cell damage induced by gene therapy
3. to study the response of low molecular weight metabolites to PCD induced cell death in the glioma and to correlate this with cell numbers
4. to characterize the accumulation of lipids in the BT4C glioma model during PCD, and to reveal their source
5. to examine the biochemical features contributing to the choline region resonating at 3.2 ppm *in vivo*, and study their reactions to PCD induced cell loss in the BT4C glioma model

4 Materials and methods

4.1 Cell line and culture

BT4C glioma cells were incubated at +37 °C in Dulbecco's Modified Eagles Medium (DMEM, Cambrex Bio Science Verviers, Belgium) containing 10% fetal bovine serum (FBS) and 1% penicillin/streptomycin. A stable producer clone of pseudotype retrovirus (clone 3.0 D5) developed by Sandmair *et al.* (Sandmair et al., 2000b), was used for the transduction of HSV-tk gene accompanied with neomycin resistance gene into the BT4C cells. The BT4C cells with HSV-tk (BT4C-tk) were selected from the wild type BT4C (BT4C-wt) cells by adding geneticin into the growth medium (400 μg/ml). The geneticin killed the BT4C-wt cells and only the BT4C-tk cells expressing the neomycin resistance gene survived. The expression of HSV-tk gene was verified by incubating the cells with GCV (10 μg/ml), and the vitality of the cells was studied using a MTT-assay.

4.2 Glioma model

Animals were treated according to the animal license approved by the National Laboratory Center, Kuopio, Finland.

Since BT4C cells are originally derived from BDIX rats, no immunological reactions against tumour cells are activated when they are reintroduced into animals from the same inbred strain (Laerum et al., 1977). Before inoculation, the BT4C-tk glioma cells were trypsinized from the petri dish, centrifuged (800 rpm, 6 minutes) and suspended into Optimem medium (Life Technologies, Paisley, UK). The number of the cells were counted with a hemocytometer (Bürker, Marienfeld, Germany) and the number of cells was adjusted to 200 000 cells in 100 μl of Optimem. Female BDIX rats (180-270 g, n = 20 (**I**), 12 (**II**), 15 (**III**), 34 (**IV**), 33 (**V**); University of Bergen, Norway and Harlan, The Netherlands) were anesthetized by injecting a mixture of Hypnorm: Dormicum: sterile water (in volume ratio of 1:1:2) subcutaneously (s.c.) and 1 x 10^4 cells in 5 μl Optimem was inoculated into the corpus callosum of the rats. Cells were implanted through a burr hole made 1 mm to the right and 2 mm posterior to the bregma point using a 10 μl Hamilton syringe (Hamilton, Bonaduz Ab, Switzerland), mounted into the microinjection unit of a stereotactic frame. The cells were inoculated at a depth of 2.5 mm during two minutes. After this, the needle was left in the injection canal for about eight minutes and slowly taken out over the space in two minutes to avoid any backflow of the cells. The skin was then closed with stitches (4-0 Dexon, Davis and Geck, Hampshire, U.K.).

Approximately after three weeks, according to T_2 MRI, the treatment of the animals was started with intraperitoneal (i.p.) injections of ganciclovir, GCV, (Cymevene®, Hoffmann-La Roche AG, Grenzach-Wyhlen, Germany). The drug was delivered at the rate of 25 mg/kg, twice daily, for 0 to 8 days (**I, III – V**), or 0 to 9 days (**II**).

4.2.1 Tissue sampling for histology or *ex vivo* / *in vitro* NMR

Animals were stunned with CO_2 and transcardially perfused with 250 ml of phosphate buffered saline (PBS) followed by 300 ml of 4 % paraformaldehyde in 0.1 M phosphate

buffer, pH 7.4 (**I – V**). The formaldehyde fixed brains were then removed from the scull, rinsed in PBS and embedded in optimal cutting temperature (OCT) compound (Bayer Corp., Emerville, CA) for cryosectioning.

Under terminal anesthesia induced by pentobarbital (i.p. 100 mg / kg) another set of animals were funnel frozen with liquid nitrogen *in situ* (Pontén et al., 1973) (**III – V**), to minimize post mortem metabolism. The brains were sectioned frozen on dry ice and the tumour was dissected for *ex vivo* and *in vitro* experiments. Samples from contralateral hemisphere were taken from some of the animals. Samples were maintained in liquid nitrogen until MAS or extraction procedures.

4.3 Histology

Nissl' staining was performed on every 15th section, sectioned by cryostat (20 μm in thickness, Microm HM 560 M, Microm Laborgeräte GmbH, Walldorf) and quantitative cell counting was performed using the Stereo Investigator software in a NeuroLucida morphometry system (MicroBrightField, Colchester, VT) (**I – V**). Cells were also counted from the three sections that corresponded to the mid-most slice of the T_2 images derived from the same animal (**I**). This was done by dividing the tumour into three sections: the central region accounted for the innermost third of the tumour radius (center), the intermediate third (middle) and from a rim region representing the outermost third of tumour radii (border). Four adjoining sections from the middle of the tumour were stained for terminal deoxyribonucleotidyl transferase-mediated dUTP nick end labeling (TUNEL) (ApopTag Plus, Oncor, Gaithersburg, MD) to detect apoptotic nuclei, using a methyl green as a counterstain (**I**, **III – V)**. Apoptotic nuclei in tumour were counted from five arbitrarily chosen high-power microscopy fields (HPF) (x20, Olympus AX-70 microscope, Tokyo, Japan) within the same regions as mentioned above.

4.4 Tissue extraction for NMR spectroscopy

A standard PCA extraction procedure was used for the extraction of acid-soluble metabolites (**III – V**). The frozen samples were weighted and homogenized in ice cold 0.9 M PCA using a Potter-Elvehjelm homogenizer. After centrifugation (13 000 rpm, 15 minutes, + 4 °C) the clear supernatants of the samples were neutralized with 3M KOH to pH 7.0 – 7.3 and re-centrifuged. The supernatants were re-neutralized if necessary, after which they were freeze-dried and stored at – 70 °C until needed.

The extraction of tissue lipids were performed with the standard chloroform-methanol procedure described elsewhere (Folch et al., 1957) (**IV**).

4.5 NMR imaging and spectroscopy

4.5.1 *In vivo* MRI and MRS

For NMR measurements animals were anesthetized with 0.8 % to 1.0 % halothane in a 7 : 3 N_2O : O_2 mixture. The core body temperature was monitored and maintained close to 37 °C by circulating warm water through a water blanket under the rat inside the magnet bore. MRI

was performed using a horizontal 4.7 T magnet (Magnex Scientific Ltd., Abigdon, United Kingdom), equipped with actively shielded field gradients (Magnex Scientific) interfaced to a Varian ^{UNITY}INOVA console (Varian, Inc., Palo Alto, CA). A quadrature surface coil (High field Imaging, Minneapolis, MH) was used in a receive/transmit mode. Animals were fixed into a custom built head holder using a mouth bar and ear pins.

Tumour volumes were determined from T_2 weighted multislice spin echo images [pulse repetition time (TR) = 2.5 s (2 s at **II**), echo time (TE) = 55 (**I, IV**), 60 (**II**) or 90 ms (**III, V**), matrix size 256 x 128, field of view (FOV) = 35 x 35 mm^2, two scans per line, contiguous slices of 1 mm in thickness], and the absolute T_2 images were acquired (in studies **I** and **IV**) by combining Hahn spin echo data obtained at four TEs between 20 and 110 ms using TR = 1.5 s, FOV = 35 x 35 mm^2, matrix size 128 x 64, slice thickness of 1.5 mm, and an adiabatic BIR-4 refocusing pulse (Garwood and DelaBarre, 2001). The signal intensities of T_2 weighted MR images were determined in the slice through the middle of the tumour and ipsilateral to the normal brain cortex (**V**). Absolute diffusion images were obtained using a spin echo sequence (TR = 1.5 s, TE = 55 ms, t_D = 4.8 ms). For the achievement of weighting by the diffusion tensor ($D_{av} = 1/3 Trace\overline{\overline{D}}$) in a single acquisition, four bipolar gradient pairs in each direction was used (Mori and van Zijl, 1995). Data from three acquisition with different diffusion weighting (b-values of 40, 500 and 1000 s/mm^2) were used for the calculation of absolute D_{av} images using a MatLab routine (Mathworks, Natick, MA) (**I**,**III**,**IV**).

(**II**) Utilizing an adiabatic Carr-Purcell (CP) type spin echo sequence (Bartha et al., 2002b), with four different TE values in the range of 36.8 – 134.9 ms, TR = 2 s, (number of acquisitions 2 – 4) was used to acquire data for CP-T_2 images from a 1 mm thick slice in the middle of the tumour. The preselected reduced FOV was 15 x 25 mm^2 covered with 32 x 128 points. Long-τ_{CP} T_2 was achieved by increasing the time between centers of the π pulses (τ_{CP}, 6.1 – 22.5 ms). Similarly, the short-τ_{CP} T_2 was achieved by increasing the number of π pulses from 6 to 22 ms, keeping τ_{CP} constant at 6.1 ms. The shapes of the RF amplitude and frequency modulations of the adiabatic π pulses were based on hyperbolic secant and tangent functions (Garwood and DelaBarre, 2001; Silver et al., 1984). The specific parameters used in this measurement were: a frequency-sweep amplitude (A) of 35,000 rad/s, a peak RF amplitude (B_1^{max}) of 0.4 G, and a pulse length (T_p) of 2.5 ms. To further reduce the likelihood of pulse imperfections, the initial phases of the adiabatic π pulses were prescribed according to the MLEV scheme (Levitt and Freeman, 1981). $T_{1\rho}$ was measured using variable length adiabatic spin lock pulses (10 – 70 ms; B_1 = 0.2 G and 0.8 G) in front of the same imaging sequence with prelocalization of the reduced field of view with six adiabatic π pulses (τ_{CP} = 6.6 ms). The on-resonance spin lock was a single RF pulse consisting of three segments: a 4-ms-long adiabatic half-passage followed by the spin lock period and finally a reverse adiabatic half-passage pulse, which returned the magnetization back to the z axis.

For the detection of water signal diffusion (**I**), NMR spectroscopy was used with a variety of acquisition parameters. T_2 weighted localizer images (TR = 2 s, TE = 90 ms, FOV = 40 mm) were used for the placement of a voxel inside the tumour. Next, shimming was done with the FASTMAP routine (Gruetter, 1993) to yield a typical water line widths of 12 – 16 Hz. Symmetrically placed pairs of unipolar diffusion-weighting gradients around the second and third π / 2 pulses in a stimulated echo acquisition mode (STEAM) pulse sequence without outer volume presaturation (Tkac et al., 1999) (TR = 2 s, TE = 19 ms, middle period (TM) = Δ – 10 ms, and eight scans / spectrum) were also used. Diffusion gradients were applied along

the x-, y-, and z-directions simultaneously to achieve the highest attainable b-values at given t_D.

The quantification of tumour metabolites (**III**, **IV**) was performed by using a STEAM sequence [TR = 3 s (2 s in **IV**), middle period delay = 30 ms, TE = 2 ms, sweep width (SW) = 2.5 kHz, 2000 data points (2048 in **IV**)] incorporating an outer volume saturation and a variable pulse power. An optimized relaxation delay (VAPOR) water suppression scheme and asymmetric excitation pulses were also used (Tkac et al., 1999). The voxel was placed inside the tumour according to the multislice T_2 weighted localizer images obtained as described above. For some animals (**III**) ^{1}H spectra were also acquired from the same voxel using the localization by adiabatic selective refocusing (LASER) method as described previously (Garwood and DelaBarre, 2001) (TR = 8.8 s, TE = 32 ms, SW = 2.5 kHz, 13k data points). Diffusion sensitizing gradients were incorporated into the STEAM sequence (TR = 2.5 s, TE = 45 ms) for the quantification of the ADC of the lipid peaks using a diffusion time of 76 ms and b-values from 0 to 21,316 s/mm^2 (**IV**). Metabolite and lipid concentrations were quantified from the STEAM spectra using non-suppressed water as a concentration reference (0.787 kg/kg of fresh tumour tissue) (Hakumäki et al., 2002). These values were corrected for the T_1 saturation effects (**III**) derived from water accumulation during PCD, using the tumour T_1 values reported recently (Hakumäki et al., 2002). A LASER spin echo sequence (Garwood and DelaBarre, 2001) was used for the semi-quantitative assessment of tumour lipids *in vivo* by ^{1}H NMR spectroscopy (TR = 8.8 s, TE = 32 ms, SW = 2.5 kHz and 13k data points) (**IV**).

4.5.2 *Ex vivo* HRMAS

For *ex vivo* ^{1}H NMR spectroscopy (**III – V**), tumour samples (5-10 mg of wet weight) were placed into a zirconium oxide MAS rotor with 10 µl of D_2O (deuterium lock reference) containing 10 mM trimethylsilyl propionic acid (TSP, chemical shift reference (δ) at 0.0 ppm). To optimize magnetic homogeneity the magnet was shimmed for the improvement of the line shape and to minimize the line width of TSP (typically to ~ 1 Hz). ^{1}H HRMAS NMR spectra were acquired using a Bruker AVANCE spectrometer operating at either 400 MHz (**V**), 600 MHz (**III – V**) or 700 MHz (**V**) at 277 K interfaced to a high resolution MAS probe (Bruker GmBH, Rheinestetten, Germany). A conventional solvent suppressed pulse/acquire sequence, a so-called NOESY presaturation sequence (Bruker), was used to suppress baseline artifacts resulting from B_0 and B_1 field inhomogeneities with a fixed evolution time (**V**) of 100 µs, and a mixing time of 150 ms [TR = 4.28 s, SW = 10 kHz, 32,768 complex data points, 4 kHz (at 400 MHz), 5 kHz (at 600 MHz) and 6 kHz (at 700 MHz) spinning rate]. The same sequence was used in studies **III** and **IV** with following parameters: TR = 2 s, SW = 10 kHz, 32,768 data points (32k **III**), 5 kHz spinning rate; water suppression during the mixing time of 150 ms and relaxation delay. Spectra were also acquired with a Carr-Purcell-Meiboom-Gill (CPMG) pulse sequence (**III-V**). In studies **III** and **V** TE = 40 ms, interpulse interval 500 µs, total number of spin echoes = 40, and other parameters as described above for NOESY. To examine the T_2 behavior of lipids (study **IV**), interpulse delay was 500 µs and effective TEs ranged from 10 to 320 ms. To confirm some of the spectral assignments (**V**), a J-resolved 2D spectrum (JRES) was acquired at 700 MHz, from a tumour on day 6 of the GCV treatment. The JRES was collected with 128 acquisitions per 48 increments using a spectral width of 7 kHz in the F2 dimension and 50 Hz in the F1 dimension. The data were then processed using zero-filling to 96 in the F1 domain, and an un-shifted sine-bell apodization function was applied in both directions prior to the FT. The spinning rate and/or the temperature were varied in some experiments (**IV**), in order to investigate their effects on spectral

characteristics. The FIDs were multiplied by an exponential apodization function equivalent to 1 Hz line broadening and FT into a real transform size of 16,384 data points, yielding 8,192 points of zero filling (**IV**).

A stimulated echo pulse sequence incorporated by bipolar gradients (Wu et al., 1995) was used for diffusion spectroscopy (**IV**), with 32 increments of a 53.2 gauss/cm field gradient placed along the magic angle axis. Sine-shaped gradients of 2.5 ms (δ/2 for a bipolar sequence) were used with a 100 ms delay between the gradients yielding a Δ of 98.3 ms. The delay was repeated three times for each tumour sample. 32 transients were acquired for each increment using a 16k time domain over a spectral width of 8.4 kHz. Finally, the ADCs were computed by fitting the NMR signal as a function of b-value into a single exponential in the XWINNMR program (Bruker GmBH).

4.5.3 In vitro MRS

High resolution pulse-acquired ^{1}H NMR spectra were collected at 500 MHz using a Bruker Avance spectrometer at 20 °C (III and V). Presaturation solvent suppression was used during the relaxation delay (TR = 12.7 s, SW = 6 kHz, 16k data points) for the measurement of the freeze-dried PCA samples. These extracts had been previously dissolved in D_2O containing 20 µl TSP for chemical shift and concentration reference. The same instrument was also used to acquire the proton-decoupled ^{31}P NMR spectra (TR = 2.4 s, SW = 40 kHz, 16k data points). For the assignment of the peaks tentatively identified as 'nucleotides' in the ^{1}H and ^{31}P NMR spectra, some of the extracts were spiked with uridine diphosphate (UDP) and cytidine diphosphate (CDP) (III).

For the characterization of *in vivo* and *ex vivo* detected lipid moieties, tissue lipid extracts were reconstituted in 500 µl of $CDCI_3/CD_3OH$ (3:1) and analyzed by high resolution ^{1}H and ^{13}C NMR spectroscopy using a triple gradient axis, inverse geometry probe (Bruker GmBH) (**IV**). Solvent suppressed TOCSY and HMBC spectroscopy were performed. The total spin lock time was 80 ms alongside sine-shaped gradients of 2 ms duration for the TOCSY (Bax and Davis, 1985; Hurd, 1990) and a ^{1}J(C,H) filter of ~140 Hz and selection for ^{2}J(C,H) and ^{3}J(C,H) ~8 Hz couplings for the HMBC (Willker et al., 1993).

4.6 NMR data analysis

4.6.1 MRI

From the midmost D_{av} and T_2 images the tumours were divided into three sections in a visually controlled manner, to match the regional analysis of histological sections as closely as possible under a MatLab routine (**I**). The spin density was corrected from the M_0 obtained from the T_2 fits and corrected for the T_1 saturation effect using T_1 values reported recently for the BT4C gliomas treated with the same gene therapy procedure (Hakumäki et al., 2002).

4.6.2 Diffusion MRS

Water signal intensity from diffusion MRS experiments was fitted into Equation (15).

$$S = S_0\left[\sum_{i=1}^{n} f_i e^{-bD_i}\right] \qquad (15)$$

Where S_0 and S indicate the magnetization in the absence and presence of the diffusion gradient, respectively. f_i and D_i correspond to population fraction and diffusion constant of the i^{th} component, respectively. Consistent biexponentiality (i.e. $N = 2$ in Eq. (15)) was observed at all t_D values measured (**I**). The non-linear problem with four unknown parameters i.e. S_0, f_1, D_1 and D_2 using $f_2 = (1 - f_1)$, was solved by using an iterative home-programmed Gauss-Newton (GN) algorithm under the MatLab routine. The root mean square displacement of water (r) was computed from the Einstein-Smoluchowski Equation (16).

$$\left\langle (r - r_0)^2 \right\rangle = 6D_i t_D \qquad (16)$$

D_i refers to the diffusion coefficient of the i^{th} components. For the present analysis, two components were used. The mean apparent residence time (τ) for the slow diffusion coefficient pool was estimated under experimental conditions probing only the restricted water pool at high constant gradient (q) values. τ in the compartment with a slow diffusion coefficient is given by Equation (17), where t_D is the diffusion time.

$$\tau_{slow} = -\left(\frac{\partial \ln S(q^2, t_D)}{\partial t_D}\Big|_{q=const}\right) \qquad (17)$$

4.6.3 CP-T_2 and $T_{1\rho}$

Parametric maps for CP-T_2 and $T_{1\rho}$ were calculated using the MatLab routine. Maps representing the τ_{CP}-dependent changes were achieved by subtracting the long-τ_{CP} image from the short-τ_{CP} image with the same TE (134.9 ms) and normalizing this to the long-τ_{CP} image (**II**).

4.6.4 NMR spectroscopy

In vivo spectra were analyzed in the time domain using jMRUI software (web site URL: http://www.carbon.uab.es/mrui) (**III** and **IV**). They were also analyzed in the frequency domain *in vitro* (**III** and **V**) and *ex vivo* (**V**) with the PERCH software (web site URL: http://www.perchsolutions.com). The *ex vivo* spectra (**III** and **IV**) were examined in the frequency domain using WXINNMR (Bruker GmBH).

4.6.5 Statistics

Student's unpaired t-test was used for the statistical analysis of results (**I** – **IV**). Linear regression analysis was used to estimate the significance of the correlation between cell density and metabolite concentrations *in vivo* and *in vitro* (**III**). Principal Component Analysis was used to analyze the data from study (**III**) in an effort to investigate the non-lipid metabolite changes (in HRMAS ^{1}H NMR CPMG spectra (TE = 40 ms)) that accompanied the PCD occurring in the tumours (Beckwith-Hall et al., 1998). The principal component

representations of variation across the data set were investigated in terms of clusterings relating to tissue type and progression through PCD. A pattern recognition method was used for the analysis of the *ex vivo* results (PLS model) (**IV**). Finally, one-way ANOVA with a Dunnet's post hoc test was used for the analysis of metabolite concentrations in treated tumours versus the control samples (**V**).

5 Results

5.1 Diffusion MRI and cell counts in the BT4C rat glioma (I)

T_2 weighted MRI showed that gliomas stopped growing on day 4 of the GCV treatment and by day 6 the tumour volumes had decreased significantly from their peak volumes (**I:** Fig. 2A). Even though the tumours showed no regression in size by the day 4 of treatment, there was already a detectable decrease in the volume averaged cell count by (**I:** Fig. 2B) 13%. A precipitous drop in cell count was evident on day 6 of the GCV treatment and interestingly, the number of apoptotic cells (as determined by TUNEL assays) also peaked at the same time point (Table 4). Both the D_{av} and the T_2 values in treated gliomas had increased by day 4, showing similar kinetics during subsequent days. Similarly, the spin density ratio increased along with the absolute T_2 values in treated tumours (**I:** Fig. 3A, E and I). The correlation analysis of the volume averaged cell counts to D_{av}, T_2 and spin density ratio measurements, determined in the volumes matching histology, was performed for each animal. This analysis revealed that all of the measured MR parameters significantly correlated with the cell density ($p < 0.001$). From these observations, it can be concluded that the more cells in the treated tumours, the lower the D_{av}, T_2 and spin density ratio values are.

Table 4. Cell density, number of apoptotic cells, and relative tumour volumes of BT4C gliomas (± SEM). Day 0 volume was taken to be one in each animal and the subsequent values were referenced to this value.

Treatment	Cell density ($x10^3$ cells/mm^3) ($n = 14$)	TUNEL (cells/hpf) ($n = 14$)	Tumour volume (relative) ($n = 20$)
Day 0	178.35 ± 10.4	4.0 ± 0.1	1 ± 0
Day 2	183.55 ± 12.7	5.7 ± 0.8	1.31 ± 0.05
Day 4	154.70 ± 13.9	11.3 ± 0.5$^{\#\#}$	1.36 ± 0.05
Day 6	109.72 ± 3.9$^{\#\#}$	22.3 ± 1.8$^{\#\#}$	1.09 ± 0.08*
Day 8	71.32 ± 1.1$^{\#\#}$	14.2 ± 1.9$^{\#\#}$	0.79 ± 0.09**

$^{\#\#}$ $p < 0.01$ relative to untreated tumour, Student's unpaired *t*-test
* $p < 0.05$ relative to day 4 value, Student's unpaired *t*-test
** $p < 0.01$ relative to day 4 value, Student's unpaired *t*-test

The regional analysis of cell count by histological methods revealed the fastest decline in cell density in the central section of the tumour during GCV treatment (**I:** Fig. 2D). Already by day 2 a significant decrease in cell count was observed in this tumour zone. In the peripheral parts of the tumours cell loss was evident from day 4 onwards. These histological observations show heterogeneity in the treatment response and also revealed areas of continued tumour growth, despite GCV treatment. The apoptotic activity was observed throughout the treatment period, beginning with an examination of the central and border sections on day 2 (**I:** Fig. 2E). The highest number of TUNEL positive cells was determined in the border zone on day 6 of treatment. In this zone cell death lagged behind that of the central parts of the tumour. Cell counts were still high in the border zone on day 8 of the GCV treatment.

Surprisingly, regional analysis of the D_{av}, T_2 and spin density ratio revealed that changes in the middle section were detectable first (**I:** Fig. 3). D_{av} had increased on day 2 and T_2 on day 4 of treatment in the middle zone. Similar changes in D_{av} and T_2 values were observed in the

central and border zones by day 4. Please note that the changes in T_2 values occurred somewhat later than those observed for the D_{av}. Spin density ratios increased first in the middle and border zones on day 4 of treatment. Increases in this MR variable was seen by day 6 in the central section. Changes in all of these MRI variables mirrored closely the decline in cell count in the regionally matched tumour volumes.

The signals from tissues acquired by diffusion spectroscopy with varying t_D and b-values display a multicompartmental behaviour. In the present study we have used a biexponential function to fit the water diffusion spectroscopy data. A significant increase in the diffusion of the D_1 component was observed in the tumours, after 4 days of GCV treatment in the experiments using $t_D \geq 47$ ms (**I:** Fig. 4A). Thus, changes in the D_1 coefficient closely resembles that of the volume averaged D_{av}. The size of f_1 increased evenly throughout the t_D range starting on day 4 of treatment (**I:** Fig. 4C). The coefficient D_2 increased by day 6 in the spectra acquired with $t_D \geq 47$ ms and this change was evident at long t_D values (> 142 ms) (**I:** Fig. 4B). The diffusion characteristics of D_1, D_2 and f_1 changed by 5 % to 10 % at long TM (> 140 ms) relative to intermediate range (TM of 60 – 100 ms). This effect may be due to T_1 saturation.

One can compute the apparent water residence characteristics from the diffusion spectroscopy data. The root mean square displacement (r) of water in untreated tumours for the D_1 and D_2 components ranged as a function of t_D from 11.7 ± 0.6 and 5.5 ± 0.2 μm to 31.6 ± 0.7 and 15.1 ± 0.4 μm, respectively (**I:** Fig. 5). The r values (at $t_D \geq 47$ ms) from D_1 and D_2 increased by day 4 and day 6 of GCV treatment, respectively. No restriction in water diffusivity was observed within the time scale covered by the t_D values (up to 194 ms). Apparent water residence time in the untreated tumours was very similar to that determined in the normal brain (38.4 ± 1.9 ms compared to 38.3 ms, respectively). The apparent residence time remained at this level until day 4, after which a trend to shorter times was observed, which reached significance by day 8 of the GCV treatment (**I:** Fig. 5C).

5.2 MRI contrasts for gene therapy response (II)

Long-τ_{CP} T_2 MRI provided pronounced contrast between untreated tumour and normal brain tissue (**II:** Fig. 2). CP-T_2 values of 53.5 ± 0.7 ms and 58.6 ± 0.6 ms were determined with this MRI technique in these tissue types, respectively. Corresponding CP-T_2 values obtained with short-τ_{CP} were 60.6 ± 0.7 ms and 64.4 ± 0.8 ms in gliomas and normal rat brain tissue, respectively. However, $T_{1\rho}$ MRI showed barely visible contrast between the gliomas and the brain, but the tumours could be delineated because of borders with a dark appearance. No significant changes in either short-τ_{CP} or long-τ_{CP} CP-T_2 values were observed in the untreated tumours during the observation time extended to 8 days. Histology performed on tumours after 8 days of GCV injections showed that individual gliomas responded very differently to gene therapy. One group of tumours showed a moderate decrease in cell count (less than 20 %) as quantified from Nissl stained sections (**II:** Fig. 1B). Additionally in these tumours, T_2 MRI indicated that increases in tumour volume were occurring. This group of animals was labeled non-responders. Another group of animals responded well to GCV treatment, as indicated by a substantial decrease in the tumour volumes ($p < 0.01$) and by a cell death rate of more than 50 % by day 8 of treatment (as verified by histology (**II:** Fig. 1)).

An increasing trend was observed in all relaxation times studied in the non-responders (**II:** Fig. 3A). In contrast, in the responders significant changes in MRI variables in tumours were

detected (**II:** Fig. 3B). Short-τ_{CP} T_2 values increased by day 2 of treatment from a pre-treatment value of 61.3 ± 1.0 to 64.2 ± 1.1 ms ($p < 0.05$), increasing further to 76.7 ± 3.6 ms ($p < 0.01$) by day 8. Long-τ_{CP} T_2 also displayed significant increase by day 6 of the GCV treatment. The sensitivity of the $T_{1\rho}$ MRI, acquired with a B_1 of 0.2 G, to reveal the GCV treatment response, was comparable to that obtained by the short-τ_{CP} T_2method. Relative difference images were obtained by subtracting the long-τ_{CP} image from the short-τ_{CP} image (both acquired with the same effective TE). The difference image was normalized to that acquired with the long-τ_{CP} (**II:** Fig. 4). Dynamic susceptibility images highlighted the τ_{CP}-dependent signal changes. Only a weak contrast was observed between glioma and normal brain tissues before treatment. However, the contrast had intensified greatly by day 4 in the responders. Our data indicated that the short-τ_{CP} T_2 MRI seemed to unveil positive HSV-tk mediated gene therapy treatment responses in BT4C gliomas with comparable time course to that seen with D_{av}.

5.3 ^{1}H NMR spectroscopy of a glioma during programmed cell death (III)

In each subset of HSV-tk positive gliomas, the reactivity to GCV treatment was verified by MRI and histological methods (**III:** Fig. 1). D_{av} showed scattered increases in water diffusivity in the GCV treated tumours by day 4. This was followed by a decline in the tumour volume between days 4 and 6. Substantial cell loss and scar formation was apparent in histological sections of the tumours at this time as well. The TUNEL staining revealed a more than 4-fold increase in apoptotic nuclei by day 4 of the GCV treatment. All these observations confirm that increased apoptotic cell death occurs in the treated gliomas.

^{1}H NMR spectra from BT4C gliomas *in vivo* show strong signals at 1.3 and 0.9 ppm arising from lipid –CH_2**CH_2**CH_2– and –CH_2**CH_3** groups, respectively (**III:** Fig. 2). The spectral peaks derived from PUFA are also detectable at 5.4 ppm (from –C**H**=C**H**–), 2.8 ppm (from –CH=CH**CH_2**CH=CH–), and 2.0 ppm (from –**CH_2**CH=CH–). STEAM ^{1}H NMR spectroscopy of an untreated tumour revealed well resolved peaks derived from Cr at 3.92 ppm, glutamate + glutamine (Glx) at 3.76, *myo*-Ins + glycine (Gly) at 3.6 ppm, Tau at 3.43 ppm, tCho with a contribution from Tau at 3.23 ppm, and Cr at 3.03 ppm (**III:** Fig. 2A and B). All these peaks were also observed in LASER spectra acquired with a TE of 30 ms (**III:** Fig. 2C and D). No resolvable resonances were seen in the spectra *in vivo*, downfield from 6 ppm, even after an improvement in the signal-to-noise ratio achieved by summing several spectra collected from different tumours. Qualitative time-dependent changes in the ^{1}H NMR detected metabolites were observed during GCV treatment. Concentrations of *myo*-Ins + Gly, Tau and Cr displayed a significant negative slope with cell density, in tumours undergoing PCD, however tCho remained unchanged (**III:** Fig. 3A-C). Additionally, a non-significant slope of Glx was evident. The ^{1}H NMR PUFA (from –C**H**=C**H**– at 5.4 ppm) and saturated (from –CH=CH**CH_2**CH=CH– at 1.3 ppm) lipids showed a positive slope in the tumours with declining cell count (**III:** Fig. 3D). This observation was consistent with a previous studies on BT4C-tk gliomas (Hakumäki et al., 1999) (**IV**).

Metabolite concentrations of Gly, Cr and Ala determined from tumour extracts *in vitro* indicated decreasing trends ($p < 0.10$) for these parameters as a function of decreasing cell density (**III:** Fig. 3E-G). Tau, Glx and tCho showed virtually zero slopes. The slope of *myo*-Ins was positive during PCD, which was unexpected from the *in vivo* observations.

HRMAS ^{1}H NMR spectroscopy makes it possible to separate the individual signals of the tCho peak, which comprises of data derived from Cho, PC, GPC as well as the overlapping peaks from Tau (**III:** Fig. 5). Principal component analysis of metabolites in the CPMG spectra separated tumour and control tissues (**III:** Fig. 6). Spectral regions responsible for distinguishing tumour and normal tissue were identified as follows. In tumours, the relative resonance intensities derived from –C**H$_3$** lipid, –C**H$_2$**CH=CH– lipids and *myo*-Ins were stronger than in the normal brain. Additionally, normal brain cortical tissues were characterized by resonances derived from Lac, NAA, glutamate and Cr. No metabolite changes were associated with PCD.

In the downfield part of HRMAS ^{1}H NMR derived spectra of tumour tissues had numerous peaks that were not observed in the normal brain (**III:** Fig. 5F). The peaks were more abundant in CPMG spectra than in pulse-acquire data sets. Since it is known that nucleic acid polymers (i.e. chromosomes and RNA) breakdown into their individual components (i.e. nucleotides such as ATP and CDP), during PCD, it was reasoned that some of these extra peaks might be derived from these compounds. The possible presence of either UDP or CDP in the tumours was performed by studying aqueous tumour extracts with ^{31}P NMR spectroscopy. The confirmation of UDP was achieved by spiking experiments using ^{31}P NMR as well as ^{1}H NMR. The relative ratio of UDP to ATP remained approximately constant during PCD at 0.58 ± 0.20 (from ^{1}H NMR) and 0.53 ± 0.10 (from ^{31}P NMR) in the extracts of gliomas.

5.4 ^{1}H NMR visible lipids in gliomas undergoing programmed cell death (IV)

^{1}H NMR spectra *in vivo* showed well-resolved peaks at 5.4 and 2.8 ppm from PUFAs as well as peaks at 0.9 and 1.3 ppm from saturated lipids in BT4C-tk gliomas undergoing PCD due to GCV treatment (Poptani et al., 1998a) (**IV:** Fig. 2). In addition, PUFAs were found to increase by 3-fold during the course of the GCV treatment, whereas the saturated lipids increased by up to 2-fold. This suggests that about 70 % of the lipid accumulation, detected by ^{1}H NMR, during PCD was attributable to PUFA accumulation. LASER spectra with different volumes were acquired from the tumour at the treatment day 8 (**IV:** Fig. 3). A large voxel was used to cover as large a volume of the tumour as possible and a small voxel was placed to cover the T_2 hyperintense core. Interestingly, the ^{1}H NMR spectra obtained were very similar from these two voxels. This suggests the uniform presence of ^{1}H NMR lipids in dead tumour tissue as well as in tissue undergoing PCD.

Diffusion ^{1}H NMR spectroscopy was used to examine the diffusivity of metabolites in the GCV treated gliomas. The ADC of the lipid peaks at 5.4 and 1.3 ppm did not change as a function of the treatment (**IV:** Table 1).

Ex vivo MAS NMR confirmed the changes in the PUFA lipid peaks seen by ^{1}H NMR spectroscopy *in vivo* (**IV:** Fig. 4). Neither spin rate nor temperature variations influenced the line widths of the lipid peaks of tumours in HRMAS spectra (**IV:** Fig. 5). These facts indicate that the NMR detectable lipids possess a high degree of rotational freedom and thus, cannot be derived from membrane bound lipid domains. In this light, the data obtained does not conflict with the theory that the intracellular lipid droplets are the source of NMR detectable lipids (Hakumäki and Kauppinen, 2000). In contrast, the peaks derived from small molecular weight metabolites were strongly affected by the spinning rate (**IV:** Fig. 5A and H). A short-range TOCSY spectrum was used for the assignments of the PUFA lipid resonances (**IV:** Fig.

6). TOCSY spectra showed a strong cross peaks at 2.8;5.4 ppm from olefinic proton resonances. In addition, cross peaks from choline lipids at 4.3;3.7 ppm and multiple cross peaks from *myo*-Ins were also detected.

Increases in the resonances derived from C**H**=C**H**, CH=CHC**H$_2$**CH=CH, CH$_2$**CH$_2$**CH$_2$ and CH$_2$**CH$_3$** against time *ex vivo* were demonstrated by the PLS-based regression model (**IV:** Fig. 7). PCD induced cell mortality was strongly correlated with an increase in the PUFAs and not just with a general increase in lipid moieties. Similar results were also obtained with CPMG spectra, confirming the assumption that the lipids were rotationally mobile and existed in a relatively unrestricted environment.

For the biochemical characterization of PUFAs, lipid extracts of the tumour tissue were examined with one- and two-dimensional TOCSY, COSY, HSQC and HMBC NMR methods. A 2-fold decrease in the total PUFA resonance intensity relative to the CH$_2$C**H$_2$**CH$_2$ resonance at 1.3 ppm was observed. This was both relative to the *in vivo* and *ex vivo* values, as determined with one-dimensional ^{1}H NMR spectral analysis of the lipid extract. This observation therefore detects the release of non-NMR detectable tissue lipids by the extraction procedure. Increased intensities of acyl and cholesterol side-chain resonances were also apparent in the extracts, indicating that the lipid resonances detected *in vivo* and *ex vivo* represented a chemical group distinct from the total lipid content of the tumours. Four different CH=CHCH$_2$CH$_2$ lipid groups were detected with HMBC that had been optimized to detect three and four bond couplings between ^{13}C and ^{1}H nuclei (**IV:** Fig. 6B). Strong cross peaks for 2.8 and 5.3 ppm ^{1}H resonances arose from the 18:1 and 18:2 types of unsaturated fatty acids with small contributions from cholesterol based lipids assigned as well. It should be noted that neither in tumours *in vivo* nor *ex vivo*, were significant quantities of cholesterol detected. This indicates that a partitioning of membrane lipids could be the source of the observed changes in ^{1}H NMR detectable lipids during the treatment.

5.5 HRMAS ^{1}H NMR spectroscopy of choline containing metabolites during PCD (V)

A hyperintensity in T$_2$ weighted MRI was observed at treatment day 4, when no significant changes in the cell density were apparent (**V:** Table 1). However, on day 4 of the GCV treatment, the number of TUNEL positive cells had increased substantially compared to untreated gliomas and this preceded the decline in the cell count on day 6 of the GCV treatment (**V:** Table 1). Tumour volumes were reduced by 30 % from the peak volume by day 8 of treatment. PCD was in progress in the treated glioma tissue used for HRMAS, as shown by our MRI and cell density observations. They are consistent with previous reports (Poptani et al., 1998a) (**III**, **IV**) that confirm cell eradication and a high number of TUNEL positive cells following GCV treatment in these gliomas.

Both water-suppressed pulse/acquire and CPMG HRMAS ^{1}H NMR spectra displayed a good separation in the peaks arising from individual choline containing metabolites (CCM), as well as Tau, *myo*-Ins and broad unassigned resonances (MM) in the same spectral area. Cho, PC and GPC could be resolved as separate peaks when measured at 700 MHz, but at 400 and 600 MHz only a partial separation was achieved (**V:** Fig. 2). However, deconvolution analysis of these resonances, using the peak fitting routine within PERCH, made it possible to separate the individual resonances at all three frequencies. 2D JRES spectrum confirmed the assignment of the two triplets of Tau at 3.27 and 3.45 ppm, as well as identified a triplet at 3.23 ppm (**V:** Fig. 3). This latter triplet is consistent with that assigned to PE, by Rémy et al

(Rémy et al., 1994). Another triplet was found to resonate at 3.02 ppm that is consistent with either γ-amino butyrate or lysine. However, *in vitro* ^{1}H NMR spectrum shows multiplet resonances at 1.73 and 1.91 ppm, as well as triplet at 3.76 ppm. This data supports the assignment of this triplet to lysine.

The absolute concentration of Cr was determined by *in vitro* NMR spectroscopy of PCA tissue extracts. The concentrations of metabolites in tissue samples *ex vivo* were determined from pooled data sets from all three frequencies (**V:** Table 2). Concentration calculation was based on the metabolite peak areas relative to the Cr peak area. The absolute Cr concentrations were determined *in vitro* from the corresponding tissue samples from the other half of the tumour not analysed with HRMAS. In tumour samples, both NMR methods (pulse/acquire and CPMG) gave consistent values for the metabolites within a range of ± 5 %. The concentrations of tCho and Tau in untreated tumours were higher than in the normal brain cortex (**V:** Table 2). Interestingly, in the early phase of the GCV treatment, an increase in both PC and GPC was evident *ex vivo*, while Cho and Tau remained unchanged. Only the concentrations of Tau were observed to follow the cell density (declining by > 60 % on day 8), whereas those for tCho and *myo*-Ins were not influenced by apoptotic cell death. The concentrations of PC and GPC returned back to the pre-treatment levels by day 8 of treatment.

A broad 'hump' was present in both pulse/acquire and CPMG HRMAS experiments in normal brain cortex and tumours (**V:** Fig. 2). At 700 MHz, the fitting routine resolved two broad peaks between PC and Tau (**V:** Fig. 2D). These were not affected by TE filtering, which suggests that these peaks have relatively long T_2 relaxation times. The resonance integral of the broad peaks(s) referenced to Cr was similar, both in normal brain cortex and untreated tumours. The concentration of MM in tumours decreased during the GCV treatment, being ~ 55 % by day 6, compared to the untreated tumour values (**V:** Table 2). There are several possible species of molecules that may contribute to these broad peaks. One of these being macromolecular species, which have been detected, both in normal brain (Behar and Ogino, 1991; Pfeuffer et al., 1999) and brain tumours (van Zijl et al., 2003).

6 Discussion

6.1 Mechanisms of diffusion contrast change in the BT4C gliomas undergoing apoptosis

The present results show that both diffusion and T_2 contrasts reveal apoptotic treatment response in BT4C gliomas with comparable sensitivities and temporal patterns. This observation agrees with other recent studies on the same tumour model (Hakumäki et al., 1998; Poptani et al., 1998a). It is interesting to note that some other MRI studies on experimental brain tumours undergoing gene therapy have indicated that diffusion MRI is more sensitive to early changes associated with positive treatment results (Chenevert et al., 1997; Ross et al., 2002). It is equally important to note that in many of these studies, diffusion has been quantified in absolute terms, but only T_2 weighted MRI has been used. These technical differences may explain the discrepancy between the results presented here and those obtained by others (Chenevert et al., 1997; Ross et al., 2002). Part of the difference may also be due to the inherent properties of the tumour models used. In BT4C glioma both diffusion and T_2 changes are strongly associated with a loss in the numbers of viable tumour cells as well as increases in spin density ratio which reflects the accumulation of water into the eradicating tumour. Cell death was found to be apoptotic in the GCV treated BT4C-tk gliomas (Poptani et al., 1998a; Sandmair et al., 2000a), where the TUNEL positivity precedes actual cell mortality. In this study TUNEL-positive cells were first found in great density in the central zone, where early cell loss was also apparent. Histological observations revealed that cell death became more evident over time, with the highest number of TUNEL-positive cells at day 6 which preceded a period of precipitous cell loss. Good correlations between absolute D_{av} and T_2 MRI data and cell counts, urge the use of quantitative MRI for imaging of treatment response in a clinical settings. This is consistent with previous studies indicating that absolute MRI variables are much more sensitive to changes brought about by pathological processes than the weighted images. It has been reported that in acute ischemic stroke both D_{av} and T_2 show abnormal absolute values well before net water accumulation in the affected tissue (Calamante et al., 1999; Gröhn et al., 1998). A factor further favoring the use of D_{av} over diffusion coefficients acquired with a single gradient axis is that D_{av} is an orientation unbiased MR index of diffusion, where possible anisotropic diffusion inside brain tumours (Mori et al., 2002) does not influence the MRI signal intensity.

Potentially, cell shrinkage during PCD should influence the diffusivity of water, because the intracellular space decreases in shrinking cells. However, this process is associated with a corresponding increase in the extracellular space, which has potentially less restriction for water diffusion. Under these conditions, NMR methods used for determining diffusion may be unable to separate these two events. Indeed, diffusion NMR spectroscopy revealed no indications for an increased restriction in water diffusion during PCD, under the present experimental conditions. Instead, decreased cell counts were strongly associated with an increase in the diffusion coefficient D_1. This D_1 coefficient was obtained by a bi-exponential fit of the diffusion spectroscopy and the D_{av} by MRI. The cell loss causes both a decline in the intracellular space and a corresponding increase in the extracellular volume. This phenomenon, combined with the decreased tortuosity of the extracellular space, could be one of the reasons affecting the diffusion contrast. The change in extracellular/intracellular volume ratio is also supported by diffusion spectroscopy, where an elevation in the f_1 value is observed throughout the t_D range. However, one should always be careful when interpreting the reasons of the changes observed in diffusion constants. Even though they are often

referred to be due to changes in extra- or intra-cellular volume fractions, there are also results suggesting similar water ADCs in both compartments (Duong et al., 1998).

We show that PCD is associated with an increase in the spin density ratio, indicating a net water accumulation. This is a new observation in this gene therapy model. A characteristic of apoptotic cell death is shrinkage in the cytoplasm, so it is highly unexpected that cellular water content would increase during the cell death process. It is therefore more probable that the water retention in eradicating tumour area is primarily taking place in the extracellular space. Increased water content is the most obvious explanation for Hahn echo T_2 MRI contrast. Decreases in the overall protein/water content is likely to contribute to the water diffusion coefficient, as the water molecules translational movement increases because of a dilution of amounts of cell debris, proteins and macromolecules (Cameron et al., 1997) in the enlarging extracellular space during PCD. As well as the viscous tortuosity constituted by cell debris and other cell structural constituents, geometric tortuosity is expected to decrease as well. This is due to the reduced cell density and the enlarged extracellular space (Rusakov and Kullmann, 1998).

It has been reported that the ADC of tCho decreases in the BT4C-tk gliomas during PCD induced by GCV treatment (Hakumäki et al., 1998). This decline should be possible only within compartments surrounded by plasma membrane. Therefore, decreases in tCho ADC may indicate increased viscosity in shrunken cells, a phenomenon known to happen during apoptosis (Kerr et al., 1972). However, we found no signs of increased restriction in water diffusion with scanning parameters used. Instead, we observed a shortening of the apparent water residence time in the D_2 component in the advanced state of PCD. This could be due to the reduction in cell density and the subsequent increasing contribution of extracellular-like water (Pfeuffer et al., 1998). Alternatively, cell shrinkage during apoptosis may account for this phenomenon. It has been suggested that altered water exchange, and the consequent change in their residence times, contributes to the diffusion contrast in drug-treated breast cancer xenografts (Galons et al., 1999). Our results show that water residence time changes only in the advanced stage of PCD, indicating that this mechanism is of significance only in the areas where the tumour has been eradicated.

In diffusion MR experiments *in vivo*, the data acquisition parameters play a key role in the selection of water pools with varying diffusional properties (van Zijl et al., 1994). The benefits of using largely varying b-values in diffusion MRI for assessment of acute brain ischemia (Niendorf et al., 1996), human brain structures and fiber orientations (Clark et al., 2002) have been demonstrated. The clinical scanners are often capable of delivering diffusion MRI with b-values up to 1500 s/mm^2 without prohibitively long TE values, making a low b-value range important. In experimental brain tumours low b-values are commonly used for MRI (Eis et al., 1995; Hakumäki et al., 2002; Poptani et al., 1998a) such as here. We observed that the low b-value range was sensitive to the water diffusion changes associated with both the cell loss and the water accumulation. Indeed, recent clinical studies have shown that in brain tumour patients b-values of 1000 s/mm^2 reveal treatment response to drug therapy better than conventional MRI contrasts (Chenevert et al., 2000; Mardor et al., 2001). This suggests that treatment protocols can be adjusted on a day-to-day basis, depending upon the imaging observations (Mardor et al., 2001).

6.2 CP-T_2 MRI of PCD

A novel T_2 MRI method was introduced for the early detection of gene therapy induced PCD (Hakumäki et al., 2002; Poptani et al., 1998a). A significant change in the CP-T_2 measured with short-τ_{CP} was found in responding tumours on day 2 of the gene therapy regime. The sensitivity of short-τ_{CP} T_2 MRI was roughly equivalent to that of $T_{1\rho}$ in revealing positive treatment responses. A significant advantage of using the short-τ_{CP} CP-T_2 is that the tissue is exposed to much less RF energy than that routinely used in $T_{1\rho}$ MRI (average 48 % of that required by $T_{1\rho}$). High RF energy deposition has been one of the limiting factors in the clinical exploitation of the spin lock methods, such as $T_{1\rho}$. However, adiabatic CP-T_2 measurements have been performed previously on the human head at field strengths up to 7 T (Bartha et al., 2002b), and therefore should be feasible in clinical settings.

The contrast between glioma and normal brain tissue before treatment was weakest with $T_{1\rho}$ and highest with long-τ_{CP} T_2 MRI. These observations disagree with the data of a previous report (Poptani et al., 2001). These discrepancies could be due to differences in the nature of tumour types used. A phenomenon called dynamic dephasing is a substantial contributor to the T_2 signal decay in a tissue. Dynamic dephasing is governed by a loss in the phase coherence as water protons either exchange or diffuse between sites possessing different magnetic properties. The effects of dynamic dephasing in tumour tissue are expected to be small in the spin lock experiments as well as in the short-τ_{CP} T_2 MRI, when conditions approaching spin locking may be reached. Under these MRI conditions the relaxation processes are expected to be weighted more to dipolar interactions, such as possible cross-relaxations, and exchange close to the frequency imposed by the spin lock field. It is known that dipolar effects are sensitive to changes in molecular rotation and vibration rates as well as the distances between the interacting molecules. Changes in cytoarchitecture, cell density and pH occur in tumours undergoing PCD. These factors could also influence the dynamic dephasing contrast and the dipolar interactions, reflected in the different relaxation times determined in responding gliomas.

It was demonstrated that the T_2 contrast can be modified to detect cellular/tissue alterations and thus aid in revealing early treatment response to GCV gene therapy before decreases either in cell count or tumour volume. The long-τ_{CP} T_2 contrast obtained with six π pulses and incremented τ_{CP} (6 – 22 ms) closely resembled the time course and sensitivity reported previously for the Hahn echo T_2 contrast with TEs in the range of 20 – 110 ms (Hakumäki et al., 2002; Poptani et al., 1998a). The time course of CP-T_2 contrast obtained with a constant, short-τ_{CP} was comparable to $T_{1\rho}$ MRI. This is good because the latter MRI measurement is known to precede changes detectable by diffusion MRI (Hakumäki et al., 2002) and is thus one of the most sensitive contrasts to detect cytotoxicity induced cell death in experimental tumour models. It should be noted that exchange is one of the key factors influencing $T_{1\rho}$ signal *in vitro* (Mäkelä et al., 2001) and *in vivo* (Duvvuri et al., 2001). It is speculated that the acidification of the cells cytoplasm (equivalent to an increase in the concentration of free hydrogen ions) in the early moments of apoptosis (Barry and Eastman, 1992; Wolf and Eastman, 1999) may influence the $T_{1\rho}$ contrast obtained at the beginning of the GCV treatment (Hakumäki et al., 2002). However, other factors, such as the increase in tumour water content, are likely to supersede $T_{1\rho}$ contrast during the progression of PCD.

6.3 Metabolite changes in PCD

^{1}H NMR detectable metabolites *in vivo* behave very differently from each other during PCD induced cell loss in the BT4C glioma. In the first group, which includes Gly, Tau and Cr, the concentration of metabolites decline in a time dependent manner largely in a step with the decrease in cell numbers. In the second group, represented by the CCM, ^{1}H NMR detected concentrations stay unchanged despite the decline in cell count until a precipitous collapse of viable cells occurs (Hakumäki et al., 1998). The third group, represented by saturated and polyunsaturated lipids, extensively increase during PCD induced cell death (Hakumäki et al., 1999), a phenomenon which has been also demonstrated in cells (Blankenberg et al., 1996). Thus, the behavior of ^{1}H NMR visible lipids during PCD shows an inverse correlation to those of low molecular weight metabolites such as Gly and Cr. The ^{1}H NMR lipid observation is accounted for by an accumulation of triacylglycerols (Al-Saffar et al., 2002), FFA and cholesterol esters into the tumours which then leads to increases in intracellular and other lipid vesicles (Hakumäki et al., 1999).

A direct comparison of *in vitro* and *in vivo* metabolites against tumour cell count is not straightforward. This is because tissue extractions have been made from only one part of the total tumour volume, whereas the cell counts are derived from the global tumour volume. Nevertheless, *in vivo* and *in vitro* ^{1}H NMR spectroscopic data show a good degree of consistency for several metabolites such as CCM, Gly and Cr. In contrast, the concentrations of *myo*-Ins and Glx both showed discrepancies between the results obtained *in vivo* and *in vitro*. The reasons for these mismatching data are not evident from our results, however, the solubility of metabolites in the PCA may vary. Furthermore, metabolites may also be released during extraction from compartments that do not contribute to the NMR signal *in vivo*. This is possibly the reason behind the greater concentrations of glutamate detected *in vitro* after PCA extraction than inferred by ^{1}H NMR *in situ* (Kauppinen and Williams, 1991).

The present observations strongly indicate that the decline in tCho *in vivo* is only a marker of advanced PCD in ^{1}H NMR spectroscopy. In a human brain tumour study *in vivo*, tCho concentration has been found to correlate with cell density (Gupta et al., 1999). A severe decline in tCho has also been observed in tumours responding to RT (Kizu et al., 1998). In addition, previous BT4C glioma gene therapy studies using STEAM ^{1}H NMR spectroscopy with TE > 20 ms at 9.4 T have noted a decline in Cho *in vivo* (Hakumäki et al., 1998; Hakumäki et al., 1999). Technical differences, such as differing field strengths and TEs, in respect to this study, may explain the discrepancy in ^{1}H NMR tCho behavior in PCD *in vivo*.

Accumulation of CDP-Cho during PCD could maintain the choline containing peak despite severe cell loss, as was demonstrated by multinuclear NMR analyses of leukemia HL-60 cells *in vitro* (Williams et al., 1998). However, we have found no support for this hypothesis, either from ^{1}H or ^{31}P NMR of extracted tumours. CDP-Cho has a singlet at 3.23 ppm and thus overlaps with the tCho peak *in vivo* and the PC peak *in vitro* in the BT4C tumour extracts and *ex vivo* in intact tumours. CDP-Cho co-resonates with PC and GPC, and the upfield component of triplet derived from Tau also contributes to this set of resonances. These peaks, however, can be separated using HRMAS ^{1}H NMR spectroscopy *ex vivo*, and the concentration of Tau was found to decrease as a function of cell numbers, both *in vivo* and *in vitro*. This decrease was found to offset any possible changes in CDP-Cho that may become detectable *in vivo* as part of a combined choline containing resonance. It is likely that previous reports that correlated Cho changes from short TE ^{1}H NMR with the progression of PCD are likely to be confounded by the Tau triplet at 3.26 ppm.

Another plausible explanation for the retained intensity of tCho *in vivo* during PCD, despite high cell death, may be associated with a repartitioning of the metabolites between NMR visible and invisible environments. Components of the ^{1}H NMR detected tCho are unlikely to be membrane bound, because it has been shown that the spinning rates used here are too low to remove the effects of large dipolar couplings between lipids in the cell membranes (Siminovitch et al., 1988). Increases in tCho have been detected after the disruption of cell membrane in cultured hepatocytes, an event that results from the redistribution of membrane PC to the cytosol (Griffin et al., 2001). It is conceivable that in advanced PCD, ^{1}H NMR detected tCho may change due to the disruption of cell membranes and the subsequent leakage of CCM into the cytosol and/or extracellular fluid. This would explain why the tCho resonance remains fairly constant despite severe losses in viable cell numbers, whereas some other low molecular weight metabolites decrease in resonance intensity.

We detected a doublet at 8.01 ppm and two broader resonances at 6.08 and 6.13 ppm in the ^{1}H NMR spectrum of tumours. These are consistent with the C6, C1 and C5 resonances derived from UDP, respectively. The assignments were confirmed by ^{31}P NMR spectroscopy of tissue extracts combined with UDP spiking. Nucleotide resonances have also been detected before in proliferating cell cultures using cell extracts of lymphocytes and HRMAS ^{1}H NMR spectroscopy of intact endometrial cells (Griffin et al., 2003; Sze and Jardetzky, 1994). Uridine is a component of RNA and the pool of UDP may signify the increased synthesis of nucleotides necessary for the replication of proliferative cells. Relatively large concentrations of uridine containing metabolites has also been detected in lymphocytes (Sze and Jardetzky, 1994), testis (Griffin et al., 2000), immortalized cell lines (Griffin et al., 2003), and as these results demonstrate, in rat gliomas.

6.4 Chemical nature and origin of ^{1}H NMR detected lipids

The progression of PCD is characterized by an increase in the ^{1}H NMR lipid derived peaks, in particular in the PUFAs at 5.4 and 2.8 ppm. Since it is known that this technique detects only a special class of cellular lipid (Hakumäki and Kauppinen, 2000). The increase in lipid peaks is thought to reflect an increased number of lipid droplets in the cytoplasm, a phenomenon shown to happen in cells destined to die (Barba et al., 1999; Hakumäki et al., 1998; Lahrech et al., 2001). The HRMAS ^{1}H NMR results from tumour samples *ex vivo* showed no spectral resolution enhancement of lipid peaks when the spinning rates were increased. This argues that the lipids detected are in a rotationally and translationally unrestricted environment with high degree of NMR visibility. However, MAS did result major resolution enhancement of the lower molecular weight metabolites, particularly *myo*-Ins and CCM. These results are consistent with the idea that ^{1}H NMR detectable lipids indeed reside in these cytoplasmic lipid vesicles of cells (Al-Saffar et al., 2002; Barba et al., 1999) and tissue *in vivo* (Hakumäki et al., 1999; Lahrech et al., 2001) The size of vesicles has been determined to be 5 – 10 μm in C6 gliomas (Lahrech et al., 2001). In the droplets, dipolar couplings and magnetic susceptibility effects are still large enough to obscure ^{1}H NMR fine structures in the lipid resonances, as could be done in HRMAS in regard to low molecular weight metabolites. It should be noted that the spin rates used for HRMAS have been found to cause neither functional (Griffin et al., 2002) nor structural (Cheng et al., 1997) damage for the biological specimens. Thus, the recently proposed cytoplasmic lipid droplet formation in PCD (Hakumäki and Kauppinen, 2000; Murphy, 2001) is an attractive explanation for the ^{1}H NMR spectral changes reported here.

Triglycerides (Al-Saffar et al., 2002; Millis et al., 1997; Rosi et al., 1999) and/or other neutral lipids (Delikatny et al., 2002) are the predominant lipid groups contributing to the ^{1}H NMR visible lipids detected in cancer tissue. Accumulation of triglycerides has been attributed to the increase in the 1.3 ppm ^{1}H NMR lipid peak in Jurkat T cells (Al-Saffar et al., 2002) and human breast cancer cells during drug-induced cell death (Delikatny et al., 2002). The biochemical assays performed on BT4C gliomas (Hakumäki et al., 1999) as well as human malignant gliomas (Tugnoli et al., 2001) have shown that they contain high concentrations of triglycerides, which are virtually absent in the normal brain. In addition, they also form the main lipid class in the cytoplasmic lipid vesicles with minor contributions derived from other lipids (Hakumäki and Kauppinen, 2000). During PCD, triglycerides, amongst other lipids, (including cholesterol esters and free fatty acids) increase (Hakumäki et al., 1999). The present *in vivo* and *ex vivo* results indicate that the changes in PUFAs signals are the most descriptive variables for PCD in this rat glioma. In tissue lipid extracts, this biochemical effect is diluted by the extraction of membrane bound lipids that contain a high proportion of saturated lipids. Since only lipids present in vesicles are ^{1}H NMR visible *in situ* (Al-Saffar et al., 2002; Barba et al., 1999; Lahrech et al., 2001), these PUFA resonances and the PUFAs themselves are expected to emanate from the cytoplasmic vesicles. This claim is strongly supported by the diffusion data both *in vivo* and *ex vivo*.

Cells submitted to apoptosis by exposure to cytotoxic drugs show an inhibition in CDP-choline:1,2-diacyl glycerol choline phosphotransferase activity, which leads to the accumulation of CDP-Cho and lipid triglycerides (Anthony et al., 1999; Williams et al., 1998). This biochemical change would provide a reservoir for the triglycerides destined for the lipid vesicles. It would also prevent the clearance of cytoplasmic lipids to PtdCho with a subsequent repartitioning of this compound into cellular membranes. Lipids in vesicles have a greater degree of mobility than in a membranous environment, as supported by diffusion and T_2 NMR data. This would make them become observable by NMR. A hypothesis has been proposed according to which damaged mitochondrial membranes are a source of the ^{1}H NMR observable lipids (Delikatny et al., 2002). It has been reported that during treatment with cytotoxic drugs, the increase in ^{1}H NMR lipids resonating at 5.35, 1.3, and 0.9 ppm was associated with mitochondrial damage, lipid droplet development and formation of autophagic vacuoles. Interestingly, mitochondrial membranes are known to be rich in PUFAs, where they provide increased membrane fluidity. Thus, the 18:1 and 18:2 fatty acids detected are most likely to be contained in the lipid moieties released from these membranes. In fact, our previous biochemical analysis from BT4C glioma indicate that phospholipase A2 activity increase during PCD (Hakumäki et al., 1999), supporting the idea that membrane lipid partitioning could contribute to the increase in ^{1}H NMR spectrometrically detectable lipids.

The observation by Blankenberg *et al.* (Blankenberg et al., 1996) argued for an apoptosis-dependent pathway in cells which also shows an accumulation of $CH_2\mathbf{CH_2}CH_2$ moieties. More recently, Delikatny *et al.* reported that in human breast carcinoma cells, ^{1}H NMR detected lipids accumulate also during necrotic cell damage and in excised brain tumours (Delikatny et al., 2002), suggesting that ^{1}H NMR detected saturated lipids are associated with necrotic histopathology (Kuesel et al., 1994; Tugnoli et al., 2001). In this study, the appearance of PUFAs is evidently associated with PCD. Interestingly localized ^{1}H NMR, performed on tumour scar tissue with low numbers of viable cells, shows that the PUFA and other lipid resonances are still visible with the same ratios as in late stage PCD, suggesting that these lipid bodies remain after cell morbidity. Thus, it is not unexpected that the studies using excised tissue will arrive at the conclusion above, since the separation of necrosis from late stage PCD by histology may not be feasible. Nevertheless, our results demonstrate a time

window in the cell death process when ^{1}H NMR visible PUFA resonances undergo dynamic changes.

6.5 Choline containing compounds and apoptosis

In vivo, the separation of metabolites contributing to the tCho peak is not possible, but it has been used as a marker for treatment success of brain tumours with RT (Kizu et al., 1998; Nelson et al., 1997; Taylor et al., 1996). As a distinction to *in vivo* measurements, Cho, PC and GPC resonances could be resolved as separate peaks when measured with HRMAS *ex vivo* at 700 MHz. At 400 and 600 MHz the resolution was not perfect between PC and GPC, but deconvolution of these resonances was possible at all field strengths using the peak fitting routine within PERCH. ^{1}H HRMAS spectroscopy additionally allows the separation of Tau and *myo*-Ins from tCho without difficulty.

The concentrations of PC and GPC increase in the early phase of PCD at a point when DNA fragmentation occurs but cell density is unchanged. The increased PC and GPC levels may reflect altered metabolism as a result of choline kinase activation, accompanied by simultaneous membrane breakdown through the action of phospholipase enzymes. None of the choline containing metabolites were found to correlate with the decreased cell density during PCD and only the concentration of Tau was found to follow the cell count. Furthermore, no correlation was found between TUNEL-staining and metabolite concentrations, suggesting that the changes in metabolite concentrations occurred on a different time scale from the DNA breakdown measured by TUNEL-staining. A triplet was identified at 3.23 ppm (J_{HH} = 6.7 Hz) in the J-resolved 2D spectrum obtained at 700 MHz, that is consistent with PE, as reported by Rémy *et al.* for the rat C6 glioma model (Rémy et al., 1994). PE has also been observed by Pfeuffer *et al.* (Pfeuffer et al., 1999) in the rat brain *in vivo*, when short TE (2 ms) ^{1}H NMR spectroscopy was used. The PE triplet was only partially observable in some spectra acquired at 700 MHz after good peak fitting with PERCH. In summary, this means that PE will contribute to the resonance intensities of both PC and GPC in the HRMAS spectra.

The broad peaks seen in the spectra could be caused by several small molecular weight metabolites, such as glycerophosphoethanolamine, betaine, carnitine, anserine, phenylalanine and sugar moieties (Fan, 1996). Resonances from macromolecular species, as detected in the aliphatic chemical shift region of cerebral ^{1}H MRS spectra (Behar and Ogino, 1991; Kauppinen et al., 1992; Pfeuffer et al., 1999), could also contribute to these ^{1}H MAS peaks in question. Membrane bound PtdCho (Millis et al., 1999) could also be part of the broad MM peak at 3.27 ppm, however, recent evidence point out to a very short T_2 of membranous CCM (Govindaraju et al., 2000). Indeed, PtdCho has not been detected *in vivo* in spectra using very short TE (2 ms) at a 9.4 T magnetic field strength (Pfeuffer et al., 1999). Another possibility is that one of the assigned species in this chemical shift region of the spectrum is present in a different physico-chemical environment, such as different sub-cellular compartments (Bollard et al., 2003). Although this hypothesis can not be explicitly ruled out by our data, we believe that these broad peaks arise both from the small molecular species indicated above and the macromolecular species known to be ^{1}H NMR detectable both in normal brain (Behar and Ogino, 1991; Kauppinen et al., 1992; Pfeuffer et al., 1999) and in brain tumours (van Zijl et al., 2003).

This study shows that the use of tCho signal at 3.23 ppm in the assessment of the degree of the apoptotic cell death may not be straightforward, as measured *in vivo* with short TE and at high magnetic field strength. tCho does not decline in apoptotic tumours as a function of cell density, but rather their ^{1}H NMR observed concentrations decrease at an advanced stage of PCD (Hakumäki et al., 1999) (**III**). There appears to be major differences in ^{1}H NMR detectable tCho changes between PCD and necrosis (Nelson et al., 1999; Podo, 1999). In treated brain tumours low levels of tCho detected by *in vivo* ^{1}H MRS has been associated to necrosis by histopathology (Nelson et al., 1999). This is also the case in ischemic stroke, which leads to necrotic tissue damage. Here, a decline in tCho is detected by ^{1}H MRS within the first day after the insult (van der Toorn et al., 1994).

The diversity of the brain tumours provides a great challenge for the treatment planning of brain tumour patients. This means that the same protocol does not work for every patient and thus creates great difficulties in finding the correct type of therapy of the individual patient. Methods which would allow us to maintain the effects of treatments clearly would help in the fight against this type of neoplasm. That is the most important reason to study what happens in tumorous tissue after efficient therapy, and to develop methods to reveal the changes. In these studies we have shown the ability of *in vivo* NMR techniques to reveal apoptosis in the experimental glioma prior tumour growth arrest or shrinkage. The extrapolation of the results achieved as such to human brain tumours might not be straightforward, due to the differences between experimental and human glioma as mentioned earlier (see section 2.2.4.3). Additionally in some situations higher magnetic fields and gradient strengths were used than is possible in clinical settings. Even though, there are potential endogenous biomarkers for apoptosis, and we have also shown that a clinically important MRI method that can reveal cytotoxic treatment response earlier than was possible with conventional T_2 MRI. With the NMR methods used here, the visualization of successful treatment response can be seen substantially earlier than the changes in the size of the tumours are observable. This, we believe, will help to make decisions in treatment planning in clinical settings easier.

7 Summary and conclusion

Due to a deficiency in the apoptotic pathway, cells may continue to divide more than is necessary, and this may possibly be the origin of certain types of cancer. Treatment of cancer with chemotherapy or radiation therapy, has been found to lead to apoptotic cell death (Thompson, 1995). Surgery has been traditionally used to remove and classify tumours. However this creates the problem of unintentionally spreading cancers cells. Therefore methods which monitor and classify tumours non-invasively would be a great help. Many studies have been made and methods have been developed for the activation of apoptotic cell death in cancer tissues. As well, very important way of research is concentrated to the non-invasive way of visualizing apoptosis *in situ*. The present results show that *in vivo* NMR techniques can reveal several changes in the tumours undergoing apoptosis that precede tumour growth arrest, cell death and shrinkage. These changes may provide biomolecular markers for monitoring cancer therapy.

The key observations of our study were:

1. Absolute D_{av} and T_2 values were shown to increase with decreasing cell density, highlighting PCD in BT4C gliomas induced by HSV-tk gene therapy. The water microenvironment was altered during the eradication of the tumours, as demonstrated by the increased spin density ratio and water ADC from the fast diffusion component as well as the fractional size of it. There was also a decrease in the water apparent residence time of the slow diffusion component and an increase in the net water content. These support the observation of a reduction in the intracellular volume and an increase in the extracellular space during PCD in the rat BT4C glioma.

2. A novel contrast method for imaging treatment response in the rat BT4C-tk glioma model was introduced. Using CP-T_2 with short spacing between adiabatic refocusing pulses (τ_{CP}), an enhanced sensitivity for cytotoxic cell damage was observed already by day 2 of treatment with GCV, before visible cell loss or a decrease in tumour volume. Thus, CP-T_2 with short-τ_{CP} reacts to changes in a tumour much earlier than has been observed with conventional T_2 MRI (Hakumäki et al., 1999; Poptani et al., 1998a). This improves the MRI contrast technique in a way that is also suitable for clinical use.

3. Only ^{1}H NMR detectable lipids proved to be good indicators of ongoing PCD, whereas no changes were observed within tCho despite severe cell loss. This casts a doubt to the validity of tCho resonance as a good diagnostic marker for PCD *in vivo*. Nucleotides, especially UDP, were detected in the tumour spectra only after treatment, but there were no changes in the concentrations thereafter. Thus, the accumulation of saturated and unsaturated lipids was shown to be the best marker of cell death in BT4C gliomas during HSV-tk gene therapy.

4. As demonstrated in a previous study, the accumulation of lipids is characteristic to this glioma model during HSV-tk GCV induced PCD (Hakumäki et al., 1999). For the characterization of these lipids, *ex vivo* and *in vitro* studies were performed. PUFAs were found to be the most significant contributors to the increased lipid resonances during PCD, mainly constituting from the 18:1 and 18:2 fatty acids. There was no enhancement in resolution after spinning the samples at different rates by MAS,

arguing that lipids are rotationally and translationally in an unrestricted environment. This supports the claim that the lipids in the cytoplasmic vesicles are the source of ^{1}H NMR visible lipids (Barba et al., 1999; Delikatny et al., 2002; Hakumäki et al., 1999; Lahrech et al., 2001). Partitioning of the membrane lipids was proposed to underlie the observed dynamic ^{1}H NMR changes in lipid derived spectral peaks.

5. The metabolites contributing to the tCho peak *in vivo*, and their reactions to the decreased cell density during PCD in BT4C gliomas were studied. Cho, PC, GPC, Tau, *myo*-Ins and macromolecules were shown to contribute to the tCho region seen *in vivo* by using HRMAS. None of the choline containing compounds decreased with cell density down to 60 % of the original level. Only the concentrations of Tau followed cell density, possibly being responsible for the observed decrease in tCho concentration after RT *in vivo* (Rémy et al., 1994). In summary, over a 50 % cell loss in a glioma after PCD is not necessarily associated with decline in choline containing compounds.

In this study, we have examined the apoptotic cell death from several points of view in the rat BT4C-tk glioma model treated with GCV, using multimodal NMR techniques. Several potential biomarkers for apoptosis can be revealed, expanding our understanding of the biomolecular and biophysical changes behind the NMR data in the apoptotic BT4C glioma. With the methods used here, the cytotoxic treatment response can be observed in an early phase of therapy. It may also be possible to use some of them in a clinical environment, allowing for the more efficient management of cancer.

8 References

Aboagye, E. O., and Bhujwalla, Z. M. (1999). Malignant transformation alters membrane choline phospholipid metabolism of human mammary epithelial cells. Cancer Res *59*, 80-84.

Ackerstaff, E., Pflug, B. R., Nelson, J. B., and Bhujwalla, Z. M. (2001). Detection of increased choline compounds with proton nuclear magnetic resonance spectroscopy subsequent to malignant transformation of human prostatic epithelial cells. Cancer Res *61*, 3599-3603.

Aghi, M., Hochberg, F., and Breakefield, X. O. (2000). Prodrug activation enzymes in cancer gene therapy. J Gene Med *2*, 148-164.

Aguayo, J. B., Blackband, S. J., Schoeniger, J., Mattingly, M. A., and Hintermann, M. (1986). Nuclear magnetic resonance imaging of a single cell. Nature *322*, 190-191.

Aguilar, L. K., and Aguilar-Cordova, E. (2003). Evolution of a gene therapy clinical trial. From bench to bedside and back. J Neurooncol *65*, 307-315.

Ala-Korpela, M., Posio, P., Mattila, S., Korhonen, A., and Williams, S. R. (1996). Absolute quantification of phospholipid metabolites in brain-tissue extracts by 1H NMR spectroscopy. J Magn Reson B *113*, 184-189.

Al-Saffar, N. M., Titley, J. C., Robertson, D., Clarke, P. A., Jackson, L. E., Leach, M. O., and Ronen, S. M. (2002). Apoptosis is associated with triacylglycerol accumulation in Jurkat T-cells. Br J Cancer *86*, 963-970.

Andrew, E. (1971). The narrowing of NMR spectra of solids by high-speed specimen rotation and the resolution of chemical shift and spin multiplet structures for solids, Vol 8 (Oxford, Pergamon Press).

Anthony, M. L., Zhao, M., and Brindle, K. M. (1999). Inhibition of phosphatidylcholine biosynthesis following induction of apoptosis in HL-60 cells. J Biol Chem *274*, 19686-19692.

Aronen, H. J., Gazit, I. E., Louis, D. N., Buchbinder, B. R., Pardo, F. S., Weisskoff, R. M., Harsh, G. R., Cosgrove, G. R., Halpern, E. F., Hochberg, F. H., and et al. (1994). Cerebral blood volume maps of gliomas: comparison with tumor grade and histologic findings. Radiology *191*, 41-51.

Asher, A. L., Mule, J. J., Kasid, A., Restifo, N. P., Salo, J. C., Reichert, C. M., Jaffe, G., Fendly, B., Kriegler, M., and Rosenberg, S. A. (1991). Murine tumor cells transduced with the gene for tumor necrosis factor-alpha. Evidence for paracrine immune effects of tumor necrosis factor against tumors. J Immunol *146*, 3227-3234.

Barba, I., Cabanas, M. E., and Arus, C. (1999). The relationship between nuclear magnetic resonance-visible lipids, lipid droplets, and cell proliferation in cultured C6 cells. Cancer Res *59*, 1861-1868.

Barry, M. A., and Eastman, A. (1992). Endonuclease activation during apoptosis: the role of cytosolic Ca2+ and pH. Biochem Biophys Res Commun *186*, 782-789.

Bartha, R., Michaeli, S., Merkle, H., Adriany, G., Andersen, P., Chen, W., Ugurbil, K., and Garwood, M. (2002a). In vivo $^{1}H_2O$ T_2^* Measurement in the Human Occipital Lobe at 4T by Carr-Purcell MRI: Detection of Microscopic Susceptibility Contrast. Magnetic resonance in medicine, 742-750.

Bartha, R., Michaeli, S., Merkle, H., Adriany, G., Andersen, P., Chen, W., Ugurbil, K., and Garwood, M. (2002b). In vivo 1H2O T2+ measurement in the human occipital lobe at 4T and 7T by Carr-Purcell MRI: detection of microscopic susceptibility contrast. Magn Reson Med *47*, 742-750.

Barton, S. J., Howe, F. A., Tomlins, A. M., Cudlip, S. A., Nicholson, J. K., Bell, B. A., and Griffiths, J. R. (1999). Comparison of in vivo 1H MRS of human brain tumours with 1H HR-MAS spectroscopy of intact biopsy samples in vitro. Magma *8*, 121-128.

Bax, A., and Davis, D. G. (1985). Practical Aspects of Two-Dimensional Transverse NOE Spectroscopy. Journal of Magnetic Resonance *63*, 207-213.

Beckwith-Hall, B. M., Nicholson, J. K., Nicholls, A. W., Foxall, P. J., Lindon, J. C., Connor, S. C., Abdi, M., Connelly, J., and Holmes, E. (1998). Nuclear magnetic resonance spectroscopic and principal components analysis investigations into biochemical effects of three model hepatotoxins. Chem Res Toxicol *11*, 260-272.

Behar, K. L., and Ogino, T. (1991). Assignment of resonance in the 1H spectrum of rat brain by two-dimensional shift correlated and J-resolved NMR spectroscopy. Magn Reson Med *17*, 285-303.

Benchetrit, F., Ciree, A., Vives, V., Warnier, G., Gey, A., Sautes-Fridman, C., Fossiez, F., Haicheur, N., Fridman, W. H., and Tartour, E. (2002). Interleukin-17 inhibits tumor cell growth by means of a T-cell-dependent mechanism. Blood *99*, 2114-2121.

Benedetti, S., Bruzzone, M. G., Pollo, B., DiMeco, F., Magrassi, L., Pirola, B., Cirenei, N., Colombo, M. P., and Finocchiaro, G. (1999). Eradication of rat malignant gliomas by retroviral-mediated, in vivo delivery of the interleukin 4 gene. Cancer Res *59*, 645-652.

Bese, N. S., Uzel, O., Turkan, S., and Okkan, S. (1998). Continuous hyperfractionated accelerated radiotherapy in the treatment of high-grade astrocytomas. Radiother Oncol *47*, 197-200.

Beuthien-Baumann, B., Hahn, G., Winkler, C., and Heubner, G. (2003). Differentiation between recurrent tumor and radiation necrosis in a child with anaplastic ependymoma after chemotherapy and radiation therapy. Strahlenther Onkol *179*, 819-822.

Bhakoo, K. K., Williams, S. R., Florian, C. L., Land, H., and Noble, M. D. (1996). Immortalization and transformation are associated with specific alterations in choline metabolism. Cancer Res *56*, 4630-4635.

Blackband, S. J., Buckley, D. L., Bui, J. D., and Phillips, M. I. (1999). NMR microscopy--beginnings and new directions. Magma *9*, 112-116.

Blankenberg, F. G., Katsikis, P. D., Storrs, R. W., Beaulieu, C., Spielman, D., Chen, J. Y., Naumovski, L., and Tait, J. F. (1997). Quantitative analysis of apoptotic cell death using proton nuclear magnetic resonance spectroscopy. Blood *89*, 3778-3786.

Blankenberg, F. G., Storrs, R. W., Naumovski, L., Goralski, T., and Spielman, D. (1996). Detection of apoptotic cell death by proton nuclear magnetic resonance spectroscopy. Blood *87*, 1951-1956.

Blankenberg, F. G., Tait, J. F., and Strauss, W. (2000a). Apoptotic cell death: its impilcations for imaging in the next millenium. European Journal of Nuclear Medicine *27*, 359-367.

Blankenberg, F. G., Tait, J. F., and Strauss, W. (2000b). Apoptotic cell death: its implications for imaging in the next millennium. European Journal of Nuclear Medicine *27*, 359-367.

Bollard, M. E., Murray, A. J., Clarke, K., Nicholson, J. K., and Griffin, J. L. (2003). A study of metabolic compartmentation in the rat heart and cardiac mitochondria using high-resolution magic angle spinning 1H NMR spectroscopy. FEBS Lett *553*, 73-78.

Brown, M. A., and Semelka, R. C. (1995). MRI: Basic principles and applicatons, John Wiley & Sons).

Bryant, R. G., Marill, K., Blackmore, C., and Francis, C. (1990). Magnetic Relaxation in Blood and Blood Clots. Magnetic resonance in medicine *13*, 133-144.

Burger, P. C., Vogel, F. S., Green, S. B., and Strike, T. A. (1985). Glioblastoma multiforme and anaplastic astrocytoma. Pathologic criteria and prognostic implications. Cancer *56*, 1106-1111.

Calamante, F., Lythgoe, M. F., Pell, G. S., Thomas, D. L., King, M. D., Busza, A. L., Sotak, C. H., Williams, S. R., Ordidge, R. J., and Gadian, D. G. (1999). Early changes in water diffusion, perfusion, T1, and T2 during focal cerebral ischemia in the rat studied at 8.5 T. Magn Reson Med *41*, 479-485.

Cameron, I. L., Kanal, K. M., Keener, C. R., and Fullerton, G. D. (1997). A mechanistic view of the non-ideal osmotic and motional behavior of intracellular water. Cell Biol Int *21*, 99-113.

Carr, H., and Purcell, E. (1954). Effects of diffusion on free precession in nuclear magnetic resonance experiments. Physical Review *94*, 630-638.

Castillo, M., Smith, J. K., and Kwock, L. (2000). Correlation of myo-inositol levels and grading of cerebral astrocytomas. AJNR Am J Neuroradiol *21*, 1645-1649.

Castillo, M., Smith, J. K., Kwock, L., and Wilber, K. (2001). Apparent diffusion coefficients in the evaluation of high-grade cerebral gliomas. AJNR Am J Neuroradiol *22*, 60-64.

Cha, S., Johnson, G., Wadghiri, Y. Z., Jin, O., Babb, J., Zagzag, D., and Turnbull, D. H. (2003). Dynamic, contrast-enhanced perfusion MRI in mouse gliomas: correlation with histopathology. Magn Reson Med *49*, 848-855.

Chan, A. A., Lau, A., Pirzkall, A., Chang, S. M., Verhey, L. J., Larson, D., McDermott, M. W., Dillon, W. P., and Nelson, S. J. (2004). Proton magnetic resonance spectroscopy imaging in the evaluation of patients undergoing gamma knife surgery for Grade IV glioma. J Neurosurg *101*, 467-475.

Chang, J. W., Lee, H., Kim, E., Lee, Y., Chung, S. S., and Kim, J. H. (2000). Combined antitumor effects of an adenoviral cytosine deaminase/thymidine kinase fusion gene in rat C6 glioma. Neurosurgery *47*, 931-938; discussion 938-939.

Chang, S. M., Lamborn, K. R., Malec, M., Larson, D., Wara, W., Sneed, P., Rabbitt, J., Page, M., Nicholas, M. K., and Prados, M. D. (2004). Phase II study of temozolomide and thalidomide with radiation therapy for newly diagnosed glioblastoma multiforme. Int J Radiat Oncol Biol Phys *60*, 353-357.

Chen, J. H., Enloe, B. M., Weybright, P., Campbell, N., Dorfman, D., Fletcher, C. D., Cory, D. G., and Singer, S. (2002). Biochemical correlates of thiazolidinedione-induced adipocyte differentiation by high-resolution magic angle spinning NMR spectroscopy. Magn Reson Med *48*, 602-610.

Chen, S.-H., Shine, H. D., Goodman, J. C., and Grossman, R. G. (1994). Gene therapy for brain tumors: Regression of experimental gliomas by adenovirus-mediated gene transfer in vivo. Proceedings of the National Academy of Sciences of the USA *91*, 3054-3057.

Chenevert, T. L., McKeever, P. E., and Ross, B. D. (1997). Monitoring early response of experimental brain tumors to therapy using diffusion magnetic resonance imaging. Clin Cancer Res *3*, 1457-1466.

Chenevert, T. L., Stegman, L. D., Taylor, J. M., Robertson, P. L., Greenberg, H. S., Rehemtulla, A., and Ross, B. D. (2000). Diffusion magnetic resonance imaging: an early surrogate marker of therapeutic efficacy in brain tumors. J Natl Cancer Inst *92*, 2029-2036.

Cheng, L. L., Chang, I. W., Smith, B. L., and Gonzalez, R. G. (1998). Evaluating human breast ductal carcinomas with high-resolution magic-angle spinning proton magnetic resonance spectroscopy. J Magn Reson *135*, 194-202.

Cheng, L. L., Lean, C., Bogdanova, A., Wright, S. C., Jr, Ackerman, J. L., Brady, T. J., and Garrido, L. (1996a). Enhanced, Resolution of Proton NMR Spectra of Malignant Lymph Nodes Using Magic-Angle Spinning. Magnetic resonance in medicine *36*, 653-658.

Cheng, L. L., Lean, C. L., Bogdanova, A., Wright, S. C., Jr., Ackerman, J. L., Brady, T. J., and Garrido, L. (1996b). Enhanced resolution of proton NMR spectra of malignant lymph nodes using magic-angle spinning. Magn Reson Med *36*, 653-658.

Cheng, L. L., Ma, M., Becerra, L., Ptak, T., Tracey, I., Lackner, A., and González, R. G. (1997). Quantitative neuropathology by high resolution magic angle spinning proton magnetic resonance spectroscopy. Proceedings of the National Academy of Sciences of the USA *94*, 6408-6413.

Chiocca, E. A., Abbed, K. M., Tatter, S., Louis, D. N., Hochberg, F. H., Barker, F., Kracher, J., Grossman, S. A., Fisher, J. D., Carson, K.*, et al.* (2004). A phase I open-label, dose-escalation, multi-institutional trial of injection with an E1B-Attenuated adenovirus, ONYX-015, into the peritumoral region of recurrent malignant gliomas, in the adjuvant setting. Mol Ther *10*, 958-966.

Clark, C. A., Hedehus, M., and Moseley, M. E. (2002). In vivo mapping of the fast and slow diffusion tensors in human brain. Magn Reson Med *47*, 623-628.

Conn, G., Soderman, D. D., Schaeffer, M. T., Wile, M., Hatcher, V. B., and Thomas, K. A. (1990). Purification of a glycoprotein vascular endothelial cell mitogen from a rat glioma-derived cell line. Proc Natl Acad Sci U S A *87*, 1323-1327.

Cooper, G. M. (2000). The Cell, A Molecular Approach, 2nd edn).

Croteau, D., Scarpace, L., Hearshen, D., Gutierrez, J., Fisher, J. L., Rock, J. P., and Mikkelsen, T. (2001). Correlation between Magnetic Resonance Spectroscopy Imaging-guided Biopsies: Semiquantitative and Qualitative Histopathological Analyses of Patients with Untreated Glioma. Neurosurgery *49*, 823-829.

Dalrymple, S. J., Parisi, J. E., Roche, P. C., Ziesmer, S. C., Scheithauer, B. W., and Kelly, P. J. (1994). Changes in proliferating cell nuclear antigen expression in glioblastoma multiforme cells along a stereotactic biopsy trajectory. Neurosurgery *35*, 1036-1044; discussion 1044-1035.

Darzynkiewicz, Z. (1995). Apoptosis in antitumor strategies: modulation of cell cycle or differentiation. J Cell Biochem *58*, 151-159.

Daumas-Duport, C., Scheithauer, B., O'Fallon, J., and Kelly, P. (1988). Grading of astrocytomas. A simple and reproducible method. Cancer *62*, 2152-2165.

Delikatny, E. J., Cooper, W. A., Brammah, S., Sathasivam, N., and Rideout, D. C. (2002). Nuclear magnetic resonance-visible lipids induced by cationic lipophilic chemotherapeutic agents are accompanied by increased lipid droplet formation and damaged mitochondria. Cancer Res *62*, 1394-1400.

Dilber, M. S., Abedi, M. R., Christensson, B., Bjorkstrand, B., Kidder, G. M., Naus, C. C., Gahrton, G., and Smith, C. I. (1997). Gap junctions promote the bystander effect of herpes simplex virus thymidine kinase in vivo. Cancer Res *57*, 1523-1528.

Dowling, C., Bollen, A. W., Noworolski, S. M., McDermott, M. W., Barbaro, N. M., Day, M. R., Henry, R. G., Chang, S. M., Dillon, W. P., Nelson, S. J., and Vigneron, D. B. (2001). Preoperative proton MR spectroscopic imaging of brain tumors: correlation with histopathologic analysis of resection specimens. AJNR Am J Neuroradiol *22*, 604-612.

Dranoff, G., Jaffee, E., Lazenby, A., Golumbek, P., Levitsky, H., Brose, K., Jackson, V., Hamada, H., Pardoll, D., and Mulligan, R. C. (1993). Vaccination with irradiated tumor cells engineered to secrete murine granulocyte-macrophage colony-stimulating factor stimulates potent, specific, and long-lasting anti-tumor immunity. Proc Natl Acad Sci U S A *90*, 3539-3543.

Dubben, H. H., Thames, H. D., and Beck-Bornholdt, H. P. (1998). Tumor volume: a basic and specific response predictor in radiotherapy. Radiother Oncol *47*, 167-174.

Duong, T. Q., Ackerman, J. J., Ying, H. S., and Neil, J. J. (1998). Evaluation of extra- and intracellular apparent diffusion in normal and globally ischemic rat brain via 19F NMR. Magn Reson Med *40*, 1-13.

Duvvuri, U., Goldberg, A. D., Kranz, J. K., Hoang, L., Reddy, R., Wehrli, F. W., Wand, A. J., Englander, S. W., and Leigh, J. S. (2001). Water magnetic relaxation dispersion in biological systems: the contribution of proton exchange and implications for the noninvasive detection of cartilage degradation. Proc Natl Acad Sci U S A *98*, 12479-12484.

Edelman, R. R., and Warach, S. (1993). Magnetic Resonance Imaging. The New England Journal of Medicine *382*, 708-716, 785-791.

Eis, M., Els, T., and Hoehn-Berlage, M. (1995). High resolution quantitative relaxation and diffusion MRI of three different experimental brain tumors in rat. Magnetic resonance in medicine *34*, 835-844.

Erickson, S. J., Prost, R. W., and Timins, M. E. (1993). The "Magic Angle" Effect: Background Physics and Clinical Relevance. Radiology, 23-25.

Escargueil-Blanc, I., Salvayre, R., and Negre-Salvayre, A. (1994). Necrosis and apoptosis induced by oxidized low density lipoproteins occur through two calcium-dependent pathways in lymphoblastoid cells. Faseb J *8*, 1075-1080.

Evelhoch, J. L., Gillies, R. J., Karczmar, G. S., Koutcher, J. A., Maxwell, R. J., Nalcioglu, O., Raghunand, N., Ronen, S. M., Ross, B. D., and Swartz, H. M. (2000). Applications of magnetic resonance in model systems: cancer therapeutics. Neoplasia *2*, 152-165.

Evelhoch, J. L., LoRusso, P. M., He, Z., DelProposto, Z., Polin, L., Corbett, T. H., Langmuir, P., Wheeler, C., Stone, A., Leadbetter, J.*, et al.* (2004). Magnetic resonance imaging measurements of the response of murine and human tumors to the vascular-targeting agent ZD6126. Clin Cancer Res *10*, 3650-3657.

Fan, T. (1996). Metabolite profiling by one- and two-dimensional NMR analysis of complex mixtures. Prog Nucl Magn Reson Spectr *28*, 161-219.

Feldman, A. L., and Libutti, S. K. (2000). Progress in antiangiogenic gene therapy of cancer. Cancer *89*, 1181-1194.

Ferrara, N., and Henzel, W. J. (1989). Pituitary follicular cells secrete a novel heparin-binding growth factor specific for vascular endothelial cells. Biochem Biophys Res Commun *161*, 851-858.

Fine, H. A., Dear, K. B., Loeffler, J. S., Black, P. M., and Canellos, G. P. (1993). Meta-analysis of radiation therapy with and without adjuvant chemotherapy for malignant gliomas in adults. Cancer *71*, 2585-2597.

Florell, R. C., Macdonald, D. R., Irish, W. D., Bernstein, M., Leibel, S. A., Gutin, P. H., and Cairncross, J. G. (1992). Selection bias, survival, and brachytherapy for glioma. J Neurosurg *76*, 179-183.

Folch, J., Lees, M., and Sloane Stanley, G. H. (1957). A simple method for the isolation and purification of total lipides from animal tissues. J Biol Chem *226*, 497-509.

Folkman, J., and Shing, Y. (1992). Angiogenesis. J Biol Chem *267*, 10931-10934.

Frankel, B., Longo, S. L., Kyle, M., Canute, G. W., and Ryken, T. C. (2001). Tumor Fas (APO-1/CD95) up-regulation results in increased apoptosis and survival times for rats with intracranial malignant gliomas. Neurosurgery *49*, 168-175; discussion 175-166.

Fulham, M. J., Bizzi, A., Dietz, M. J., Shih, H. H., Raman, R., Sobering, G. S., Frank, J. A., Dwyer, A. J., Alger, J. R., and Di Chiro, G. (1992). Mapping of brain tumor metabolites with proton MR spectroscopic imaging: clinical relevance. Radiology *185*, 675-686.

Gadi, V. K., Alexander, S. D., Waud, W. R., Allan, P. W., Parker, W. B., and Sorscher, E. J. (2003). A long-acting suicide gene toxin, 6-methylpurine, inhibits slow growing tumors after a single administration. J Pharmacol Exp Ther *304*, 1280-1284.

Gadian, D. G. (1995). NMR and its applications to living systems, 2nd edn, Oxford University Press).

Galons, J. P., Altbach, M. I., Paine-Murrieta, G. D., Taylor, C. W., and Gillies, R. J. (1999). Early increases in breast tumor xenograft water mobility in response to paclitaxel therapy detected by non-invasive diffusion magnetic resonance imaging. Neoplasia *1*, 113-117.

Gansbacher, B., Bannerji, R., Daniels, B., Zier, K., Cronin, K., and Gilboa, E. (1990). Retroviral vector-mediated gamma-interferon gene transfer into tumor cells generates potent and long lasting antitumor immunity. Cancer Res *50*, 7820-7825.

Garwood, M., and DelaBarre, L. (2001). The return of the frequency sweep: designing adiabatic pulses for contemporary NMR. J Magn Reson *153*, 155-177.

Gatenby, R. A., Kessler, H. B., Rosenblum, J. S., Coia, L. R., Moldofsky, P. J., Hartz, W. H., and Broder, G. J. (1988). Oxygen distribution in squamous cell carcinoma metastases and its relationship to outcome of radiation therapy. Int J Radiat Oncol Biol Phys *14*, 831-838.

Gauvain, K. M., McKinstry, R. C., Mukherjee, P., Perry, A., Neil, J. J., Kaufman, B. A., and Hayashi, R. J. (2001). Evaluating pediatric brain tumor cellularity with diffusion-tensor imaging. AJR Am J Roentgenol *177*, 449-454.

Ge, K., Xu, L., Zheng, Z., Xu, D., Sun, L., and Liu, X. (1997). Transduction of cytosine deaminase gene makes rat glioma cells highly sensitive to 5-fluorocytosine. Int J Cancer *71*, 675-679.

Gill, S. S., Thomas, D. G., Van Bruggen, N., Gadian, D. G., Peden, C. J., Bell, J. D., Cox, I. J., Menon, D. K., Iles, R. A., Bryant, D. J., and et al. (1990). Proton MR spectroscopy of intracranial tumours: in vivo and in vitro studies. J Comput Assist Tomogr *14*, 497-504.

Goldman, C. K., Kendall, R. L., Cabrera, G., Soroceanu, L., Heike, Y., Gillespie, G. Y., Siegal, G. P., Mao, X., Bett, A. J., Huckle, W. R., *et al.* (1998). Paracrine expression of a native soluble vascular endothelial growth factor receptor inhibits tumor growth, metastasis, and mortality rate. Proc Natl Acad Sci U S A *95*, 8795-8800.

Govindaraju, V., Young, K., and Maudsley, A. A. (2000). Proton NMR chemical shifts and coupling constants for brain metabolites. NMR Biomed *13*, 129-153.

Gribbestad, I. S., Petersen, S. B., Fjosne, H. E., Kvinnsland, S., and Krane, J. (1994). 1H NMR spectroscopic characterization of perchloric acid extracts from breast carcinomas and non-involved breast tissue. NMR Biomed *7*, 181-194.

Griebel, J., Mayr, N. A., de Vries, A., Knopp, M. V., Gneiting, T., Kremser, C., Essig, M., Hawighorst, H., Lukas, P. H., and Yuh, W. T. (1997). Assessment of tumor microcirculation: a new role of dynamic contrast MR imaging. J Magn Reson Imaging *7*, 111-119.

Griffin, J. L., Bollard, M., Nicholson, J. K., and Bhakoo, K. (2002). Spectral profiles of cultured neuronal and glial cells derived from HRMAS (1)H NMR spectroscopy. NMR Biomed *15*, 375-384.

Griffin, J. L., Mann, C. J., Scott, J., Shoulders, C. C., and Nicholson, J. K. (2001). Choline containing metabolites during cell transfection: an insight into magnetic resonance spectroscopy detectable changes. FEBS Lett *509*, 263-266.

Griffin, J. L., Pole, J. C., Nicholson, J. K., and Carmichael, P. L. (2003). Cellular environment of metabolites and a metabonomic study of tamoxifen in endometrial cells using gradient high

resolution magic angle spinning 1H NMR spectroscopy. Biochim Biophys Acta *1619*, 151-158.

Griffin, J. L., Troke, J., Walker, L. A., Shore, R. F., Lindon, J. C., and Nicholson, J. K. (2000). The biochemical profile of rat testicular tissue as measured by magic angle spinning 1H NMR spectroscopy. FEBS Lett *486*, 225-229.

Grohn, O. H., Lukkarinen, J. A., Oja, J. M., van Zijl, P. C., Ulatowski, J. A., Traystman, R. J., and Kauppinen, R. A. (1998). Noninvasive detection of cerebral hypoperfusion and reversible ischemia from reductions in the magnetic resonance imaging relaxation time, T2. J Cereb Blood Flow Metab *18*, 911-920.

Gross, M. W., Weber, W. A., Feldmann, H. J., Bartenstein, P., Schwaiger, M., and Molls, M. (1998). The value of F-18-fluorodeoxyglucose PET for the 3-D radiation treatment planning of malignant gliomas. Int J Radiat Oncol Biol Phys *41*, 989-995.

Gruetter, R. (1993). Automatic, localized in vivo adjustment of all first- and second-order shim coils. Magn Reson Med *29*, 804-811.

Gupta, R. K., Cloughesy, T. F., Sinha, U., Garakian, J., Lazareff, J., Rubino, G., Rubino, L., Becker, D. P., Vinters, H. V., and Alger, J. R. (2000). Relationships between choline magnetic resonance spectroscopy, apparent diffusion coefficient and quantitative histopathology in human glioma. J Neurooncol *50*, 215-226.

Gupta, R. K., Sinha, U., Cloughesy, T. F., and Alger, J. R. (1999). Inverse correlation between choline magnetic resonance spectroscopy signal intensity and the apparent diffusion coefficient in human glioma. Magn Reson Med *41*, 2-7.

Hakumäki, J. M., Grohn, O. H., Tyynela, K., Valonen, P., Yla-Herttuala, S., and Kauppinen, R. A. (2002). Early gene therapy-induced apoptotic response in BT4C gliomas by magnetic resonance relaxation contrast T1 in the rotating frame. Cancer Gene Ther *9*, 338-345.

Hakumäki, J. M., and Kauppinen, R. A. (2000). 1H NMR visible lipids in the life and death of cells. Trends Biochem Sci *25*, 357-362.

Hakumäki, J. M., Poptani, H., Puumalainen, A. M., Loimas, S., Paljarvi, L. A., Ylä-Herttuala, S., and Kauppinen, R. A. (1998). Quantitative 1H nuclear magnetic resonance diffusion spectroscopy of BT4C rat glioma during thymidine kinase-mediated gene therapy in vivo: identification of apoptotic response. Cancer Res *58*, 3791-3799.

Hakumäki, J. M., Poptani, H., Sandmair, A.-M., Ylä-Herttuala, S., and Kauppinen, R. A. (1999). 1H MRS detects polyunsaturated fatty acid accumulation during gene therapy of glioma: Implications for the in vivo detection of apoptosis. Nature medicine *5*, 1323-1327.

Hawighorst, H., Engenhart, R., Knopp, M. V., Brix, G., Grandy, M., Essig, M., Miltner, P., Zuna, I., Fuss, M., and van Kaick, G. (1997). Intracranial meningeomas: time- and dose-dependent effects of irradiation on tumor microcirculation monitored by dynamic MR imaging. Magn Reson Imaging *15*, 423-432.

Hawighorst, H., Knopp, M. V., Debus, J., Hoffmann, U., Grandy, M., Griebel, J., Zuna, I., Essig, M., Schoenberg, S. O., DeVries, A.*, et al.* (1998). Pharmacokinetic MRI for assessment of malignant glioma response to stereotactic radiotherapy: initial results. J Magn Reson Imaging *8*, 783-788.

Hein, P. A., Kremser, C., Judmaier, W., Griebel, J., Pfeiffer, K. P., Kreczy, A., Hug, E. B., Lukas, P., and DeVries, A. F. (2003). Diffusion-weighted magnetic resonance imaging for monitoring diffusion changes in rectal carcinoma during combined, preoperative chemoradiation: preliminary results of a prospective study. Eur J Radiol *45*, 214-222.

Hengartner, M. O. (2000). The biochemistry of apoptosis. Nature *407*, 770-776.

Hirakawa, T., Maruyama, K., Kohl, N. E., Kodama, T., and Ruley, H. E. (1991). Massive accumulation of neutral lipids in cells conditionally transformed by an activated H-ras oncogene. Oncogene *6*, 289-295.

Hollstein, M., Shomer, B., Greenblatt, M., Soussi, T., Hovig, E., Montesano, R., and Harris, C. C. (1996). Somatic point mutations in the p53 gene of human tumors and cell lines: updated compilation. Nucleic Acids Res *24*, 141-146.

Hollstein, M., Sidransky, D., Vogelstein, B., and Harris, C. C. (1991). p53 mutations in human cancers. Science *253*, 49-53.

Holsti, L. R., Roberts, P. J., and Teppo, L., eds. (1992). Syöpätaudit (Kustannus Oy Duodecim).

Howe, F., Barton, S., Cudlip, S., Stubbs, M., Saunders, D., Murphy, M., Wilkins, P., Opstad, K., McLean, M., Bell, B., and Griffiths, J. (2003). Metabolic Profiles of Human Brain Tumors Using Quantitative In Vivo 1H Magnetic Resonance Spectroscopy. Magnetic resonance in Medicine *49*, 223-232.

Huisman, T. A. (2003). Diffusion-weighted imaging: basic concepts and application in cerebral stroke and head trauma. Eur Radiol *13*, 2283-2297.

Hurd, R. E. (1990). Gradient-enhanced spectroscopy. Journal of Magnetic Resonance *87*, 422-428.

Huxtable, R. J. (1992). Physiological actions of taurine. Physiol Rev *72*, 101-163.

Ikeda, E., Achen, M. G., Breier, G., and Risau, W. (1995). Hypoxia-induced transcriptional activation and increased mRNA stability of vascular endothelial growth factor in C6 glioma cells. J Biol Chem *270*, 19761-19766.

Im, S. A., Gomez-Manzano, C., Fueyo, J., Liu, T. J., Ke, L. D., Kim, J. S., Lee, H. Y., Steck, P. A., Kyritsis, A. P., and Yung, W. K. (1999). Antiangiogenesis treatment for gliomas: transfer of antisense-vascular endothelial growth factor inhibits tumor growth in vivo. Cancer Res *59*, 895-900.

Immonen, A., Vapalahti, M., Tyynela, K., Hurskainen, H., Sandmair, A., Vanninen, R., Langford, G., Murray, N., and Yla-Herttuala, S. (2004). AdvHSV-tk gene therapy with intravenous ganciclovir improves survival in human malignant glioma: a randomised, controlled study. Mol Ther *10*, 967-972.

Ishimaru, H., Morikawa, M., Iwanaga, S., Kaminogo, M., Ochi, M., and Hayashi, K. (2001). Differentiation between high-grade glioma and metastatic brain tumor using single-voxel proton MR spectroscopy. Eur Radiol *11*, 1784-1791.

Isobe, T., Matsumura, A., Anno, I., Yoshizawa, T., Nagamoto, Y., Itai, Y., and Nose, T. (2002). Quantification of cerebral metabolites in glioma patients with proton MR spectroscopy using T2 relaxation time correction. Magnetic Resonance Imaging *20*, 343-349.

Jackowski, S. (1994). Coordination of membrane phospholipid synthesis with the cell cycle. J Biol Chem *269*, 3858-3867.

Jackowski, S. (1996). Cell cycle regulation of membrane phospholipid metabolism. J Biol Chem *271*, 20219-20222.

Jackson, A., Kassner, A., Annesley-Williams, D., Reid, H., Zhu, X. P., and Li, K. L. (2002). Abnormalities in the recirculation phase of contrast agent bolus passage in cerebral gliomas: comparison with relative blood volume and tumor grade. AJNR Am J Neuroradiol *23*, 7-14.

Jemal, A., Murray, T., Samuels, A., Ghafoor, A., Ward, E., and Thun, M. J. (2003). Cancer statistics, 2003. CA Cancer J Clin *53*, 5-26.

Kallinowski, F., Schlenger, K. H., Kloes, M., Stohrer, M., and Vaupel, P. (1989a). Tumor blood flow: the principal modulator of oxidative and glycolytic metabolism, and of the metabolic micromilieu of human tumor xenografts in vivo. Int J Cancer *44*, 266-272.

Kallinowski, F., Schlenger, K. H., Runkel, S., Kloes, M., Stohrer, M., Okunieff, P., and Vaupel, P. (1989b). Blood flow, metabolism, cellular microenvironment, and growth rate of human tumor xenografts. Cancer Res *49*, 3759-3764.

Kang, M. A., Kim, K. Y., Seol, J. Y., Kim, K. C., and Nam, M. J. (2000). The growth inhibition of hepatoma by gene transfer of antisense vascular endothelial growth factor. J Gene Med *2*, 289-296.

Kauppinen, R. A. (2002). Monitoring cytotoxic tumour treatment response by diffusion magnetic resonance imaging and proton spectroscopy. NMR Biomed *15*, 6-17.

Kauppinen, R. A., Nissinen, T., Karkkainen, A. M., Pirttila, T. R., Palvimo, J., Kokko, H., and Williams, S. R. (1992). Detection of thymosin beta 4 in situ in a guinea pig cerebral cortex preparation using 1H NMR spectroscopy. J Biol Chem *267*, 9905-9910.

Kauppinen, R. A., and Williams, S. R. (1991). Nondestructive detection of glutamate by 1H nuclear magnetic resonance spectroscopy in cortical brain slices from the guinea pig: evidence for changes in detectability during severe anoxic insults. J Neurochem *57*, 1136-1144.

Kerr, J., Wyllie, A., and Currie, A. (1972). Apoptosis: A basic phenomenon with wide-ranging implications in tissue kinetics. British journal of cancer, 239-257.

Kim, K. J., Li, B., Winer, J., Armanini, M., Gillett, N., Phillips, H. S., and Ferrara, N. (1993). Inhibition of vascular endothelial growth factor-induced angiogenesis suppresses tumour growth in vivo. Nature *362*, 841-844.

Kinoshita, Y., Kajiwara, H., Yokota, A., and Koga, Y. (1994). Proton magnetic resonance spectroscopy of brain tumors: an in vitro study. Neurosurgery *35*, 606-613; discussion 613-604.

Kizu, O., Naruse, S., Furuya, S., Morishita, H., Ide, M., Maeda, T., and Ueda, S. (1998). Application of proton chemical shift imaging in monitoring of gamma knife radiosurgery on brain tumors. Magnetic Resonance Imaging *16*, 197-204.

Kono, K., Inoue, Y., Nakayama, K., Shakudo, M., Morino, M., Ohata, K., Wakasa, K., and Yamada, R. (2001). The role of diffusion-weighted imaging in patients with brain tumors. AJNR Am J Neuroradiol *22*, 1081-1088.

Koot, R. W., Maarouf, M., Hulshof, M. C., Voges, J., Treuer, H., Koedooder, C., Sturm, V., and Bosch, D. A. (2000). Brachytherapy: Results of two different therapy strategies for patients with primary glioblastoma multiforme. Cancer *88*, 2796-2802.

Kucharczyk, J., Mintorovitch, J., Asgari, H. S., and Moseley, M. (1991). Diffusion/perfusion MR imaging of acute cerebral ischemia. Magn Reson Med *19*, 311-315.

Kuesel, A. C., Donnelly, S. M., Halliday, W., Sutherland, G. R., and Smith, I. C. (1994). Mobile lipids and metabolic heterogeneity of brain tumours as detectable by ex vivo 1H MR spectroscopy. NMR Biomed *7*, 172-180.

Laerum, O. D., Rajewsky, M. F., Schachner, M., Stavrou, D., Haglid, K. G., and Haugen, A. (1977). Phenotypic properties of neoplastic cell lines developed from fetal rat brain cells in culture after exposure to ethylnitrosourea in vivo. Z Krebsforsch Klin Onkol Cancer Res Clin Oncol *89*, 273-295.

Lahrech, H., Zoula, S., Farion, R., Remy, C., and Decorps, M. (2001). In vivo measurement of the size of lipid droplets in an intracerebral glioma in the rat. Magn Reson Med *45*, 409-414.

Lam, P. Y., and Breakefield, X. O. (2001). Potential of gene therapy for brain tumors. Hum Mol Genet *10*, 777-787.

Lam, W. W., Poon, W. S., and Metreweli, C. (2002). Diffusion MR imaging in glioma: does it have any role in the pre-operation determination of grading of glioma? Clin Radiol *57*, 219-225.

Lang, F. F., Yung, W. K., Sawaya, R., and Tofilon, P. J. (1999). Adenovirus-mediated p53 gene therapy for human gliomas. Neurosurgery *45*, 1093-1104.

Laperriere, N. J., Leung, P. M., McKenzie, S., Milosevic, M., Wong, S., Glen, J., Pintilie, M., and Bernstein, M. (1998). Randomized study of brachytherapy in the initial management of patients with malignant astrocytoma. Int J Radiat Oncol Biol Phys *41*, 1005-1011.

Law, M., Yang, S., Wang, H., Babb, J. S., Johnson, G., Cha, S., Knopp, E. A., and Zagzag, D. (2003). Glioma grading: sensitivity, specificity, and predictive values of perfusion MR imaging and proton MR spectroscopic imaging compared with conventional MR imaging. AJNR Am J Neuroradiol *24*, 1989-1998.

Le Belle, J. E., Harris, N. G., Williams, S. R., and Bhakoo, K. K. (2002). A comparison of cell and tissue extraction techniques using high-resolution 1H-NMR spectroscopy. NMR Biomed *15*, 37-44.

Levin, V. A., Leibel, S. A., and Gutin, P. H. (2001). Neoplasms of the Nervous Systems. In Cancer: Principles andpractice of Oncology, V. T. DeVita, S. Hellman, and S. A. Rosenberg, eds. (Philadelphia, Lippincott Williams and Wilkins), pp. 2100-2160.

Levin, V. A., Silver, P., Hannigan, J., Wara, W. M., Gutin, P. H., Davis, R. L., and Wilson, C. B. (1990). Superiority of post-radiotherapy adjuvant chemotherapy with CCNU, procarbazine, and vincristine (PCV) over BCNU for anaplastic gliomas: NCOG 6G61 final report. Int J Radiat Oncol Biol Phys *18*, 321-324.

Levine, A. J., Momand, J., and Finlay, C. A. (1991). The p53 tumour suppressor gene. Nature *351*, 453-456.

Levitt, M., and Freeman, R. (1981). Compensation for pulse imperfections in NMR spin-echo experiments. Journal of Magnetic Resonance *43*, 65-80.

Lowe, S. W., and Lin, A. W. (2000a). Apoptosis in cancer. Carcinogenesis *21*, 485-495.

Lowe, S. W., and Lin, A. W. (2000b). Apoptosis in cancer. Carcinogenesis *21*, 485-495.

Lowe, S. W., Schmitt, E. M., Smith, S. W., Osborne, B. A., and Jacks, T. (1993). p53 is required for radiation-induced apoptosis in mouse thymocytes. Nature *362*, 847-849.

Lyng, H., Sundfor, K., Trope, C., and Rofstad, E. K. (2000). Disease control of uterine cervical cancer: relationships to tumor oxygen tension, vascular density, cell density, and frequency of mitosis and apoptosis measured before treatment and during radiotherapy. Clin Cancer Res *6*, 1104-1112.

Macchiarini, P., Fontanini, G., Hardin, M. J., Squartini, F., and Angeletti, C. A. (1992). Relation of neovascularisation to metastasis of non-small-cell lung cancer. Lancet *340*, 145-146.

Machein, M. R., Risau, W., and Plate, K. H. (1999). Antiangiogenic gene therapy in a rat glioma model using a dominant-negative vascular endothelial growth factor receptor 2. Hum Gene Ther *10*, 1117-1128.

Maidment, S. L., and Pilkington, G. (2000). Brain Cancers. http://wwwelsnet/elsonline/html/A0001892html.

Maier, S. E., Bogner, P., Bajzik, G., Mamata, H., Mamata, Y., Repa, I., Jolesz, F. A., and Mulkern, R. V. (2001). Normal brain and brain tumor: multicomponent apparent diffusion coefficient line scan imaging. Radiology *219*, 842-849.

Majos, C., Alonso, J., Aguilera, C., Serrallonga, M., Perez-Martin, J., Acebes, J. J., Arus, C., and Gili, J. (2003). Proton magnetic resonance spectroscopy ((1)H MRS) of human brain tumours: assessment of differences between tumour types and its applicability in brain tumour categorization. Eur Radiol *13*, 582-591.

Mardor, Y., Pfeffer, R., Spiegelmann, R., Roth, Y., Maier, S. E., Nissim, O., Berger, R., Glicksman, A., Baram, J., Orenstein, A.*, et al.* (2003). Early detection of response to radiation therapy in patients with brain malignancies using conventional and high b-value diffusion-weighted magnetic resonance imaging. J Clin Oncol *21*, 1094-1100.

Mardor, Y., Roth, Y., Lidar, Z., Jonas, T., Pfeffer, R., Maier, S. E., Faibel, M., Nass, D., Hadani, M., Orenstein, A.*, et al.* (2001). Monitoring response to convection-enhanced taxol delivery in brain tumor patients using diffusion-weighted magnetic resonance imaging. Cancer Res *61*, 4971-4973.

Mayr, M. T., Crocker, I. R., Butker, E. K., Williams, H., Cotsonis, G. A., and Olson, J. J. (2002). Results of interstitial brachytherapy for malignant brain tumors. Int J Oncol *21*, 817-823.

Mesnil, M., and Yamasaki, H. (2000). Bystander effect in herpes simplex virus-thymidine kinase/ganciclovir cancer gene therapy: role of gap-junctional intercellular communication. Cancer Res *60*, 3989-3999.

Meyerand, M. E., Pipas, J. M., Mamourian, A., Tosteson, T. D., and Dunn, J. F. (1999). Classification of biopsy-confirmed brain tumors using single-voxel MR spectroscopy. AJNR Am J Neuroradiol *20*, 117-123.

Michaeli, S., Garwood, M., Zhu, X.-H., DelaBarre, L., Andersen, P., Adriany, G., Merkle, H., Ugurbil, K., and Chen, W. (2002). Proton T_2 Relaxation Study of Water, N-acetylaspartate, and Creatine in Human Brain Using Hahn and Carr-Purcell Spin Echoes at 4T and 7T. Magnetic resonance in medicine, 629-633.

Millauer, B., Shawver, L. K., Plate, K. H., Risau, W., and Ullrich, A. (1994). Glioblastoma growth inhibited in vivo by a dominant-negative Flk-1 mutant. Nature *367*, 576-579.

Miller, B. M., Chang, L., Booth, R., Ernst, T., Cornford, M., Nikas, D., McBride, D., and Jenden, D. J. (1996). In Vivo 1H MRS Choline: Correlation With In Vitro Chemistry/Histology. Life Sciences *58*, 1929-1935.

Miller, C. R., Williams, C. R., Buchsbaum, D. J., and Gillespie, G. Y. (2002). Intratumoral 5-fluorouracil produced by cytosine deaminase/5-fluorocytosine gene therapy is effective for experimental human glioblastomas. Cancer Res *62*, 773-780.

Millis, K. K., Maas, W. E., Cory, D. G., and Singer, S. (1997). Gradient, High-Resolution, Magic-Angle Spinning Nuclear Magnetic Resonance Spectroscopy of Human Adipocyte Tissue. Magnetic resonance in medicine *38*, 399-403.

Millis, K. K., Weybright, P., Campbell, N., Fletcher, J. A., Fletcher, C. D., Cory, D. G., and Singer, S. (1999). Classification of Human Liposarcoma and Lipoma Using Ex Vivo Proton NMR Spectroscopy. Magnetic resonance in medicine *41*, 257-267.

Mogard, J., Kihlstrom, L., Ericson, K., Karlsson, B., Guo, W. Y., and Stone-Elander, S. (1994). Recurrent tumor vs radiation effects after gamma knife radiosurgery of intracerebral metastases: diagnosis with PET-FDG. J Comput Assist Tomogr *18*, 177-181.

Moolten, F. L. (1986). Tumor chemosensitivity conferred by inserted herpes thymidine kinase genes: paradigm for a prospective cancer control strategy. Cancer Res *46*, 5276-5281.

Moreno, A., Rey, M., Montane, J. M., Alonso, J., and Arus, C. (1993). 1H NMR spectroscopy of colon tumors and normal mucosal biopsies; elevated taurine levels and reduced polyethyleneglycol absorption in tumors may have diagnostic significance. NMR Biomed *6*, 111-118.

Mori, S., Frederiksen, K., van Zijl, P. C., Stieltjes, B., Kraut, M. A., Solaiyappan, M., and Pomper, M. G. (2002). Brain white matter anatomy of tumor patients evaluated with diffusion tensor imaging. Ann Neurol *51*, 377-380.

Mori, S., and van Zijl, P. C. (1995). Diffusion weighting by the trace of the diffusion tensor within a single scan. Magn Reson Med *33*, 41-52.

Mullen, C. A., Coale, M. M., Levy, A. T., Stetler-Stevenson, W. G., Liotta, L. A., Brandt, S., and Blaese, R. M. (1992a). Fibrosarcoma cells transduced with the IL-6 gene exhibited reduced tumorigenicity, increased immunogenicity, and decreased metastatic potential. Cancer Res *52*, 6020-6024.

Mullen, C. A., Kilstrup, M., and Blaese, R. M. (1992b). Transfer of the bacterial gene for cytosine deaminase to mammalian cells confers lethal sensitivity to 5-fluorocytosine: a negative selection system. Proc Natl Acad Sci U S A *89*, 33-37.

Murphy, D. J. (2001). The biogenesis and functions of lipid bodies in animals, plants and microorganisms. Prog Lipid Res *40*, 325-438.

Murphy, M., Loosemore, A., Clifton, A. G., Howe, F. A., Tate, A. R., Cudlip, S. A., Wilkins, P. R., Griffiths, J. R., and Bell, B. A. (2002). The contribution of proton magnetic resonance spectroscopy (1HMRS) to clinical brain tumour diagnosis. Br J Neurosurg *16*, 329-334.

Mäkelä, H. I., Gröhn, O. H., Kettunen, M. I., and Kauppinen, R. A. (2001). Proton exchange as a relaxation mechanism for T1 in the rotating frame in native and immobilized protein solutions. Biochem Biophys Res Commun *289*, 813-818.

Nafe, R., Herminghaus, S., Raab, P., Wagner, S., Pilatus, U., Schneider, B., Schlote, W., Zanella, F., and Lanfermann, H. (2003). Preoperative proton-MR spectroscopy of gliomas - correlation with quantitative nuclear morphology in surgical specimen. Journal of Neuro-Oncology *63*, 233-245.

Namba, H., Iwadate, Y., Tagawa, M., Kimura, M., Shimizu, H., Sato, Y., Sueyoshi, K., and Sakiyama, S. (1996). Evaluation of the bystander effect in experimental brain tumors bearing herpes simplex virus-thymidine kinase gene by serial magnetic resonance imaging. Hum Gene Ther *7*, 1847-1852.

Nanda, D., Vogels, R., Havenga, M., Avezaat, C. J., Bout, A., and Smitt, P. S. (2001). Treatment of malignant gliomas with a replicating adenoviral vector expressing herpes simplex virus-thymidine kinase. Cancer Res *61*, 8743-8750.

Negendank, W. G., Sauter, R., Brown, T. R., Evelhoch, J. L., Falini, A., Gotsis, E. D., Heerschap, A., Kamada, K., Lee, B. C., Mengeot, M. M., *et al.* (1996). Proton magnetic resonance spectroscopy in patients with glial tumors: a multicenter study. Journal of Neurosurgery *84*, 449-458.

Nelson, J. S., Tsukada, Y., Schoenfeld, D., Fulling, K., Lamarche, J., and Peress, N. (1983). Necrosis as a prognostic criterion in malignant supratentorial, astrocytic gliomas. Cancer *52*, 550-554.

Nelson, S. J., Huhn, S., Vigneron, D. B., Day, M. R., Wald, L. L., Prados, M., Chang, S., Gutin, P. H., Sneed, P. K., Verhey, L., *et al.* (1997). Volume MRI and MRSI techniques for the quantitation of treatment response in brain tumors: presentation of a detailed case study. J Magn Reson Imaging *7*, 1146-1152.

Nelson, S. J., Vigneron, D. B., and Dillon, W. P. (1999). Serial evaluation of patients with brain tumors using volume MRI and 3D 1H MRSI. NMR Biomed *12*, 123-138.

Nicolay, K., Braun, K. P., Graaf, R. A., Dijkhuizen, R. M., and Kruiskamp, M. J. (2001). Diffusion NMR spectroscopy. NMR Biomed *14*, 94-111.

Nicolay, K., van der Toorn, A., and Dijkhuizen, R. M. (1995). In vivo diffusion spectroscopy. An overview. NMR Biomed *8*, 365-374.

Nieder, C., Andratschke, N., Wiedenmann, N., Busch, R., Grosu, A. L., and Molls, M. (2004). Radiotherapy for High-Grade GliomasDoes Altered Fractionation Improve the Outcome? Strahlenther Onkol *180*, 401-407.

Niendorf, T., Dijkhuizen, R. M., Norris, D. G., van Lookeren Campagne, M., and Nicolay, K. (1996). Biexponential diffusion attenuation in various states of brain tissue: implications for diffusion-weighted imaging. Magn Reson Med *36*, 847-857.

Nitta, T., Hishii, M., Sato, K., and Okumura, K. (1994). Selective expression of interleukin-10 gene within glioblastoma multiforme. Brain Res *649*, 122-128.

Opstad, K. S., Murphy, M. M., Wilkins, P. R., Bell, B. A., Griffiths, J. R., and Howe, F. A. (2004). Differentiation of metastases from high-grade gliomas using short echo time 1H spectroscopy. J Magn Reson Imaging *20*, 187-192.

Party, M. R. C. B. T. W. (2001). Randomized trial of procarbazine, lomustine, and vincristine in the adjuvant treatment of high-grade astrocytoma: a Medical Research Council trial. J Clin Oncol *19*, 509-518.

Peeling, J., and Sutherland, G. (1992). High-resolution 1H NMR spectroscopy studies of extracts of human cerebral neoplasms. Magn Reson Med *24*, 123-136.

Pfeuffer, J., Flogel, U., and Leibfritz, D. (1998). Monitoring of cell volume and water exchange time in perfused cells by diffusion-weighted 1H NMR spectroscopy. NMR Biomed *11*, 11-18.

Pfeuffer, J., Tkac, I., Provencher, S. W., and Gruetter, R. (1999). Toward an in vivo neurochemical profile: quantification of 18 metabolites in short-echo-time (1)H NMR spectra of the rat brain. J Magn Reson *141*, 104-120.

Pirzkall, A., McKnight, T. R., Graves, E. E., Carol, M. P., Sneed, P. K., Wara, W. W., Nelson, S. J., Verhey, L. J., and Larson, D. A. (2001). MR-spectroscopy guided target delineation for high-grade gliomas. Int J Radiat Oncol Biol Phys *50*, 915-928.

Pirzkall, A., Nelson, S. J., McKnight, T. R., Takahashi, M. M., Li, X., Graves, E. E., Verhey, L. J., Wara, W. W., Larson, D. A., and Sneed, P. K. (2002). Metabolic imaging of low-grade gliomas with three-dimensional magnetic resonance spectroscopy. Int J Radiat Oncol Biol Phys *53*, 1254-1264.

Plate, K. H., Breier, G., Weich, H. A., and Risau, W. (1992). Vascular endothelial growth factor is a potential tumour angiogenesis factor in human gliomas in vivo. Nature *359*, 845-848.

Podo, F. (1999). Tumour phospholipid metabolism. NMR in Biomedicine *12*, 413-439.

Pontén, U., Ratcheson, R., Salford, L., and Siesjö, B. (1973). Optimal freezing conditions for cerebral metabolites in rats. Journal of Neurochemistry *21*, 1127-1138.

Poptani, H., Duvvuri, U., Miller, C. G., Mancuso, A., Charagundla, S., Fraser, N. W., Glickson, J. D., Leigh, J. S., and Reddy, R. (2001). T1rho imaging of murine brain tumors at 4 T. Acad Radiol *8*, 42-47.

Poptani, H., Kaartinen, J., Gupta, R. K., Niemitz, M., Hiltunen, Y., and Kauppinen, R. A. (1999). Diagnostic assessment of brain tumours and non-neoplastic brain disorders in vivo using proton nuclear magnetic resonance spectroscopy and artificial neural networks. J Cancer Res Clin Oncol *125*, 343-349.

Poptani, H., Puumalainen, A. M., Grohn, O. H., Loimas, S., Kainulainen, R., Yla-Herttuala, S., and Kauppinen, R. A. (1998a). Monitoring thymidine kinase and ganciclovir-induced changes in rat malignant glioma in vivo by nuclear magnetic resonance imaging. Cancer Gene Ther *5*, 101-109.

Poptani, H., Puumalainen, A.-M., Gröhn, O. H., Loimas, S., Kainulainen, R., Yläherttuala, S., and Kauppinen, R. A. (1998b). Monitoring thymidine kinase and ganciclovir-induced changes in rat malignant glioma *in vivo* by nuclear magnetic resonance imaging. Cancer Gene Therapy *5*, 101-109.

Preul, C., Kuhn, B., Lang, E. W., Mehdorn, H. M., Heller, M., and Link, J. (2003). Differentiation of cerebral tumors using multi-section echo planar MR perfusion imaging. Eur J Radiol *48*, 244-251.

Preul, M. C., Caramanos, Z., Collins, D. L., Villemure, J. G., Leblanc, R., Olivier, A., Pokrupa, R., and Arnold, D. L. (1996). Accurate, noninvasive diagnosis of human brain tumors by using proton magnetic resonance spectroscopy. Nat Med *2*, 323-325.

Principi, M., Italiani, M., Guiducci, A., Aprile, I., Muti, M., Giulianelli, G., and Ottaviano, P. (2003). Perfusion MRI in the evaluation of the relationship between tumour growth, necrosis and angiogenesis in glioblastomas and grade 1 meningiomas. Neuroradiology *45*, 205-211.

Ram, Z., Culver, K. W., Walbridge, S., Blaese, R. M., and Oldfield, E. H. (1993). In Situ Retroviral-mediated Gene Transfer for the treatment of Brain Tumors in Rats. Cancer research, 83-88.

Rémy, C., Arús, C., Ziegler, A., Lai, E. S., Moreno, A., Le Fur, Y., and Décorps, M. (1994). In vivo, ex vivo, and in vitro one- and two-dimensional nuclear magnetic resonance spectroscopy of an intracerebral glioma in rat brain: assignment of resonances. J Neurochem *62*, 166-179.

Roberts, T. P., and Rowley, H. A. (2003). Diffusion weighted magnetic resonance imaging in stroke. Eur J Radiol *45*, 185-194.

Rosi, A., Luciani, A. M., Matarrese, P., Arancia, G., Viti, V., and Guidoni, L. (1999). 1H-MRS lipid signal modulation and morphological and ultrastructural changes related to tumor cell proliferation. Magn Reson Med *42*, 248-257.

Ross, B., and Bluml, S. (2001). Magnetic resonance spectroscopy of the human brain. Anat Rec *265*, 54-84.

Ross, B. D., Chenevert, T. L., and Rehemtulla, A. (2002). Magnetic resonance imaging in cancer research. Eur J Cancer *38*, 2147-2156.

Roszman, T., Elliott, L., and Brooks, W. (1991). Modulation of T-cell function by gliomas. Immunol Today *12*, 370-374.

Rubsam, L. Z., Boucher, P. D., Murphy, P. J., KuKuruga, M., and Shewach, D. S. (1999). Cytotoxicity and accumulation of ganciclovir triphosphate in bystander cells cocultured with herpes simplex virus type 1 thymidine kinase-expressing human glioblastoma cells. Cancer Res *59*, 669-675.

Rusakov, D. A., and Kullmann, D. M. (1998). Geometric and viscous components of the tortuosity of the extracellular space in the brain. Proc Natl Acad Sci U S A *95*, 8975-8980.

Rutter, A., Hugenholtz, H., Saunders, J. K., and Smith, I. C. (1995). Classification of brain tumors by ex vivo 1H NMR spectroscopy. J Neurochem *64*, 1655-1661.

Sandmair, A. M., Loimas, S., Puranen, P., Immonen, A., Kossila, M., Puranen, M., Hurskainen, H., Tyynela, K., Turunen, M., Vanninen, R.*, et al.* (2000a). Thymidine kinase gene therapy for human malignant glioma, using replication-deficient retroviruses or adenoviruses. Hum Gene Ther *11*, 2197-2205.

Sandmair, A. M., Turunen, M., Tyynela, K., Loimas, S., Vainio, P., Vanninen, R., Vapalahti, M., Bjerkvig, R., Janne, J., and Yla-Herttuala, S. (2000b). Herpes simplex virus thymidine kinase gene therapy in experimental rat BT4C glioma model: effect of the percentage of thymidine kinase-positive glioma cells on treatment effect, survival time, and tissue reactions. Cancer Gene Ther *7*, 413-421.

Santyr, G. E., Henkelman, R. M., and Bronskill, M. J. (1989). Spin locking for magnetic resonance imaging with application to human breast. Magn Reson Med *12*, 25-37.

Saransaari, P., and Oja, S. S. (2001). Tauriini - aivojen arvoituksellinen viestintäaine. Suomen lääkärilehti, 3189-3192.

Schaefer, P. W., Grant, P. E., and Gonzalez, R. G. (2000a). Diffusion-weighted MR Imaging of the Brain. Radiology *217*, 331-345.

Schaefer, P. W., Grant, P. E., and Gonzalez, R. G. (2000b). Diffusion-weighted MR imaging of the brain. Radiology *217*, 331-345.

Schlemmer, H. P., Bachert, P., Henze, M., Buslei, R., Herfarth, K. K., Debus, J., and van Kaick, G. (2002). Differentiation of radiation necrosis from tumor progression using proton magnetic resonance spectroscopy. Neuroradiology *44*, 216-222.

Schlemmer, H. P., Bachert, P., Herfarth, K. K., Zuna, I., Debus, J., and van Kaick, G. (2001). Proton MR spectroscopic evaluation of suspicious brain lesions after stereotactic radiotherapy. AJNR Am J Neuroradiol *22*, 1316-1324.

Schuller-Levis, G. B., and Park, E. (2003). Taurine: new implications for an old amino acid. FEMS Microbiology Letters *226*, 195-202.

Selker, R. G., Shapiro, W. R., Burger, P., Blackwood, M. S., Arena, V. C., Gilder, J. C., Malkin, M. G., Mealey, J. J., Jr., Neal, J. H., Olson, J.*, et al.* (2002). The Brain Tumor Cooperative Group NIH Trial 87-01: a randomized comparison of surgery, external radiotherapy, and carmustine versus surgery, interstitial radiotherapy boost, external radiation therapy, and carmustine. Neurosurgery *51*, 343-355; discussion 355-347.

Shono, T., Tofilon, P. J., Schaefer, T. S., Parikh, D., Liu, T. J., and Lang, F. F. (2002). Apoptosis induced by adenovirus-mediated p53 gene transfer in human glioma correlates with site-specific phosphorylation. Cancer Res *62*, 1069-1076.

Shweiki, D., Itin, A., Soffer, D., and Keshet, E. (1992). Vascular endothelial growth factor induced by hypoxia may mediate hypoxia-initiated angiogenesis. Nature *359*, 843-845.

Silva, A. C., Kim, S. G., and Garwood, M. (2000). Imaging blood flow in brain tumors using arterial spin labeling. Magn Reson Med *44*, 169-173.

Silver, M., Joseph, R., and Hoult, D. (1984). Highly selective $\pi/2$ and π pulse generation. Journal of Magnetic Resonance *59*, 347-351.

Siminovitch, D. J., Ruocco, M. J., Olejniczak, E. T., Das Gupta, S. K., and Griffin, R. G. (1988). Anisotropic 2H-nuclear magnetic resonance spin-lattice relaxation in cerebroside- and phospholipid-cholesterol bilayer membranes. Biophys J *54*, 373-381.

Smith, T. A., Eccles, S., Ormerod, M. G., Tombs, A. J., Titley, J. C., and Leach, M. O. (1991). The phosphocholine and glycerophosphocholine content of an oestrogen-sensitive rat mammary tumour correlates strongly with growth rate. Br J Cancer *64*, 821-826.

Somorjai, R. L., Dolenko, B., Nikulin, A. K., Pizzi, N., Scarth, G., Zhilkin, P., Halliday, W., Fewer, D., Hill, N., Ross, I.*, et al.* (1996). Classification of 1H MR spectra of human brain neoplasms: the influence of preprocessing and computerized consensus diagnosis on classification accuracy. J Magn Reson Imaging *6*, 437-444.

Sotak, C. H. (1988). A volume-localized, two-dimensional NMR method for the determination of lactate using zero-quantum coherence created in a stimulated echo pulse sequence. Magn Reson Med *7*, 364-370.

Spence, A. M., Peterson, R. A., Scharnhorst, J. D., Silbergeld, D. L., and Rostomily, R. C. (2004). Phase II study of concurrent continuous Temozolomide (TMZ) and Tamoxifen (TMX) for recurrent malignant astrocytic gliomas. J Neurooncol *70*, 91-95.

Steller, H. (1995). Mechanisms and Genes of Cellular Suicide. Science *267*, 1445-1449.

Stenning, S. P., Freedman, L. S., and Bleehen, N. M. (1987). An overview of published results from randomized studies of nitrosoureas in primary high grade malignant glioma. Br J Cancer *56*, 89-90.

Stewart, L. A. (2002). Chemotherapy in adult high-grade glioma: a systematic review and meta-analysis of individual patient data from 12 randomised trials. Lancet *359*, 1011-1018.

Sugahara, T., Korogi, Y., Kochi, M., Ikushima, I., Shigematu, Y., Hirai, T., Okuda, T., Liang, L., Ge, Y., Komohara, Y.*, et al.* (1999). Usefulness of diffusion-weighted MRI with echo-planar technique in the evaluation of cellularity in gliomas. Journal of magnetic resonance imaging *9*, 53-60.

Sun, Y., Schmidt, N. O., Schmidt, K., Doshi, S., Rubin, J. B., Mulkern, R. V., Carroll, R., Ziu, M., Erkmen, K., Poussaint, T. Y.*, et al.* (2004). Perfusion MRI of U87 brain tumors in a mouse model. Magn Reson Med *51*, 893-899.

Sze, D. Y., and Jardetzky, O. (1994). High-resolution proton NMR studies of lymphocyte extracts. Immunomethods *4*, 113-126.

Tada, M., and de Tribolet, N. (1993). Recent advances in immunobiology of brain tumors. J Neurooncol *17*, 261-271.

Tate, A. R., Griffiths, J. R., Martinez-Perez, I., Moreno, A., Barba, I., Cabanas, M. E., Watson, D., Alonso, J., Bartumeus, F., Isamat, F.*, et al.* (1998). Towards a method for automated classification of 1H MRS spectra from brain tumours. NMR Biomed *11*, 177-191.

Tate, A. R., Majos, C., Moreno, A., Howe, F. A., Griffiths, J. R., and Arus, C. (2003). Automated classification of short echo time in in vivo 1H brain tumor spectra: a multicenter study. Magn Reson Med *49*, 29-36.

Taylor, J. S., Langston, J. W., Reddick, W. E., Kingsley, P. B., Ogg, R. J., Pui, M. H., Kun, L. E., Jenkins, J. J., 3rd, Chen, G., Ochs, J. J.*, et al.* (1996). Clinical value of proton magnetic

resonance spectroscopy for differentiating recurrent or residual brain tumor from delayed cerebral necrosis. Int J Radiat Oncol Biol Phys *36*, 1251-1261.

Tedeschi, G., Lundbom, N., Raman, R., Bonavita, S., Duyn, J. H., Alger, J. R., and Di Chiro, G. (1997). Increased choline signal coinciding with malignant degeneration of cerebral gliomas: a serial proton magnetic resonance spectroscopy imaging study. J Neurosurg *87*, 516-524.

Thompson, C. B. (1995). Apoptosis in the pathogenesis and treatment of disease. Science *267*, 1456-1462.

Timbrell, J. A., Seabra, V., and Waterfield, C. J. (1995). The in vivo and in vitro protective properties of taurine. Gen Pharmacol *26*, 453-462.

Tkac, I., Starcuk, Z., Choi, I. Y., and Gruetter, R. (1999). In vivo 1H NMR spectroscopy of rat brain at 1 ms echo time. Magn Reson Med *41*, 649-656.

Tofts, P. S. (1997). Modeling tracer kinetics in dynamic Gd-DTPA MR imaging. J Magn Reson Imaging *7*, 91-101.

Tofts, P. S., and Kermode, A. G. (1991). Measurement of the blood-brain barrier permeability and leakage space using dynamic MR imaging. 1. Fundamental concepts. Magn Reson Med *17*, 357-367.

Trask, T. W., Trask, R. P., Aguilar-Cordova, E., Shine, H. D., Wyde, P. R., Goodman, J. C., Hamilton, W. J., Rojas-Martinez, A., Chen, S. H., Woo, S. L., and Grossman, R. G. (2000). Phase I study of adenoviral delivery of the HSV-tk gene and ganciclovir administration in patients with recurrent malignant brain tumors. Mol Ther *1*, 195-203.

Tsuyuguchi, N., Takami, T., Sunada, I., Iwai, Y., Yamanaka, K., Tanaka, K., Nishikawa, M., Ohata, K., Torii, K., Morino, M.*, et al.* (2004). Methionine positron emission tomography for differentiation of recurrent brain tumor and radiation necrosis after stereotactic radiosurgery--in malignant glioma. Ann Nucl Med *18*, 291-296.

Tugnoli, V., Tosi, M. R., Tinti, A., Trinchero, A., Bottura, G., and Fini, G. (2001). Characterization of lipids from human brain tissues by multinuclear magnetic resonance spectroscopy. Biopolymers *62*, 297-306.

Tyynelä, K., Sandmair, A.-M., Turunen, M., Vanninen, R., Vainio, P., Kauppinen, R., Johansson, R., Vapalahti, M., and Ylä-Herttuala, S. (2002). Adenovirus-mediated herpes simplex virus thymidine kinase gene therapy in BT4C rat glioma model. Cancer gene therapy, 917-924.

Tzika, A. A., Cheng, L. L., Goumnerova, L., Madsen, J. R., Zurakowski, D., Astrakas, L. G., Zarifi, M. K., Scott, R. M., Anthony, D. C., Gonzalez, R. G., and Black, P. M. (2002). Biochemical characterization of pediatric brain tumors by using in vivo and ex vivo magnetic resonance spectroscopy. J Neurosurg *96*, 1023-1031.

Uhl, M., Aulwurm, S., Wischhusen, J., Weiler, M., Ma, J. Y., Almirez, R., Mangadu, R., Liu, Y. W., Platten, M., Herrlinger, U.*, et al.* (2004). SD-208, a novel transforming growth factor beta receptor I kinase inhibitor, inhibits growth and invasiveness and enhances immunogenicity of murine and human glioma cells in vitro and in vivo. Cancer Res *64*, 7954-7961.

Usenius, J. P., Kauppinen, R. A., Vainio, P. A., Hernesniemi, J. A., Vapalahti, M. P., Paljarvi, L. A., and Soimakallio, S. (1994a). Quantitative metabolite patterns of human brain tumors: detection by 1H NMR spectroscopy in vivo and in vitro. J Comput Assist Tomogr *18*, 705-713.

Usenius, J. P., Vainio, P., Hernesniemi, J., and Kauppinen, R. A. (1994b). Choline-containing compounds in human astrocytomas studied by 1H NMR spectroscopy in vivo and in vitro. J Neurochem *63*, 1538-1543.

Utriainen, M., Komu, M., Vuorinen, V., Lehikoinen, P., Sonninen, P., Kurki, T., Utriainen, T., Roivainen, A., Kalimo, H., and Minn, H. (2003). Evaluation of brain tumor metabolism with [11C]choline PET and 1H-MRS. J Neurooncol *62*, 329-338.

Wald, L. L., Nelson, S. J., Day, M. R., Noworolski, S. E., Henry, R. G., Huhn, S. L., Chang, S., Prados, M. D., Sneed, P. K., Larson, D. A.*, et al.* (1997). Serial proton magnetic resonance spectroscopy imaging of glioblastoma multiforme after brachytherapy. Journal of Neurosurgery *87*, 525-534.

Walker, M. D., Alexander, E., Jr., Hunt, W. E., MacCarty, C. S., Mahaley, M. S., Jr., Mealey, J., Jr., Norrell, H. A., Owens, G., Ransohoff, J., Wilson, C. B.*, et al.* (1978). Evaluation of BCNU

and/or radiotherapy in the treatment of anaplastic gliomas. A cooperative clinical trial. J Neurosurg *49*, 333-343.

van der Toorn, A., Verheul, H. B., Berkelbach van der Sprenkel, J. W., Tulleken, C. A., and Nicolay, K. (1994). Changes in metabolites and tissue water status after focal ischemia in cat brain assessed with localized proton MR spectroscopy. Magn Reson Med *32*, 685-691.

van zijl, P. C., Davis, D., and Moonen, C. T. (1994). Diffusion spectroscopy in living systems. In NMR in physiology and biomedicine, R. J. Gillies, ed. (San Diego, Academic Press), pp. 185-198.

van Zijl, P. C., Zhou, J., Mori, N., Payen, J. F., Wilson, D., and Mori, S. (2003). Mechanism of magnetization transfer during on-resonance water saturation. A new approach to detect mobile proteins, peptides, and lipids. Magn Reson Med *49*, 440-449.

Vaupel, P., Fortmeyer, H. P., Runkel, S., and Kallinowski, F. (1987). Blood flow, oxygen consumption, and tissue oxygenation of human breast cancer xenografts in nude rats. Cancer Res *47*, 3496-3503.

Weidner, N., Carroll, P. R., Flax, J., Blumenfeld, W., and Folkman, J. (1993). Tumor angiogenesis correlates with metastasis in invasive prostate carcinoma. Am J Pathol *143*, 401-409.

Weidner, N., Semple, J. P., Welch, W. R., and Folkman, J. (1991). Tumor angiogenesis and metastasis--correlation in invasive breast carcinoma. N Engl J Med *324*, 1-8.

Verhoven, B., Schlegel, R. A., and Williamson, P. (1995). Mechanisms of phosphatidylserine exposure, a phagocyte recognition signal, on apoptotic T lymphocytes. Journal of Experimental Medicine *182*, 1597-1601.

Weybright, P., Millis, K., Campbell, N., Cory, D. G., and Singer, S. (1998). Gradient, high-resolution, magic angle spinning 1H nuclear magnetic resonance spectroscopy of intact cells. Magn Reson Med *39*, 337-345.

Vigneron, D., Bollen, A., McDermott, M., Wald, L., Day, M., Moyher-Noworolski, S., Henry, R., Chang, S., Berger, M., Dillon, W., and Nelson, S. (2001). Three-dimensional magnetic resonance spectroscopic imaging of histologically confirmed brain tumors. Magn Reson Imaging *19*, 89-101.

Williams, S. N., Anthony, M. L., and Brindle, K. M. (1998). Induction of apoptosis in two mammalian cell lines results in increased levels of fructose-1,6-bisphosphate and CDP-choline as determined by 31P MRS. Magn Reson Med *40*, 411-420.

Willker, W., Leibfritz, D., Kerssebaum, R., and Bermel, W. (1993). Gradient Selection in Inverse Heteronuclear Correlation Spectroscopy. Magnetic Resonance in Chemistry *31*, 287-292.

Vincent, A., Vogels, R., Someren, G., Esandi, M., Noteboom, J., Avezaat, C., Vecht, C., Bekkum, D., Valerio, D., Bout, A., and Hoogerbrugge, P. (1996). Herpes simplex virus thymidine kinase gene therapy for rat malignant brain tumors. Human Gene Therapy *7*, 197-025.

Vincent, S., and George, H. (2004). Latest intelligence in brain cancer research. In Cancer Research UK Scientific Yearbook 2003/2004, pp. 58-61.

Wolf, C. M., and Eastman, A. (1999). Intracellular acidification during apoptosis can occur in the absence of a nucleus. Biochem Biophys Res Commun *254*, 821-827.

Wu, D., Chen, A., and Johnson, C. S. J. (1995). An Improved Diffusion-Ordered Spectroscopy Experiment Incorporating Bipolar-Gradient Pulses. Journal of Magnetic Resonance, Series A *115*, 260-264.

Wyllie, A. H., Kerr, J. F., and Currie, A. R. (1980). Cell death: the significance of apoptosis. Int Rev Cytol *68*, 251-306.

Ye, F. Q., Martin, W. W., and Allen, P. S. (1996). Estimation of the Iron Concentration in Excised Gray Matter by Means of Proton Relaxation Measurements. Magnetic resonance in medicine *35*, 285-289.

Zhang, J., Richards, L. J., Yarowsky, P., Huang, H., van Zijl, P. C., and Mori, S. (2003). Three-dimensional anatomical characterization of the developing mouse brain by diffusion tensor microimaging. Neuroimage *20*, 1639-1648.

Zülch, K. (1979). Histological typing of tumours of the central nervous system, Vol No. 21 (Geneva, WHO).